Establishment of a heterotypic 3D breast cancer model based on a vascularized porous scaffold combined with an epithelial cell-laden hydrogel

Filipa Raquel Castro Teixeira

Dissertation for the Degree of Master of Science in Bioengineering at Faculdade de Engenharia da Universidade do Porto and Instituto de Ciências Biomédicas Abel Salazar da Universidade do Porto

- This page was intentionally left blank -

Establishment of a heterotypic 3D breast cancer model based on a vascularized porous scaffold combined with an epithelial cell-laden hydrogel

Filipa Raquel Castro Teixeira

FEUP – Faculdade de Engenharia da Universidade do Porto

ICBAS-UP – Instituto de Ciências Biomédicas de Abel Salazar

Dissertation for Masters in Bioengineering

Supervisor:

Sílvia Bidarra, Ph.D. **i3S**

Co-supervisor:

Cristina Barrias, Ph.D. **i3S**

i3S - Instituto de investigação e inovação em saúde, Universidade do Porto

Porto, September 2018

- This page was intentionally left blank -

“You are a wonderful creation.

You know more than you think you know,

just as you know less than you want to know.”

Oscar Wilde

- This page was intentionally left blank -

ACKNOWLEDGEMENTS

First and foremost, I would like to thank to my supervisor, Sílvia Bidarra for all the time she spent with me, patience, care, and wisdom. You are a wonderful role model and I have learned so much from you. Not less importantly, I would like to thank her for every friendly word of encouragement through all the difficulties and for sharing a small part of her knowledge, and for all the laughing, crying and crazy moments. A most sincere acknowledge for her support in the final days of this project.

To my co-supervisor, Cristina Barrias, for kindly accepting me and giving me the opportunity to work on this project. You have always believed in me even when I did not believe in myself and that has been really important throughout this process.

My sincere thanks also goes to all members of the Bioengineered 3D Microenvironments group and Biomaterial for Multistage Drug and Cell Delivery group for welcoming and for all the support and help.

To Ana Luísa Torres, I would like to thank the availability to supply the outgrowth endothelial cells and for teaching how to carefully work with these cells. Besides that, I would also like to thank you for all your patience, support, for some scares, but especially for your contagious smile.

But this work is not only a reflection of the last few months. It is also the conclusion of five years full of good memories. So, I would like to acknowledge my Professors and previous supervisors for all the transmitted knowledge. Also, I would like to express my deepest gratitude to all my friends, specially Tânia, Sofia, Francisca, João and Márcia. With them I have passed the best moments of the last few years. And with them I was able to surpass the worst moments. Thank you with all of my heart!

To my linguistic friend, Marlene for being always there and specially in the last few months. Thank you for lifting me up when I needed and for your kind words and advices (except for encouraging me several times to destroy my computer).

Last, but definitely not the least, I can only express my gratitude to all my family for their unconditional support and patience throughout this challenging stage of my life. Without them this would be definitely not possible.

The research described in this thesis was financially supported by: Project 3DEMT funded by POCI via FEDER (POCI-01-0145-FEDER-016627) and by FCT via OE (PTDC/BBB-ECT/2518/2014).

To all, THANK YOU**

ABSTRACT

Tumor angiogenesis is critical for tumor growth and metastasis, but so far little is known about the role that vascular cells play in the tumor microenvironment. The use of tissue engineering strategies for the development of *in vitro* 3D models of vascularized tumors has been providing cancer research with better tools for dissecting the tumor microenvironment in biologically relevant settings. They also afford useful platforms for more effectively screening of potential anti-cancer therapeutics.

The aim of this work was to develop a sophisticated 3D tri-culture platform combining hydrogel-embedded breast epithelial cells with a vascularized porous scaffold.

The first part of the thesis, focused on the development of alginate-based porous 3D scaffolds, which were seeded with outgrowth endothelial cells (OECs) and fibroblasts. After optimization of the structural characteristics of the scaffolds and the cell culture set-up, it was possible to promote the deposition of abundant amounts of endogenous extracellular matrix, along with the formation of endothelial vascular-like structures.

In the second part, another 3D *in vitro* model was developed, which was based on the entrapment of human mammary epithelial cells within RGD-alginate hydrogel matrices. This system provided a simple, yet biologically meaningful, cellular microenvironment, where cell-matrix interactions could be modulated in a systematic way. Three different human breast epithelial cells with distinct metastatic capacities were studied in this 3D microenvironment, namely for their ability to form spheroids and undergo normal/abnormal epithelial morphogenesis.

Finally, in the last part of the thesis, a 3D heterotopic model was developed, by combining the two previous models, i.e. the vascularized porous scaffold and the breast epithelial cells-laden hydrogels. Although the experiments performed in this final part of the thesis are still very preliminary, it was possible to detect the formation of epithelial cell spheroids within vascularized scaffolds. In the future, this *in vitro* platform is expected to provide a valuable tool to improve current knowledge on the role of vascularization on cancer dissemination, which may help in the identification of putative targets for more effective anti-cancer therapies.

- This page was intentionally left blank -

TABLE OF CONTENTS

LIST OF FIGURES

LIST OF TABLES

LIST OF ABBREVIATIONS

2D	Two dimensional
3D	Three dimensional
BSA	Bovine serum albumin
CAD	Computer-aided design
CM	Conditioned medium
EC	Endothelial cell
ECM	Extracellular matrix
EDC	1-ethyl-(dimethylaminopropyl)-carbodiimide
EGF	Epidermal growth factor
EHS	Englebreth-Holm-Swarm
EMT	Epithelial-mesenchymal transition
EPC	Endothelial progenitor cell
FGF	Fibroblast growth factor
FN	Fibronectin
GDL	Glucose delta-lactone
GelMA	Gelatin methacrylate
hMF	Human mammary fibroblasts
HMVEC	Human microvascular endothelial cell
HUVEC	Human umbilical vein endothelial cell
IGF-1	Insulin growth factor-1
MMP	Matrix metalloproteinase
OEC	Outgrowth endothelial cell
ON	Overnight
PA	Polyacrylamide

PDGF	Platelet-derived growth factor
PEG	Polyethylene glycol
PFA	Paraformaldehyde
PLA	Poly(lactic acid)
PLGA	Poly(lactide-co-glycolide)
PVGLIG	Proline-Valine-Glycine-Leucine-Isoleucine-Glycine
RGD	Arginine-Glycine-Aspartic acid
RPT	Rapid prototyping technique
RT	Room temperature
SDF-1α	Stromal cell-derived factor-1α
SEM	Scanning Electron Microscopy
Sulfo-NHS	N-Hydroxy-sulfosuccinimide
TBS	Tris-buffered saline
TGF-β	Tumor growth factor beta
TIME	Telomerase-immortalized human microvascular endothelial
TME	Tumor microenvironment
VEGF	vascular endothelial growth factor
YIGSR	Tyrosine-Isoleucine-Glycine-Serine-Arginine

- This page was intentionally left blank -

INTRODUCTION

1. General introduction

Breast cancer is a leading cause of cancer death in women worldwide[1]. Despite some improvements in cancer diagnosis and treatment, metastatic disease remains a major obstacle for effective treatment. During metastatic dissemination, cancer cells pass through a series of complex steps including the establishment of tumor-associated vascularization. Recently, studies have suggested that tumor vascularization involves not only angiogenesis (vessel sprouting from pre-existing vessels[2,3]), but also alternative mechanisms such as vasculogenesis (recruitment of endothelial progenitor cells, EPCs from bone marrow[4]). Attempts to mimic tumor-vasculature *in vitro* by means of co-culture with endothelial cells (EC) have shown limited success until now. Also, traditional two-dimensional (2D) cell cultures represent reductionist models, being currently recognized that cells behave more physiologically when cultured three-dimensionally (3D), where key cell-matrix interactions can be partially recreated. Therefore, a current challenge is the development of 3D models to study tumor angiogenesis, by replicating intricate tumor-vasculature crosstalk using tissue engineering tools. Current approaches aim to reduce the complexity associated with *in vivo* models, while incorporating a number of elements of the tumor microenvironment that are considered to be relevant enough to mimic specific tumor and associate cell-cell and cell-matrix interactions (Fig. 1).

In this context, further improvements of 3D culture systems, particularly the development of innovative heterotypic co-culture strategies and easily tunable 3D scaffolds, will be invaluable in accurately representing cancer progression and in testing novel therapeutic strategies within a biologically relevant setting.

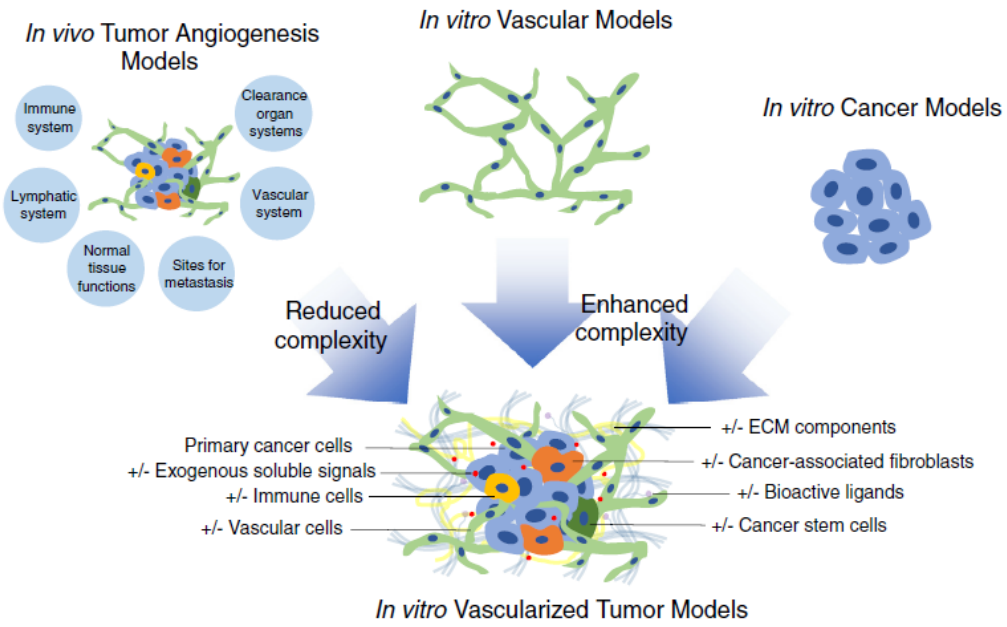

Figure 1 - Overview of current approaches to study tumor angiogenesis. Adapted from Roudsari et al. (2015)[166].

2. Life isn't flat: 2D versus 3D models

The tumor microenvironment (TME) plays an significant role in tumor progression[5–9]. In the case of breast cancer cells, it is involved on malignant growth, loss of epithelial polarity and disorganization of normal cellular architecture in the breast tissue[10–12].

Most cancer models use complex *in vivo* models or 2D monolayer cultures that do not fully mimic the TME. For many years, cancer researchers have relied on 2D monolayer culture studies and small animal models to investigate the complex tumorigenic mechanisms of angiogenesis, invasion and metastasis. Although 2D biology studies have provided extensive fundamental knowledge on cancer cell biology, they lack the structural architecture for proper cell-cell and cell-matrix interactions and are not able to replicate an *in vivo* phenotype[13,14]. Other restriction of 2D models is that cells form a monolayer of polarized cells with only one side of their surface area attached to the substrate, while the remaining surface is exposed to the culture medium. Hence cells are limited to their planar and spread morphology which can lead to the loss of some tissue-specific functions[15,16]. Multiple studies have used small animal models in cancer research, since those are able to better replicate architectural and physiological aspects of cancer biology, as compared to *in vitro* models, but even the best animal models might show to be inadequate in their ability to mimic human host-tumor biology. In fact, major limitations of animal models are related to the considerable differences between cancer

development and progression in humans and animals. For instance, animal models do not recapitulate human-specific features relating to tumors, namely autoimmune conditions, specific patterns of stem cell differentiation and tumoral responses to therapeutic drugs[17]. As such, the paradigm has been changing, and increasing numbers of cancer studies are now being performed using 3D culture models, which somehow fill the gap between the simplicity of 2D *in* vitro models and the complexity of *in vivo* animal models. Such models attempt to recapitulate the tumor biology at multiple levels, which includes specific tumor cell activities and gene signatures, the phenotypic heterogeneity of the population and, importantly, the TME. The later should ideally include matrix-related biochemical and biophysical cues and non-tumoral cell populations.

Table 1 summarizes some of the key differences between 2D and 3D cell culture systems. Several studies have shown that the distinct gene expression profiles of cells cultured in 2D vs. 3D translate into different cellular behavior, namely in terms of morphology[18,19], proliferation[20–22], and drug sensitivity[23,24] , where cells in 3D present a more *in vivo*-like behavior. For example, while malignant (T4-2) and non-malignant (S-1) HMT-3522 breast cells present a similar morphology in 2D culture, they behave very differently when cultured in 3D[18]. S-1 cells grown in a 3D basement membrane organized into polarized, acini-like structures that are analogous in morphology to those found in healthy breast tissue *in vivo*. In contrast to non-malignant cells, the T4-2 cells formed disorganized, abnormal masses that resembled tumor cell aggregates *in vivo*. Both S-1 and T4-2 cells cultured in 3D underwent concomitant down-regulation of epidermal growth factor (EGFR) and β1-integrin when treated with antibody-based inhibitors of these receptors. T4-2 cells underwent growth-arrestment, losing their abnormal structure and reverted to a normal phenotype and morphology analogous to non-malignant cells, whereas S-1 cells underwent apoptosis[18,25]. On the other hand, no down-regulation or growth arrest were noticed when T4-2 cells were cultured 2D and treated with the same antibodies[25]. This study illustrates the different behavior that cells may present under 2D vs. 3D cultures and emphasizes the importance of the microenvironment in dictating cell fate and response.

In addition to cell morphology and organization, differences in cells' proliferative capacity when cultured in 2D as compared to 3D microenvironment have also been reported, being cell type and matrix dependent. A diversity of cell lines showed reduced proliferation rate in 3D cultures compared to those in 2D[21,22,24,26], but other cell lines showed opposite proliferation patterns, growing faster in 3D than in 2D[20,27]. In general, the proliferation rate of cells grown in 3D culture more closely represent the growth of tumors *in vivo* compared to those cultured in an unnatural 2D environment[28].

Apart from differences in the cell morphology and proliferation, cells grown in 3D also exhibit differences in their sensitivity to cancer therapeutics as compared to 2D controls[23,24]. For example, the human breast cancer cell line (MCF7) and its multidrug resistant variant (MDR-MCF7) responded differently to the anti-cancer drug doxorubicin, when cultured as cell aggregates in 3D or as a cell monolayers in 2D[24]. MCF7 cells grown in 3D had reduced sensitivity to doxorubicin as compared to 2D cultures, while MDR-MCF7 cells in 3D showed no response to drug treatment and an increased invasive potential[24]. Tumor spheroids consist of multi-layers of interacting cells, whereas cells in 2D culture conditions form a monolayer of cells that become fully exposed on a surface. Therefore, the higher drug resistance displayed in cell spheroids in 3D, as compared to cells in 2D, could be explained by the diffusive blockade caused by the multiple layers of cells in a tumor spheroid structure[23], which prevent drugs from efficiently reaching cells in the inner core of the spheroid. On the other hand, the distance that anti-cancer drugs need to diffuse through a 2D monolayer is much shorter, as the drug only needs to diffuse through the cell membrane to have an effect. This decreased sensitivity may help explain the mismatched preclinical and clinical findings for cancer therapeutics that have been typically tested using 2D model systems. Overall, the above studies suggest that cells grown in 3D are more analogous to their *in vivo* counterparts and may as such be exploited as more valid *in vitro* platforms for screening anti-cancer drug candidates.

Table 1 - Key differences between two-dimensional and three-dimensional cell culture systems. Adapted from Edmondson *et al.* (2014)[29].

Cellular characteristics	2D	3D	Refs.
Morphology	Sheet-like flat and stretched cells in monolayer	Natural shape in spheroid/aggregate structures	18,19, 30, 31
Proliferation	Often proliferate at a faster rate than *in vivo*	May proliferate at a faster/slower rate compared to 2D-cultured cells depending on cell type and/or type of 3D model system	20,21,22, 24,26,27, 28,32,
Exposure to medium/drugs	Cells in monolayer are equally exposed to nutrients/growth factors/drugs that are dispersed in medium	Nutrients/growth factors drugs may not be able to fully penetrate the spheroid, reaching cells near the core	30,33
Stage of cell cycle	More cells are likely to be in the same stage of cell cycle since they are equally exposed to medium	Spheroids contain proliferating, quiescent, hypoxic and necrotic cells	30,34,35
Gene/protein expression	Often display differential gene and protein expression levels compared to *in vivo* models	Cells often exhibit gene/protein expression profiles more similar to those *in vivo* tissue origins	14,22, 28,36
Drug sensitivity	Cells often succumb to treatment and drugs appear to be very effective	Cells are often more resistant to treatment compared to those in 2D culture system, often being better predictors of *in vivo* drug responses	21,23,24, 28,27

Abbreviations: 2D, two-dimensional; 3D, three-dimensional

Several 3D cell culture models have been used to study breast cancer tumor progression *in vitro,* which take into account the spatial cell organization and extracellular matrix (ECM) and present the ability of re-establish cellular morphologies and phenotypes seen during *in vivo* tumor development[37–42]. Marked advances have been made in the development of 3D tumor models so far, namely in terms of reliably replicating the TME. Regarding the composition of the 3D scaffolds that are used to build systems, they can be constituted by both natural and synthetic materials,[34] as described in table 2. Protein-based hydrogel-based natural materials, such as collagen and Matrigel, are the most commonly used in cancer research. These ECM-based materials intrinsically provide integrin binding sites that naturally support and promote cell adhesion and cell-matrix crosstalk. Nevertheless, natural materials have several drawbacks such as limited

control over degradability, lack of mechanical stability, batch-to-batch variability. Also, they present a complex and sometimes unknown composition that challenges the reproducibility of the experiments. Therefore, there is a looming trend toward the use synthetic materials, which offer several advantages such as easiness of chemical modifications, and better control over the range of mechanical and/or biochemical properties. Yet, synthetic material lack bioligands and/or other bioactive moieties that are naturally present in natural scaffolds. Although obtained from natural sources, some types of polysaccharides, like alginate, behave in a similar way, as they also do not possess cell-interactive domains and are easily tunable, representing a good compromise between protein-based and synthetic materials. For the design of ECM-like 3D matrices with chemically defined properties, such “bioinert” hydrogels actually represent a very interesting set of materials, as they can act as blank-slates and be specifically decorated with selected bioactive cues. This provides a more controlled approach to elicit a desired response in a particular scenario. For example, conjugation of specific adhesion peptides (e.g. Arginine-Glycine-Aspartic acid (RGD)[43] and Tyrosine-Isoleucine-Glycine-Serine-Arginine (YIGSR)) gives an opportunity to adequately control cell adhesion[15]. Degradability of synthetic materials can be user-controlled and manipulated to achieve stability over desired periods of time. This can be done using different strategies. One example is the incorporation of specific matrix metalloproteinase (MMP)-sensitive sites (e.g. Proline-Valine-Glycine-Leucine-Isoleucine-Glycine, PVGLIG)[44] or specific chemical moieties[45]. Moreover, both natural and synthetic scaffolds can be used to concomitantly deliver growth factors to direct the cell fate[46]. A more detailed description on the properties of these different hydrogels and their application in the construction of 3D models will be presented in section 3.2.

Table 2 - Classes of materials used in 3D cell culture: natural (protein or polysaccharide-based) and synthetic. Advantages and disadvantages of the use of different materials are present in this table. Adapted from Gill *et al.* (2014)[6].

	Naturally derived matrices	Synthetic matrices
Examples for 3D culture	Collagen and Matrigel (protein-based), Alginate and Chitosan (polysaccharide- based) Permit 3D culture in physiological conditions with high viability	PA (toxic to 3D culture), PLA, PLG and PLGA (require processing steps) and PEG (compatible with 3D culture)
Bioactivity	Baseline bioactivity with ample ligands for cell adhesion and signaling; difficult to isolate specific bioactive factor for experimental study	Requires passive protein absorption (PLA, PLG and PLGA) or extra engineering (PEG); greater control over bioactivity with less experimental confounding
Mechanical properties	Tunable via additional crosslinking; generally alters ligand density; limited to low-range elasticities	Tunable with minimal/no bioactivity change; broad range of physiological elasticities
Matrix degradation	Cell-mediated matrix remodeling; difficult to control	Predictable degradation of synthetic material; requires modification for cell-mediated degradation
Growth factor contamination	Difficult to completely remove	None with synthetics

Abbreviations: PA, polyacrylamide; PLA, poly(lactic acid); PLG, poly(lactic-co-glycolic acid); PEG, poly(ethylene glycol).

3. Tumor vascularization

The tumor vasculature is essential for tumor growth and progression. In the early stages of tumor development, the tumor small mass is avascular, and the surrounding vasculature supplies the growing cells with oxygen and nutrients. Tumors beyond 1-2 mm^3 require contact with blood vessels to reach sufficient level of oxygen and nutrients into the tumor bulk, since cells cannot survive 200 µm away from a vascular source[47,48]. The environmental stress in the tumor core, such as hypoxia and glucose deprivation and accumulation of metabolic wastes and carbon dioxide may induce an angiogenic switch. This is frequently characterized by the secretion of pro-angiogenic growth factors, such as vascular endothelial growth factor (VEGF), fibroblast growth factor (FGF), and platelet-derived growth factor (PDGF), that act on endothelial cells from nearby vessels leading to their migration and sprouting around the tumor mass[49,50]. The new blood

vessel within the tumor can then provide nutritional supply and also a route for cancer cells to enter in the circulatory system and metastasize to distant tissues/organs - the process of intravasation, the leading cause of cancer-related death[51].

As already discussed, cancer research can greatly benefit from the development of sophisticated 3D models to mimic the complexity of the TME, since 2D cultures cannot replicate cell-cell and cell-ECM interactions in a physiologically relevant manner.

Researchers interested in tumor angiogenesis should integrate knowledge obtained from both tumor and vascular models to develop new *in vitro* models of vascularized tumor. Notably, although tissue engineered tools have been widely used in both angiogenesis and cancer research, conjugational 3D models for simultaneously study tumor angiogenesis and cancer-EC interactions are still scarce. One important aspect is the selection of the scaffold(s), which can be both of natural and synthetic origin, and may have the ability to direct both cancer and EC morphogenesis/function *in vitro*[52–55].

3.1. Engineering 3D *in vitro* vascular scaffolds

Engineered tissues of relevant sizes that exceed the diffusion limit (1-2 mm), require a vascular network capable of supplying oxygen, nutrients and, signaling molecules, while removing metabolic waste. Insufficient blood vessels cause a decrease of cell viability and function as well as tissue formation and ischemia, leading to the failure of the engineered tissue[56]. For this reason, the ability to promote the growth and development of vessels in cellularized 3D constructs has become a major goal in tissue engineering.

The use of porous biomaterials is especially important for promoting vascular invasion because pore structures alone (without biochemical cues) can support/guide cellular infiltration and vascular ingrowth[57–60]. This approach has been widely applied in vascular tissue engineering, and is generally based on the use ECs mono- and/or co-cultures[61–64].

Depending on the type of materials used and/or the type of porous structure needed, porous 3D scaffolds can be fabricated with different conventional techniques[65–67], such as freeze-drying with or without particulate leaching, gas foaming, and phase separation, among others. They can also be fabricated using more advanced techniques such as rapid prototyping techniques (RPTs). RPTs uses computer-aided design (CAD) modelling, allowing the fabrication of scaffolds with complex architecture, a precise control over internal architecture and design repeatability, not possible using conventional techniques[68–71]. By finding tuning scaffolds architecture at both micro and macro levels, RPTs may also allow the fabrication of scaffolds with improved mechanical properties[72,73]. Yet one important limitation is the smaller type of biomaterials that can be

processed by rapid prototyping compared to the conventional techniques[74]. Electrospinning and modular assembly methods are also used to fabricate scaffolds for tissue engineering applications[62,75–77]. Table 2 describes some of the most commonly used scaffold processing techniques. Before selecting the most adequate we should take into account the potential and disadvantages of each one to match the needs of each specific application. Tight control over scaffolds architecture is important for 3D tissue formation, specially pore size and interconnectivity, because it is determinant for cell migration and growth, while it also facilitates the diffusion of nutrients and oxygen essential for maintaining for cell viability[78,79]. These features also play an important role in scaffold vascularization, since an appropriate internal structure is required to provide pathways for new blood vessels ingrowth[80–86].

Apart from the structural and mechanical properties of the scaffold, attention should also be paid to its biochemical properties. As already discussed, the properties of scaffolds may also be improved by biofunctionalization with relevant moieties. These may include, for instance, incorporation of cell adhesive peptides and/or of specific MMP-sites, which may enhance different cellular activities such as adhesion, migration, proliferation or differentiation.

The development of 3D *in vitro* cultures of human ECs enabled further research on EC morphogenesis under more physiological relevant conditions. These platforms in conjunction with 3D cancer models could potentially open new avenues to understand the complex mechanisms regulating tumor angiogenesis and for the development of advanced drug screening applications.

Table 3 - Most commonly used techniques for scaffolds fabrication[57,87–91].

	Fabrication techniques	Description	Advantages	Disadvantages
Conventional techniques	**Particulate leaching**	The porogen or salt crystals (e.g. sodium chloride) with a specific size are transferred into a mold. A polymer solution is then cast into the salt-filled mold. After solvent evaporation by freeze-drying or air-drying, the salt crystals within the polymer matrix are leached away using water, forming the scaffold pores. The pore size can be controlled by the size of the salt crystals and the porosity by the salt/polymer ratio.	Simple and user friendly and no special equipment needed. Control over porosity and pore geometry, highly porous structures, crystallinity can be tailored, large range of pore sizes	Poor control over the orientation and the degree of pore interconnectivity, limited to the fabrication of thin membranes, limited mechanical property, residual solvents and porogens
	Gas foaming	High-pressure carbon dioxide gas is used to saturate the polymer. The amount of gas dissolved in the polymer solution determines the porosity and pore structure of the scaffold. When the CO_2 pressure is reduced back to atmospheric level the gas solubility in polymer decreases resulting in pore nucleation. Incorporation of particulate leaching on gas foaming process often results in formation of open pores in prepared scaffolds.	No use of organic solvents and high temperature, control over porosity and pore size, suitable for the incorporation of heat sensitive biological agents inside the scaffold	Inadequate pore interconnectivity, limited pore sizes, formation of a nonporous surface
	Phase separation	A homogeneous multicomponent system, under certain conditions, becomes thermodynamically unstable and tends to separate into more than one phase in order to lower the system free energy. A polymer solution separates into two phases, a polymer-rich phase and a polymer-lean phase. After the solvent is removed, the polymer-rich phase solidifies. Phase-separation techniques have been used to fabricate porous membranes for filtration and separation.	Easily combine with other fabrication technology, allows incorporation of bioactive agents, highly porous structures	Difficult to control precisely scaffold morphology, problems with residual solvent, limited range of pore sizes

	Freeze-drying	This technique is based on the sublimation principle, in which a solution is frozen and then the solvent is removed by freeze-drying under high vacuum.	Leaching steps are not required, high temperature is not applied	Long processing time, small pore size
Nano-scale techniques	**Electrospinning**	A polymer solution or melt is forced through a capillary, forming a drop of polymer solution at the tip. A high voltage is applied between the tip and a grounded collection target. When the electric field strength overcomes the surface tension of the droplet, a polymer solution or melt jet is initiated and accelerated towards the collection target. Finally, the ejected polymer solution and melt repel each other and the solvent evaporates to form fibers as the jet travels to the collector.	Process is simple and versatile, easily scaled-up for mass production, high aspect ratio, surface area, permeability, porosity, and tunable mechanical reliability, suitable for the surface modification of bioactive agents.	Limited mechanical property, pore size decreases with fiber thickness, inability to fabricate complex 3D structures, involvement of toxic organic solvents.
	Self-assembly	Autonomous organization of components into patterns or structures without human intervention. Such self-assembly of biological molecules can be induced by noncovalent bonds or weak covalent interactions, including electrostatic, van der Waals, hydrophobic interactions, ionic, hydrogen, and coordination bonds.	The level of porosity, pore size and the diameter of the fibers are well-controlled; tune cell behavior, since nanofibers can be chemically modified with bioactive moieties. Avoids use of organic solvents.	Designing process is complex, expensive materials required, limited scaffold size.
RPTs	**3D Printing**	The 3D printer constructs the 3D model by first spreading a layer of fresh powder over a building platform. An ‘inkjet’ print head prints or deposits the binder solution onto the powder bed. After the 2D layer profile is printed, a fresh layer of powder is laid down. The printing cycle continues and the layers merge together when fresh binder is deposited until the whole part is completed. After the binder has	Control over pore size and interconnectivity over conventional/nanoscale approaches. The layer-by-layer process allow fabrication of complex and anatomically-shaped structures.	Expensive machinery, resolution limitations at lower pore sizes.

		dried in the powder bed, the finished component is retrieved, and unbound powder removed.		
	Selective laser sintering	The selective laser sintering technique uses a CO2 laser beam to sinter thin layers of powdered polymeric materials, forming solid 3D objects. A laser is then scanned over the powder bed, which heats the powder locally and sinter-bonds the adjacent particles to form a single layer of the part. The non-sintered particles act as a support for any hollow section, overhangs or undercuts in the part. After the formation of the first layer, the next layer of powder is spread over the first layer followed by laser scanning.	Accurate control over pore size and interconnectivity. The layer-by-layer process allow fabrication of complex and anatomically-shaped structures.	Expensive machinery, resolution limitations at lower pore sizes; Polymers must be compatible with high operating temperature.
	Stereolithography	This technique is based on the use of an ultraviolet (UV) laser that is vector scanned over the top of a surface of a photopolymerizable liquid polymer material. UV laser scans create 2D patterns and then the desired 3D structure is produced by stacking the solidified 2D patterns together.	Accurate control over pore size and interconnectivity. The layer-by-layer process allow fabrication of complex and anatomically-shaped structures.	Expensive machinery, Polymers compatible with UV curing is required.
	Fused deposition modeling	The technique produces a tissue scaffold by the melt extrusion method that is making use of a layer-by-layer thermoplastic polymer.	Accurate control over pore size and interconnectivity. The layer-by-layer process allow fabrication of complex and anatomically-shaped structures with good resolution.	Limited to thermoplastics, since the technique uses polymer melts. Low pore sizes difficult to achieve while maintaining high porosity.

3.2. Engineering a 3D *in vitro* vascularized tumor model

3.2.1. Natural hydrogels

Most of the 3D approaches for tumor angiogenesis engineering are focused on using natural-based scaffolds, since they carry a variety of intrinsic signals important for cancer morphogenesis[22,92], EC capillary morphogenesis[93,94], and sprouting[95,96]. This includes collagen, Matrigel and fibrin. One of the first tumor angiogenesis models was introduced by Janvier *et al.* in 1997, who developed a sandwich model to study prostate cancer angiogenesis[97]. This model consisted of human umbilical vein endothelial cells (HUVECs) embedded in fibrin gel with a layer of collagen embedded human PC-3 prostate adenocarcinoma cells and human foreskin fibroblasts on top. After 28 days, increased HUVEC tube formation was demonstrated upon tri-culture with both fibroblasts and cancer cells. PC-3 cells cultured alone with ECs led to EC death, indicating that tube formation was fibroblast-dependent. This model provides evidence that fibroblasts play an important role in tumor angiogenesis. The main limitations of this model were mechanical stability caused by uncontrolled hydrogel degradation and shrinking during the experiment.

In another report, Correa de Sampaio and colleagues develop the “minitumor” model for the study of breast tumor angiogenesis[98]. Multicellular spheroids with endothelial cells, fibroblasts and MDA-MB-231 breast cancer cells were assessed for EC sprouting in collagen I hydrogels[98]. Results revealed that MDA-MB-231 cells could stimulate sprout formation in the absence of exogenous angiogenic growth factors and could be inhibited by a broad-spectrum inhibitor of metalloproteinases. This approach has been adapted to a bilayered bioengineered tumor, in which telomerase-immortalized human microvascular endothelial (TIME) cells were cultured on top of an acellular collagen I hydrogel, under which MDA-MB-231 or MCF7 cells were cultured in a separate collagen I hydrogel (Fig. 2)[99]. This model showed that the paracrine signaling between TIME and breast cancer cells led to augmented angiogenic activity in the absence of exogenous pro-angiogenic growth factors. ECs invaded the collagen layer and assembled into capillary-like tubule network with lumen formation and anastomosing branches in the presence of MDA-MB-231 cells but not MCF7 cells. This result was expected, as MDA-MB-231 cells present a more invasive phenotype than the less aggressive MCF7 breast cancer cell.

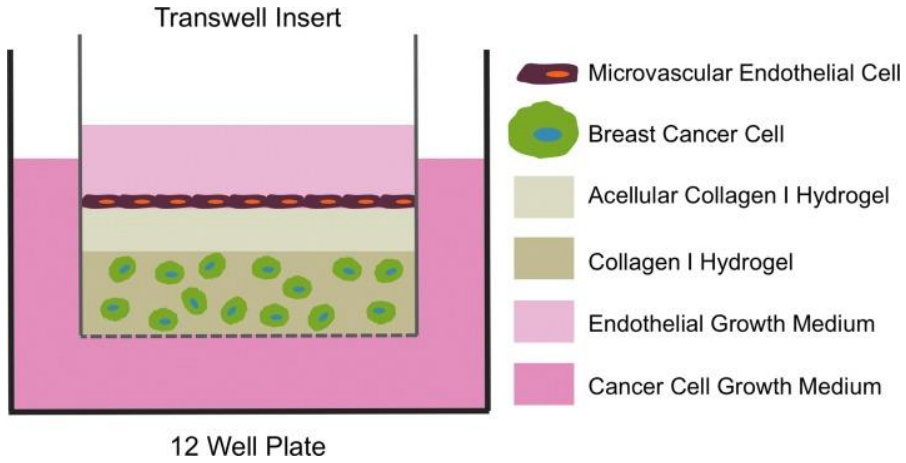

Figure 2 - Schematic illustration of the bilayered bioengineered tumor model cultured in a transwell insert developed by Rylander and colleagues. Breast cancer cells were cultured in the bulk collagen I hydrogel, and microvascular endothelial cells were cultured on the surface of an acellular layer of collagen I hydrogel that separated the two cell types. Adapted from Szot *et al.* (2013)[99].

Besides collagen, Matrigel, a basement membrane extracted from Englebreth-Holm-Swarm (EHS) tumor, has also been widely used in cancer and angiogenesis studies. For example, in Matrigel-based 3D cultures, Bissell and colleagues recapitulate *in vivo* characteristics of breast tumors using human breast cancer cells in[100,101]; while Mukai and colleagues showed the formation of vessel-like structures by umbilical cord blood EPCs and HUVECs. The inherent presence of growth factors and ECM proteins in Matrigel promoted epithelial morphogenesis allowed EC to migrate and organize into capillary-like networks, respectively[102]. Due to its potential, Matrigel has also been used as a model for tumor angiogenesis. Shekhar *et al.* explored the co-culture of human ECs, breast fibroblasts and MCF10A breast epithelial cells on Matrigel coated chamber slides[103,104]. After 3 weeks, conditioned morphogenesis of breast epithelial cells led to a more invasive phenotype. This model cannot fully mimic the TME due to its nearly 2D design (gel “on-top”), but it showed the effects of endothelial and epithelial factors in tumor angiogenesis and breast cancer morphogenesis. The importance of stromal involvement in angiogenesis was also studied in ovarian cancer by developing a multicellular model that used three of the primary cell types involved in tumor angiogenesis. This consisted on a co-culture of human SKOV-3 ovarian carcinoma cell clusters with human microvascular ECs (HMVECs), 10T1/2 cells and myofibroblasts, which was used to explore cell-cell interactions, namely between fibroblasts and tumor cells[105]. A thick layer of Matrigel was created in a well plate and, after polymerization, a plug of Matrigel with approximately 1 mm was removed and the resulting space was filled with SKOV-3 cells embedded in collagen type I. ECs and myofibroblasts were

suspended in culture medium and added to each well, and with time, cells formed tubular structures and migrated towards the tumor cell cluster, eventually invading it. These results acknowledge the importance of myofibroblasts and ECs interaction during tumor angiogenesis.

3.2.2. Synthetic hydrogels

Synthetic materials have been increasingly used to overcome the limitations of the natural materials. Werner's group developed a semi-synthetic starPEG-heparin hydrogel, composed of star-shaped poly(ethylene glycol) (PEG) and glycosaminoglycan heparin, crosslinked via cytocompatible Michael addition chemistry[106]. This hydrogel is able to bind and store growth factors and Stromal cell-derived factor-1α (SDF-1α, a potent chemoattractant known to act on EPCs) simulating this way the EC migration, proliferation and angiogenesis within the hydrogel[45,107,108]. The same group used this hydrogel to develop a 3D culture models to study liver,[109] breast and prostate cancer tumor angiogenesis[110]. The first one was developed by incorporating 7-day old human hepatocarcinoma (HepG2) cells spheroids together with the EC suspension in a fresh hydrogel. This model provides the opportunity to asses tumor-EC interactions in a 3D matrix where ECs can form tumor-invading sprouts. For the study of breast and prostate tumor angiogenesis, they encapsulated breast or prostate epithelial carcinoma cells (MCF-7, MDA-MB-231 or LNCaP, PC3) with HUVECs and mesenchymal stromal cells in a 3D tri-culture and assessed differences in tumor growth for cells in Matrigel and starPEG-heparin hydrogel. The responsiveness of tumor angiogenesis model to chemotherapeutic drugs was also compared between 2D and 3D cultures. 3D cultured breast and prostate epithelial cells were less sensitive to chemotherapy when compared with 2D cultures. Comparing both hydrogels, tumor angiogenesis models grown in the startPEG-heparin displayed a more ordered development of tumor angiogenesis and vascular recruitment, with clearly defined tumors proliferating while in connection with HUVECs. They also showed that, although the morphology of the tumor spheres was different between both hydrogels, the phenotype of the cultures remained the same. This work highlights the importance of using different culture techniques to study cancer cells behavior, including 2D versus 3D and natural versus synthetic materials.

A recent approach based on gelatin methacrylate (GelMA) hydrogel microwells to assess the interactions between human glioma (U87) spheroids and HUVECs[111,112]. U87 tumor cells were cultured in PEG hydrogel-based concave microwells for 14 days. Then the U87 glioblastoma spheroids were transferred into GelMA concave microwells and

HUVECs were carefully seeded on the outside (Fig. 3). The presence of U87 spheroids induced HUVEC migration through the hydrogel walls and promoted HUVEC growth and tubular-like structure formation. Although derived from a natural protein-based material (hydrolyzed collagen) GelMA hydrogels are chemically synthesized in a well-controlled manner and are thus often considered as “synthetic” or “artificial”, as they are not natural-occurring. Yet, they intrinsically contain RGD-binding sequences that allow cells attachment and migration into the microwells. Nguyen and colleagues were the first ones to highlight the use of GelMA as a hydrogel for tumor angiogenesis studies.

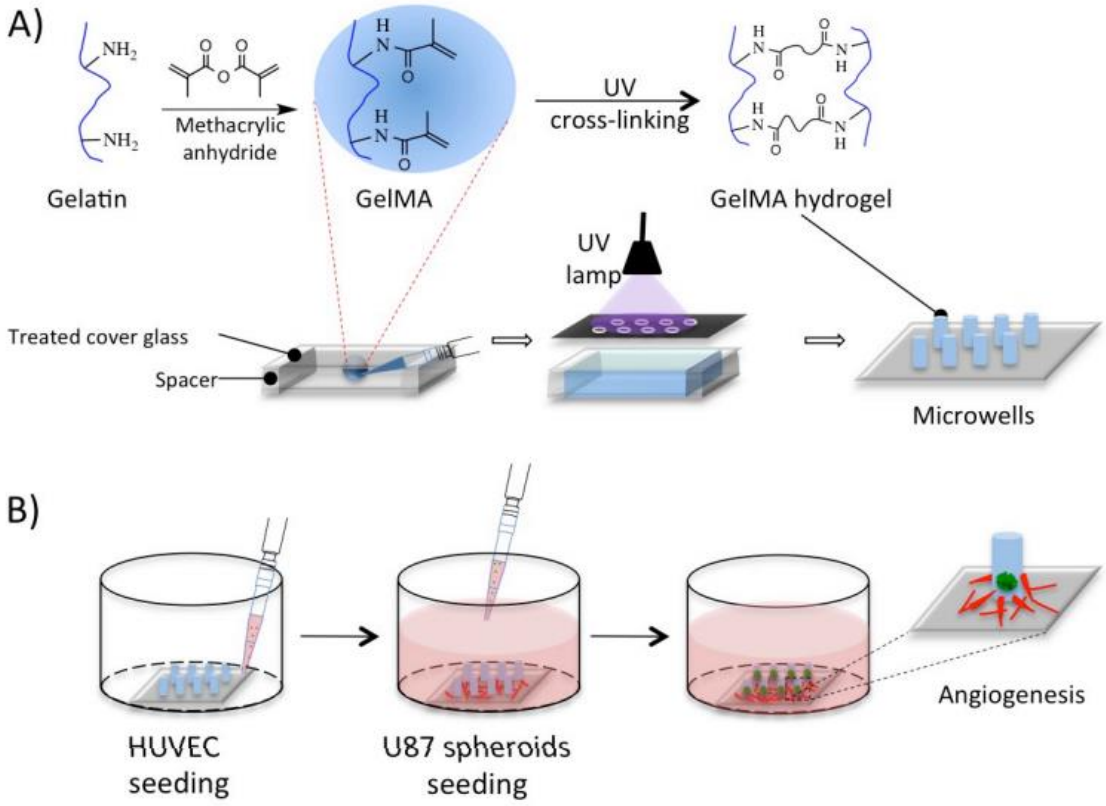

Figure 3 - Schematic representation of in vitro angiogenesis model using 3D GelMA microwell, developed by Nguyen *et al.* (A) Fabrication of GelMA microwells from photolithography process. Gelatin is modified by the direct reaction with methacrylic anhydride (MA) in PBS in order to form GelMA. Then, GelMA hydrogel was photocross-linked under UV light. The structure of GelMA microwells was determined by the design of photomask. (B) The angiogenic process - HUVEC cells were seeded carefully outside the microwells and cultured in EBM-2 medium. Then, glioblastoma cancer spheroids were seeded into the microwells. Cells were co-cultured to allow the formation of angiogenesis. Adapted from Nguyen *et al*. (2016)[111,112].

Roudsari *et al.* used cell-adhesive, proteolytically-degradable PEG-based hydrogels as highly controlled 3D substrates for lung tumor angiogenesis[113,114]. This 3D tumor angiogenesis model comprised two PEG-based hydrogel layers, each with different cell composition: the top layer with a vascular cell co-culture (ECs and pericytes) and the other with lung adenocarcinoma cells (Fig. 4). Three types of lung adenocarcinoma cells, with different metastatic potential were used (highly metastatic murine 344SQ cells, non-metastatic murine 393P cells and metastatic human A594 cells). The three cell types were able to develop into spheroids and promoted vascular invasion into the cancer cell layer. Comparing the three cell types, interaction between vessels invading the cancer layer and the cancer cell structures was higher for the highly metastatic 344SQ. 344SQ secreted more VEGF and FGFb than A594 and 393P cells, indicating that 344SQ have higher capacity to stimulate more angiogenesis than the other two cell types. Moreover, it was also observed that 344SQ spheroids at the hydrogels interface were larger and disorganized, suggestive of an invasive phenotype. This trend was not evident for A549 or 393P cell clusters. These semi-synthetic and synthetic hydrogels, unlike natural materials, present controlled composition with reduced batch-to-batch variation and can be fabricated with a wider range of mechanical properties, thus offering several possibilities to mimic the TME[37]. The use of these materials seems promising in future tumor angiogenesis research.

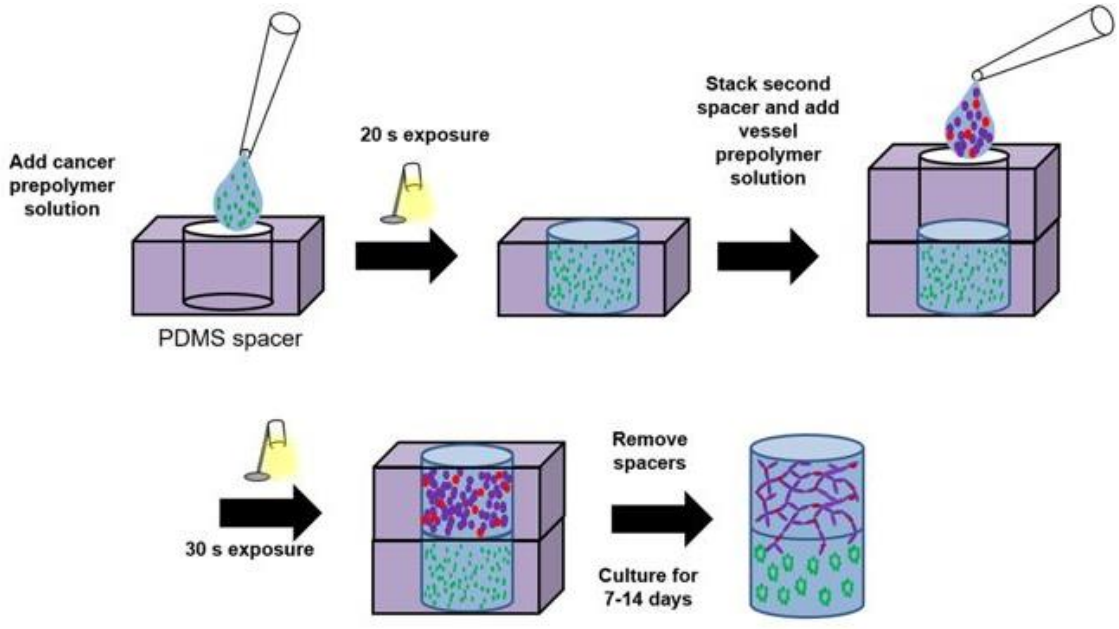

Figure 4 - Tumor angiogenesis model construction. Cancer prepolymer solution is added to a PDMS spacer well, followed by a 20 s photopolymerization. A second PDMS spacer well is stacked on top of the initial spacer well, followed by a 30 s photopolymerization and removal of PDMS spacer wells. Adapted from Roudsari *et al* (2016)[114].

3.3. Other strategies for 3D *in vitro* vascularization

Nowadays, increasingly more complex systems are being created. Different materials and processing technologies are under testing aiming at developing new methods for drug screening, diagnosis or personalized treatments related to cancer. In Table 4 some alternative strategies are described, where less common approaches have been used. These involve, for example, decellularized tissue matrices, microfluidic devices and high throughput screening platforms. All of these engineered–based systems have been developed to improve the complexity of standard models, but most of them still require further optimizations to truly fill the gap between *in vitro* and *in vivo* models.

Table 4 - Engineered-based systems for tumor angiogenesis studies.

Model	Description	Reference
Human arterial ring assay is an innovative system for the study of tumor angiogenesis.	Prostate cancer cell (LNCaP) spheroids are embedded in Matrigel in the proximity of the aortic rings (arterial explants from human umbilical cords), without the addition of exogenous angiogenic growth factors.	Seano *et al.* (2013)[115]
Decellularized scaffolds for the study of malignant peripheral nerve sheath tumors.	This model is based on a decellularized porcine jejunal segment that was seeded with primary fibroblasts and S462 tumor cells on one side and with microvascular ECs seeded on the other side. The cell-seeded scaffold was then placed inside a flow bioreactor system, exposing the cells to shear stress.	Moll *et al.* (2013)[116]
Microfluidic approach to study the effects of shear forces and blood flow on breast tumor angiogenesis.	The model consists of a single central microchannel seeded with ECs (TIME) surrounded by collagen containing MDA-MB-231 breast cancer cells; Resembling a single neovessel through which tumor-relevant hydrodynamic stresses are introduced.	Buchanan *et al.* (2014)[117]
Dynamic 3D culture method for Glioblastoma research.	Use of Rotary Cell Culture System (RCCS) to derive large macroscopic glioma aggregates; Evaluate the capacity of high-grade glial tumors of assuming an endothelial phenotype and genotype.	Smith *et al*. (2015)[118]
3D bioprinting approach for the study of glioangiogenesis.	The 3D bioprinted glioma stem cell model was established based on modified porous gelatin/alginate/fibrinogen hydrogel that mimics the ECM.	Dai *et al.* (2016)[119]

4. Aim of the thesis

Attempts to mimic tumor-vasculature in vitro by means of co-culture cancer cells with EC have shown limited success until now. Also, traditional 2D cell cultures represent reductionist models, being currently recognized that cells behave more physiologically when cultured in 3D, where key cell-matrix interactions can be partially recreated. The dynamic interactions between tumor cells and their 3D microenvironment play a critical role in cancer initiation, growth, invasion and metastasis

The primary aim of this Master Thesis was to develop a sophisticated 3D tri-culture platform that comprises two different compartments: a hydrogel-embedded breast epithelial cells and a vascularized porous scaffold.

In the first part of this thesis a 3D vascular-like compartment was established. For this purpose, an alginate-based 3D porous scaffolds were developed and characterized. Then this construct was used to generate 3D vascularized structures by co-culturing ECs and fibroblasts, in which suitable culture conditions were identified (e.g. cell seeding strategy, cell density). The second objective consisted on the establishment of a 3D tumoral-like compartment by embedding human mammary epithelial cells within alginate-RGD matrices. In this regard, three different epithelial cell lines with different tumorigenic capacities were used. Finally, a sophisticated 3D tri-culture platform combining hydrogel-embedded breast epithelial cells with a vascularized porous scaffold was created. Insights gained with the development of this 3D platform may lead to the identification of new therapeutic targets and more effective treatment options for breast cancer.

- This page was intentionally left blank -

MATERIALS AND METHODS

1. Cell maintenance

Outgrowth endothelial cells (OECs) were isolated from umbilical cord blood, as previously described by Torres and colleagues[120]. These cells were cultured in endothelial cell growth medium, EGM-2MV (Lonza). The medium was prepared by supplementing EBM-2 with ascorbic acid, hydrocortisone, 5 ng/mL epidermal growth factor (hEGF), 0.5 ng/mL vascular endothelial growth factor (VEGF), 10 ng/mL basic fibroblast growth factor-b (hFGF-b), 20 ng/mL insulin growth factor-1 (IGF-1) and 5 % v/v fetal bovine serum (FBS).

Human mammary fibroblasts (hMF) were maintained in fibroblast culture medium (ScienceCell) composed of 2% v/v of FBS, 1% v/v of Fibroblast Growth Supplement (FGS) and 1% v/v of penicilin/streptomycin (Pen/Strep). The cells were maintained in a 5% v/v CO_2 humidified incubator at 37°C in order to maintain physiological conditions.

Normal-like breast epithelial cell line, MCF10A cells were maintained in Dulbecco's Modified Eagle Medium/Nutrient Mixture F-12 with Glutamax (DMEM/F12 GlutaMAX™, Gibco) supplemented with 5% v/v Horse Serum (ThermoFisher Scientific), 20 ng/mL EGF (Sigma), 66.6 ng/mL Hydrocortisone (1 mg/mL, Sigma), 100 ng/mL Cholera Toxin (Sigma), 0.01 mg/mL Insulin solution human (Sigma) and 1% v/v Pen/Strep.

Luminal non-metastatic breast cancer cell line, MCF7 cells were maintained in phenol red-free DMEM/F12 with Glutamax (Gibco) supplemented with 10% v/v FBS (Biowest) and 1% v/v Pen/Strep.

Basal aggressive metastatic breast cancer cell line, MDA-MB-231 was maintained in DMEM with Glutamax (Gibco) supplemented with 10% v/v FBS and 1% v/v Pen/Strep.

All the cells were kept at 37°C in a 5% v/v CO_2 humidified atmosphere in order to maintain physiological conditions.

2. Synthesis of RGD-grafted alginate

Ultrapure sodium alginate (PRONOVA UP LVG, Novamatrix, FMC Biopolymers) with a molecular weight of 150 kDa and a high content of guluronic acid (≈70%) was covalently grafted with cell-adhesion peptides (glycine)4-arginine-glycine-aspartic acid-serine-proline (hereafter abbreviated as RGD, GenScript) using aqueous carbodiimide chemistry as previously described[121,122]. Briefly, alginate at 1 wt.% in 2-(N-morpholino) ethanesulfonic acid (MES buffer (Sigma): pH 6.5, 0.1 M MES, 0.3 M sodium chloride (NaCl, Sigma)) was prepared and stirred overnight (ON) at room temperature (RT). N-Hydroxy-sulfosuccinimide (Sulfo-NHS, Pierce) and 1-ethyl- (dimethylaminopropyl)-

carbodiimide (EDC, Sigma, 27.4 mg per g of alginate) were sequentially added at a molar ratio of 1:2, followed by 100 mg of RGD peptide per g of alginate. Control samples were also prepared without the addition of peptide (HMW_0). After stirring for 20 h, at RT, the reaction was quenched with hydroxylamine (NH_2OH, Sigma) and the solution was dialyzed against deionized water for 3 days (MWCO 3500, Spectrum Labs). After purification with activated charcoal (0.5 g per g of alginate, Sigma), RGD-alginate was lyophilized and stored at -20ºC until further use. The amount of grafted RGD was quantified using the BCA Protein Assay (Pierce). Briefly, samples (1 wt.% RGD-grafted alginate) were incubated in BCA reagent for 60 min at 37°C in the dark and the absorbance was read at 562 nm in a microplate reader (Biotek Synergy MX). A set of RGD solutions (0 to 1 mg/ml in 1 wt.% HMW_0) was used as standards to produce a calibration curve. Typically, the reaction yield was determined by the BCA total protein assay, as described in[44,122].

3. Preparation and characterization of RGD-alginate scaffolds

Scaffolds were prepared by internal gelation, using calcium as ionic crosslinker as described previously by[44,122,123]. For that purpose, RGD-alginate precursor solutions were sterile-filtered (0.22 µm) and homogeneously mixed with a suspension of calcium carbonate ($CaCO_3$, Fluka) in water at a $CaCO_3$/COOH molar ratio of 0.288, and the gelling process was triggered through the addition of fresh glucone solution of delta-lactone (GDL, Sigma) in water at a $CaCO_3$/GDL molar ratio of 0.125. A final RGD-modified alginate concentration of 2 wt.% with 600 µM of RGD was obtained and quickly added in a 96-well plate (250 µL/well), where it gelled. Three-dimensional scaffolds were generated by freeze-drying technique. After the gelation time (≈45 minutes, at RT) the samples were frozen at -20°C, and then lyophilized at 0.008 mBar and a temperature of -80°C. The obtained cylindric scaffolds were then cut into smaller ones (with an average height of 1.5 mm).

The scaffolds were characterized by Scanning Electron Microscopy (SEM) analysis performed on the surfaces and cross-sections, using a High-resolution Scanning Electron Microscope with X-Ray Microanalysis (JEOL JSM 6301F/ Oxford INCA Energy 350) at an accelerating voltage of 15 kV. Samples were coated with Au/Pd thin film, by sputtering for 120 seconds and with a 15 mA current, using the SPI Module Sputter Coater equipment. The average pore diameter was also analyzed by manual measurement of SEM images[57,124], using Fiji Imaging software.

3.1. Alternative strategy to produce porous alginate scaffolds

Alginate scaffolds were also prepared using the particle leaching method, in which sodium chloride (NaCl) was used as porogen to form the porous structures. NaCl particles were broken/fractioned and sieved to a particle size of 150-250 µm. Alginate precursor solutions were homogeneously mixed with a suspension of calcium carbonate in MilliQ water at a $CaCO_3$/COOH molar ratio of 0.288, and the gelling process was triggered through the addition of GDL in MilliQ water at a $CaCO_3$/GDL molar ratio of 0.125. A final alginate concentration of 2 and 4 wt.% was obtained and the particles were subsequently incorporated into the alginate solution, mixed and quickly added in a 96-well plate (250 µL/Well), where it gelled. Both 2 and 4 wt.% alginate were tested with 1.1 and 0.6 mg/mL of NaCl particles. After the gelation time (≈45 minutes, at RT) the sample were frozen at -20°C, and then lyophilized for two days at 0.008 mBar and a temperature of -80°C. The obtained cylindric scaffolds were then cut into smaller ones. The salt particles were then leached out by placing the scaffolds in distilled water for 24h with agitation. The water was changed 3 times. The leached samples were frozen at -20°C, and then freeze-dried again for 24h.

The scaffolds were characterized by Scanning Electron Microscopy (SEM) analysis as previously described.

4. Culture of fibroblast or/and endothelial cells on alginate scaffolds

The RGD-Alginate scaffolds were sterilized by washing them in ethanol 70% for 30 min, followed by rinsing in sterile TBS/$CaCl_2$, 3 times. The scaffolds were then placed in a new 48-well plate and incubated with cell culture medium, at 37°C. The medium was removed 10 min before the seeding to improve cell attachment.

For monocultures hMF and OECs cells were seeded at a density of $25x10^4$ cells/scaffold in a total volume of 30 µL of the respective culture medium. Two different seeding strategies were tested to evaluate which one would allow a better cell distribution throughout the scaffold (Fig. 5). In one strategy, 30 µL of the cell suspension was added to the top of the scaffold. For the other strategy, 15 µL of cell suspension was added at the top and 1 h later the scaffold was turned, and the remaining 15 µL was added on the other side. After allowing cell adhesion for 4h, culture medium was added, and the seeded scaffolds were incubated.

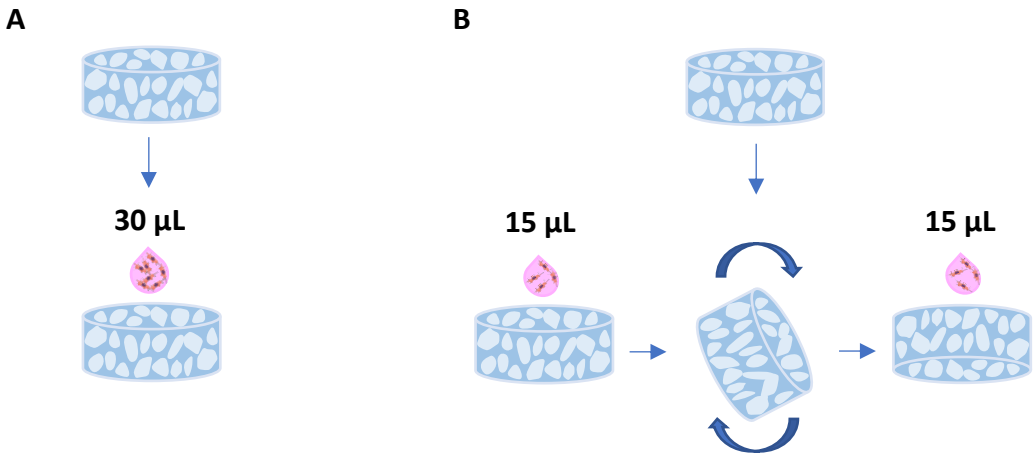

Figure 5 - Experimental procedure for scaffolds colonization. Two strategies were used: (A) 30 µL of the cell suspension was added to the top of the scaffold and (B) 15 µL of cell suspension was added at the top and 1 h later the scaffold was turned upside down, and the remaining 15 µL was added on the other side.

For co-cultures of hMF and OECs two approaches were considered. In the first one, both cell types were seeded simultaneously at a final cell density of $50x10^4$ or $1x10^6$ cells/scaffold in 30 µL of EGM-2MV, with a cell ratio of 1:1 (Fig. 6A and 6B). For the other strategy, a sequential seeding was carried out. First hMF were seeded at $50x10^4$ cells/scaffold, followed by seeding of $50x10^4$ of OECs, at day 4 (D_4) (Fig. 6C) and at day 7 (D_7) (Fig. 6D) after the pre-seeding. After allowing cell adhesion for 4h, EGM-2MV culture medium was added, and the seeded scaffolds were incubated at 37°C in a 5% v/v CO_2 humidified atmosphere.

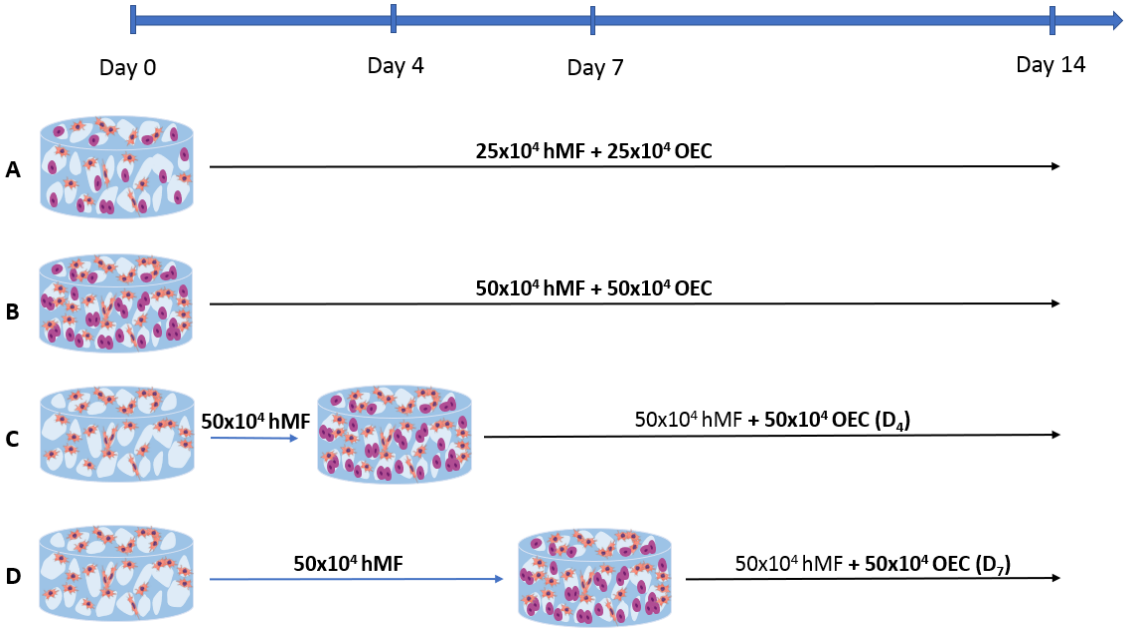

Figure 6 - Experimental design for co-culturing outgrowth endothelial cells (OECs) and human mammary fibroblasts (hMF) in RGD-alginate scaffolds. Simultaneous (A and B) and sequential (C and D) co-culture strategies were studied, with the following cell densities per scaffold: (A) $25x10^4$ hMF + $25x10^4$ OEC, (B) $50x10^4$ hMF + $50x10^4$ OEC; Pre-seeding with $50x10^4$ hMF and (C) after 4 days or (D) 7 days $50x10^4$ OEC were added to the scaffold.

5. 3D culture of epithelial cells in RGD-alginate matrices

In situ forming alginate hydrogel matrices were prepared by internal gelation, using calcium as ionic crosslinker as described previously[44,122,123]. For that purpose, RGD-alginate precursor solutions were sterile-filtered (0.22 µm) and homogeneously mixed with a sterile suspension of $CaCO_3$ in 0.9 wt.% NaCl at a $CaCO_3$/COOH molar ratio of 0.288, and the gelling process was triggered through the addition of a filtered (0.22 µm) fresh GDL in 0.9 wt.% NaCl at a $CaCO_3$/GDL molar ratio of 0.125. A final RGD-modified alginate concentration of 1 wt.% with 200 µM of RGD is obtained by adding the previous solution to the cell suspension (5 x 10^6 cells/mL). Cells were trypsinized, centrifugated (1200 rpm, 5 min) and then the supernatant was removed, and the cells were resuspended in 0.9 wt.% NaCl. Finally, the cell suspension was homogeneously mixed with the RGD-alginate solution and crosslinking agents. The 3D matrices were obtained by quickly applying small drops, of 14 and 20 µL, of the mixture between Teflon plates separated by spacers with a thickness of 500 and 750 µm, respectively (Fig. 7A and 7B). Then the Teflon plates with the 3D matrices were kept in a petri dish, at 37°C in a 5% v/v CO_2 incubator and removed 20 min after triggering the gelling process, which is after adding the GDL[125]. The 3D matrices (Fig. 7C and 7D) were transferred to a 24-well

culture plate and incubated with culture medium at 37°C and after 30 min the medium was renewed.

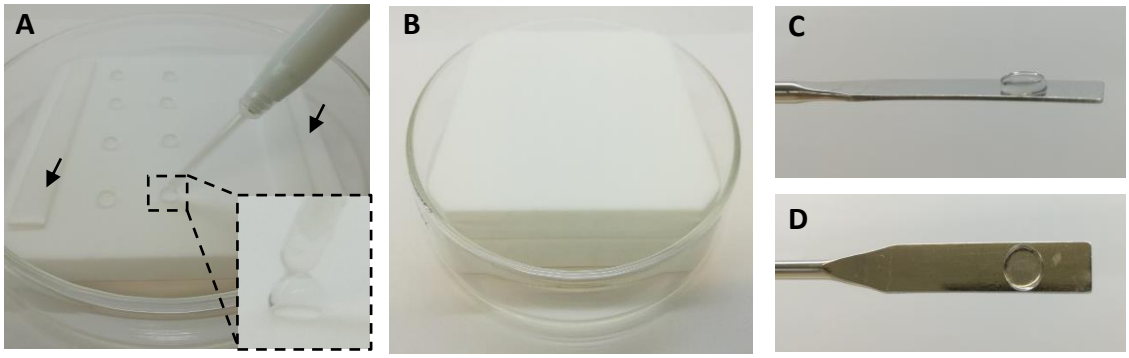

Figure 7 - Experimental procedure for the synthesis of the 3D cell-laden matrices. Small drops of cell-laden alginate were applied on top of a Teflon plate between two spacers (black arrows) (A) and then another Teflon plate was placed on top of those spacers(B). After gelation, 3D matrices were obtained (C and D).

6. Establishment of a heterotypic 3D breast cancer model

3D tri-culture platform that combined a hydrogel-embedded breast epithelial cells with a vascularized porous scaffold was developed. To achieve this, 1 wt.% RGD-alginate with epithelial cells embedded were prepared as described above (Section 5) and added to the RGD-alginate scaffolds previously co-cultured with endothelial cells and fibroblasts for 8 days ($25x10^4$ hMF + $25x10^4$ OEC seeded simultaneously, as described in section 4) (Fig. 8). Briefly, the scaffolds were placed on sterilized filter papers to remove excess culture medium from the pores, in order to facilitate the entrance of the hydrogel within the scaffold (Fig. S1A). Then the scaffolds were placed on top of a Teflon plate and 40 µL of the mixture was applied in small drops on top of each scaffold (Fig. S1B). The Teflon plate with the embedded scaffolds were kept in a petri dish, at 37°C in a 5% v/v CO_2 incubator and removed 20 min after triggering the gelling process (Fig. S1C). Finally, the 3D tri-cultures were transferred to a 24-well culture plate and incubated with EGM-2MV at 37°C and after 30 min fresh medium was added (Fig. S1D).

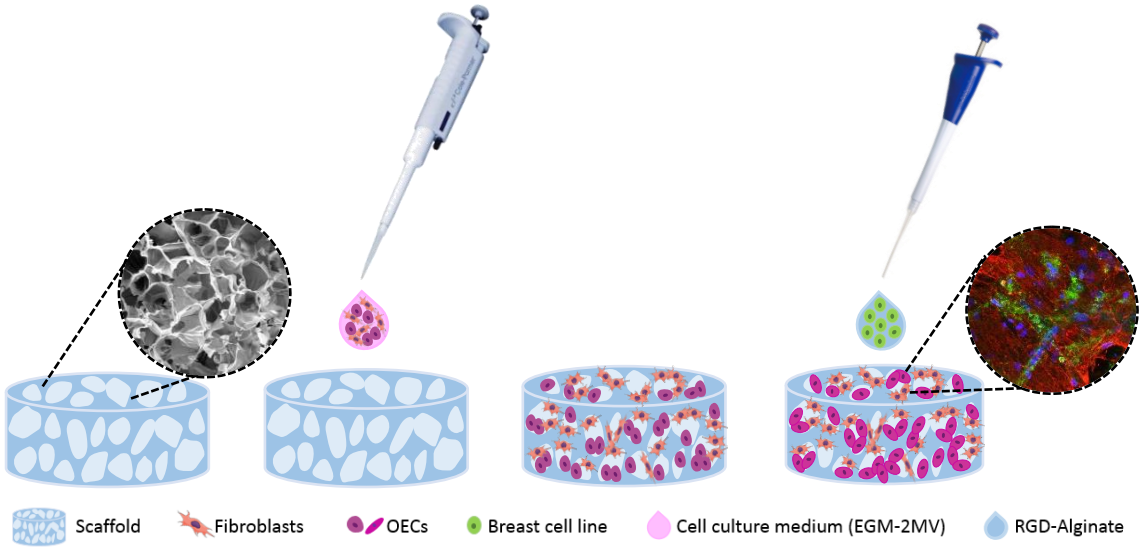

Figure 8 - Schematic representation of the 3D tri-culture platform that combined an epithelial cell-laden hydrogel with a pre-vascularized scaffold.

7. Evaluation of epithelial cells metabolic activity and cell proliferation

The metabolic activity of entrapped cells in alginate matrices was determined through a resazurin-based assay. To this end, hydrogels containing cells (height: 750µm; volume: 20µL; n=4) were incubated with 20% v/v of stock resazurin solution (0.1mg/mL, Sigma) in the respective normal cell culture medium for 2h at 37°C protected from light. Then, 200 µL of supernatant were transferred to a 96-well black plate (Greiner) and fluorescence measurements were performed using a microplate reader (Biotek Synergy MX) with excitation/emission at 530/590nm.

Cell proliferation was assessed by Ki-67 immunostaining. The 3D cultured hydrogels (height: 500 µm; volume: 14 µL) were washed 3 times with TBS-Ca (TBS with 7.5 mM $CaCl_2$), fixed with 4 wt.% paraformaldehyde (PFA, Sigma) in TBS-Ca for 20 minutes and washed again. Then were permeabilized with 0.1% v/v Triton X-100 in TBS-Ca for 5 min, and then incubated for 1 h in 1 wt.% bovine serum albumin (BSA, Sigma) in TBS-Ca to block unspecific binding. Cell-laden hydrogels were then incubated ON at 4°C with rabbit anti-Ki-67 (1:100, Abcam). Finally, samples were washed again and then incubated with goat anti-rabbit secondary antibody Alexa Fluor 488 (Invitrogen, 1:1000, 1 h at RT) and nuclei were counterstained with DAPI.

8. Matrigel-based tube formation assay

In order to evaluate the angiogenic potential of the 3 epithelial cell lines, an angiogenesis assay was performed in Matrigel® (Growth Factor Reduced Basement Membrane Matrix, Corning). The conditioned medium from each cell line was obtained by incubating the cell-laden hydrogels, after 12 days of culture, with low serum medium (phenol red-free DMEM/F12 with Glutamax with 1% v/v FBS and 1% v/v Pen/Strep) for 48h. Medium was collected, centrifuged for 5 min, and the supernatant was storage at -20°C. For the tube formation assay, 150 µL of Matrigel were added to 48-well culture plates and incubated at 37°C in a 5% v/v CO_2 humidified atmosphere for 30 min, to allow the Matrigel to gel. Then, $5x10^4$ of OECs in 500 µL of the respective conditioned medium (CM) were added per well (n=3, for each CM). The low serum medium was used as a negative control (n=3), and OEC growth medium as a positive control (n=3). The volumes of CM used were normalized to the number of viable cells entrapped within the 3D matrices. After the seeding with CM, OECs were maintained at 37°C in a 5% v/v CO_2 humidified atmosphere for 24h and ended this period of time, the cells were stained with Calcein AM (2 µg/mL, Invitrogen), for 45 min at 37°C in the dark, and then washed with the low serum medium. The capillary-like structures were observed using an inverted fluorescence microscope (Axiovert 200M, Zeiss), which were then counted.

9. Analysis of whole-mounted samples by immunostaining

9.1. 3D culture of epithelial cells

Immunocytochemistry was conducted to analyze the expression cell-cell junction markers E-cadherin and β-Catenin on epithelial cell-laden hydrogels (height: 500µm; volume: 14µL) that were collected on day 14 of culture. 3D matrices were washed 3 times with TBS-Ca, fixed with 4 wt.% PFA in TBS-Ca for 20 minutes and washed again. Before the immunostaining, the epithelial cell-laden hydrogels were incubated with 50 mM ammonium chloride (NH_4Cl) in TBS-Ca for 10 minutes, and permeabilized with 0.2% Triton X-100 in TBS-Ca for 5 minutes; both incubations were performed at RT and hydrogels were washed 3 times after each incubation. To block unspecific signal, samples were incubated with 5 wt.% BSA, in TBS-Ca during 1h, and then incubated overnight at 4°C with primary antibodies in 5 wt.% BSA TBS-Ca: rabbit anti-E-cadherin (1:100, Cell Signaling) and mouse anti-β-Catenin (1:50, BD Bioscience). After the immunoreaction, samples were washed 3 times with TBS-Ca and then incubated with secondary antibody Alexa Fluor 488 Goat Anti-Rabbit (Invitrogen, 1:1000) and Alexa Fluor 594 Goat Anti-Mouse (Invitrogen, 1:1000) in TBS-Ca for 1h in the dark. After

washing 4 times with TBS-Ca, the nuclei were counterstained with DAPI. 3D imaging of the samples was accomplished by confocal laser scanning microscopy (CLSM, SP5, Leica), and data analysis was performed using Fiji Imaging software.

9.2. Mono- and Co-cultured scaffolds

Mono- and co-cultured scaffolds were washed with TBS-Ca, fixed with 2% v/v PFA in TBS-Ca (20 min at RT) and washed again. Then, scaffolds were permeabilized with 0.2% v/v Triton X-100 for 10 min and blocked for 1 h with 1.5 wt.% BSA solution in TBS-Ca.
The mono-cultured scaffolds with hMF were incubated ON at 4°C with phalloidin 488 (1:40, Flash Phalloidin Green 488, Biolegend) and rabbit anti-fibronectin (FN, 1:100, Sigma). Afterwards, samples were washed again and then incubated with the secondary antibody, goat anti-rabbit Alexa Fluor 594 (1:1000) for 1h.
The mono-cultured scaffolds of OECs were incubated with rabbit anti-laminin (Lam, 1:50, Sigma) and mouse anti-CD31 (1:100, clone JC70A, DAKO) ON at 4°C. After washing with TBS-Ca, scaffolds were incubated with secondary antibodies Alexa Fluor 488 goat anti-rabbit (1:1000) and Alexa Fluor 594 goat anti-mouse (1:1000) for 1h.
The co-cultured scaffolds were incubated with phalloidin 647 (1:40, Flash Phalloidin Red 647, Biolegend), with mouse anti-CD31 (1:100, clone JC70A, DAKO) combined with rabbit anti-fibronectin (FN, 1:100, Sigma) and other scaffolds were incubated with goat anti-CD31 (1:100, PECAM-1, sc-1506, Santa Cruz) combined with mouse anti-collagen type IV (Col IV, 1:30, M0785, DAKO) ON at 4°C. After washing, scaffolds were incubated for 1 hour at RT with the secondary antibodies Alexa Fluor 594 goat anti-rabbit (1:500, Invitrogen), Alexa Fluor 488 rabbit anti-mouse (1:1000, Invitrogen), Alexa Fluor 488 mouse anti-goat (1:1000, Invitrogen) and Alexa Fluor 594 rabbit anti-mouse (1:500, Invitrogen).
Finally, the scaffolds were washed 4 times with TBS-Ca, the nuclei were counterstained with DAPI. 3D imaging of the samples was accomplished by CLSM (SP5, Leica) and data analysis was performed using Fiji Imaging software.

9.3. 3D Tri-culture constructs

Samples were fixed with 4% v/v PFA, permeabilized and blocked as described in the previous section 9.2. Subsequently, samples were incubated ON at 4°C with phalloidin 647 (1:40, Flash Phalloidin Red 647, Biolegend) and with the following primary antibodies: rabbit anti-fibronectin (FN, 1:100, Sigma); mouse anti-CD31 (1:50, clone JC70A, DAKO) and rabbit anti-collagen type I (Col I, 1:50, Rockland). Afterwards, samples were washed TBS/Ca and then incubated, for 1h at RT, with the secondary

antibodies: Alexa Fluor 594 goat anti-rabbit (for FN and Col I (1:1000), Invitrogen) and Alexa Fluor 488 rabbit anti-mouse (for CD31 (1:1000), Invitrogen) and nuclei were counterstained with DAPI. 3D imaging of the samples was accomplished by CLSM (SP5, Leica) and data analysis was performed using Fiji Imaging software.

10. Paraffin-embedded sections

3D tri-culture constructs were washed 3 times with TBS-Ca, fixed with 4 wt.% PFA in TBS-Ca for 20 min and washed again, and then embedded in paraffin in an automated tissue processor (Microm STP 210). Sample processing was set to graded series of 20 min each, starting by sequential immersion in ethanol (EtOH) solutions of increasing concentrations (70%, 90%, 98% and 100%), followed by immersion in ClearRite and finally immersion in preheated paraffin. Samples were embedded in para paraffin in a modular embedding system (Microm STP 120-1), with a transverse orientation, in order to show all layers. Paraffin blocks were sectioned (6 µm) using a semi-automated microtome (Leica RM2255). Paraffin-embedded sections were mounted on (3-aminopropyl)triethoxysilane (APES) coated glass slides, dried ON at 37°C and then kept at RT until use. All slides were dewaxed in xylene and dehydrated using an ethanol gradient before stained. Safranin-Light Green (SF-LG) staining was used to evaluate the presence of alginate. Images were obtained using an inverted fluorescence microscope (Axiovert 200M, Zeiss) and processed using Fiji Imaging Software.

11. Statistical analyses

Statistical analyses were performed using GraphPad Prism 7.0 software version. Normality of data was tested using D'Agostini-Pearson omnibus and Shapiro-wilk tests. For the analyzes of the metabolic activity, One-way ANOVA test was used. Results for all analysis with 'p' value less than 0.05 were considered to indicate statistically significant differences (* $p<0.05$, ** $p<0.01$ and *** $p<0.0001$).

- This page was intentionally left blank -

RESULTS AND DISCUSSION

1. Vascularized porous scaffolds

1.1. Scaffolds preparation and characterization

The scaffolds were made from a 2 wt.% RGD-modified alginate hydrogel, which was prepared in a 96-well plate, and then frozen at -20°C (Fig. 9A). 3D scaffolds were generated by freeze-drying technique, which is based upon the principle of sublimation of the ice crystals formed upon freezing, resulting in a highly porous scaffold, in which pore structures present the same morphology as the ice crystals[87,126]. It is a simple, rapid, economical and environmentally-friendly method to prepare porous structures, where the amount and size of pores can be tuned by controlling the processing conditions[127,128]. The obtained scaffolds with a cylindric and symmetric configuration (Fig. 9B and 9C) were cut into smaller ones, with an average height of 1.5 mm (Fig. 9D-F). The structure of the scaffolds structure was analyzed by SEM (Fig. 9G).

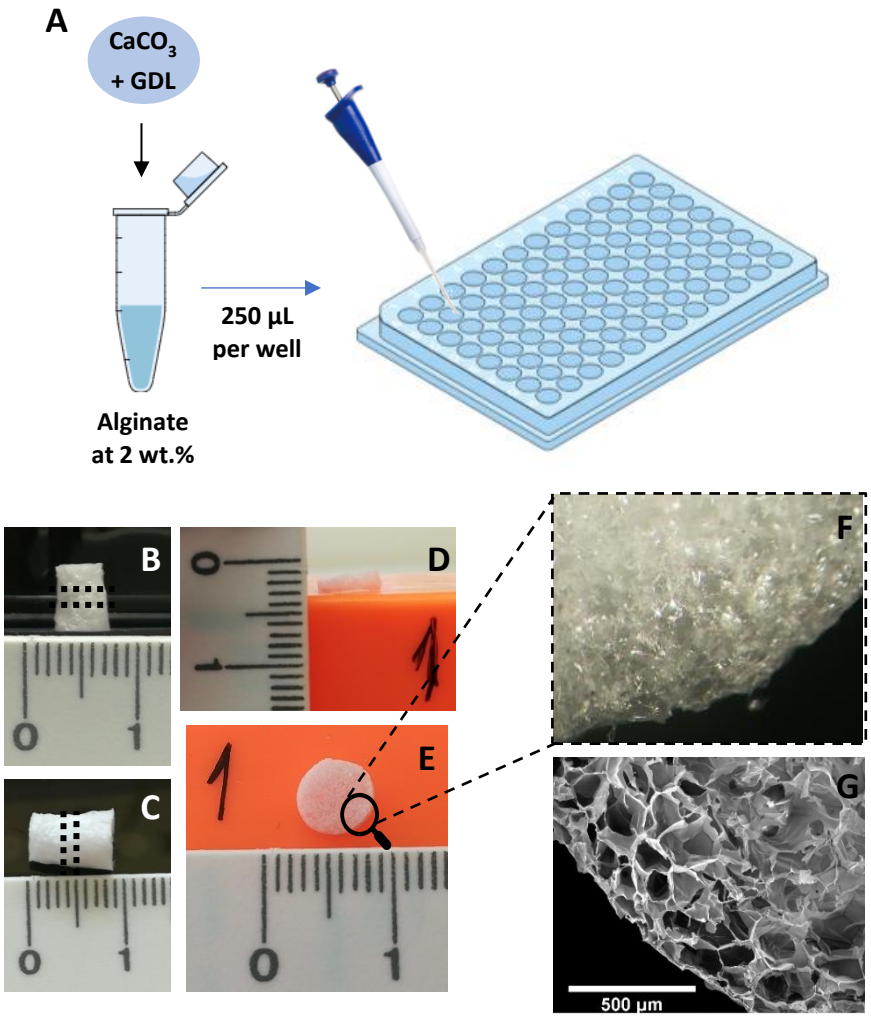

Figure 9 - Schematic representation of the process used for scaffolds preparation. Alginate hydrogels can be formed *in situ* upon release of calcium ions from an insoluble compound (calcium carbonate), triggered by the pH decrease resulting from GDL hydrolysis (A). Alginate combined with $CaCO_3$ and GDL is added to a 96 well plate giving rise to scaffolds with a cylindrical shape after lyophilization (B and C), which are cut into smaller structures (D and E). Disc-shaped scaffolds present a sponge appearance (F) and high porosity (G).

The porous architectural characteristics play an important role in scaffold vascularization, by facilitating the diffusion of nutrients and oxygen and providing pathways for new blood vessels ingrowth[80–86]. The design of porous scaffolds for tissue engineering purposes must take into consideration several parameters such as porosity extent, and pore size/size distribution, volume, pore throat size, shape, wall roughness and interconnectivity[91].

The pore size and interconnectivity are amongst the more essential factors for blood vessels growth[81–84,129], even though other parameters such as wall roughness may affect endothelial cell attachment, growth and activation[130]. Figure 10 shows SEM images of the surfaces and cross sections of a 2 wt.% alginate scaffolds. Scaffolds were highly

porous with sponge-like appearance and an average pore size of 186.7±47.6 µm (Fig. 11). Higher magnification images show pores interconnectivity. The porous structure was homogenous throughout the scaffold, without significant differences between the surface and the inner regions.

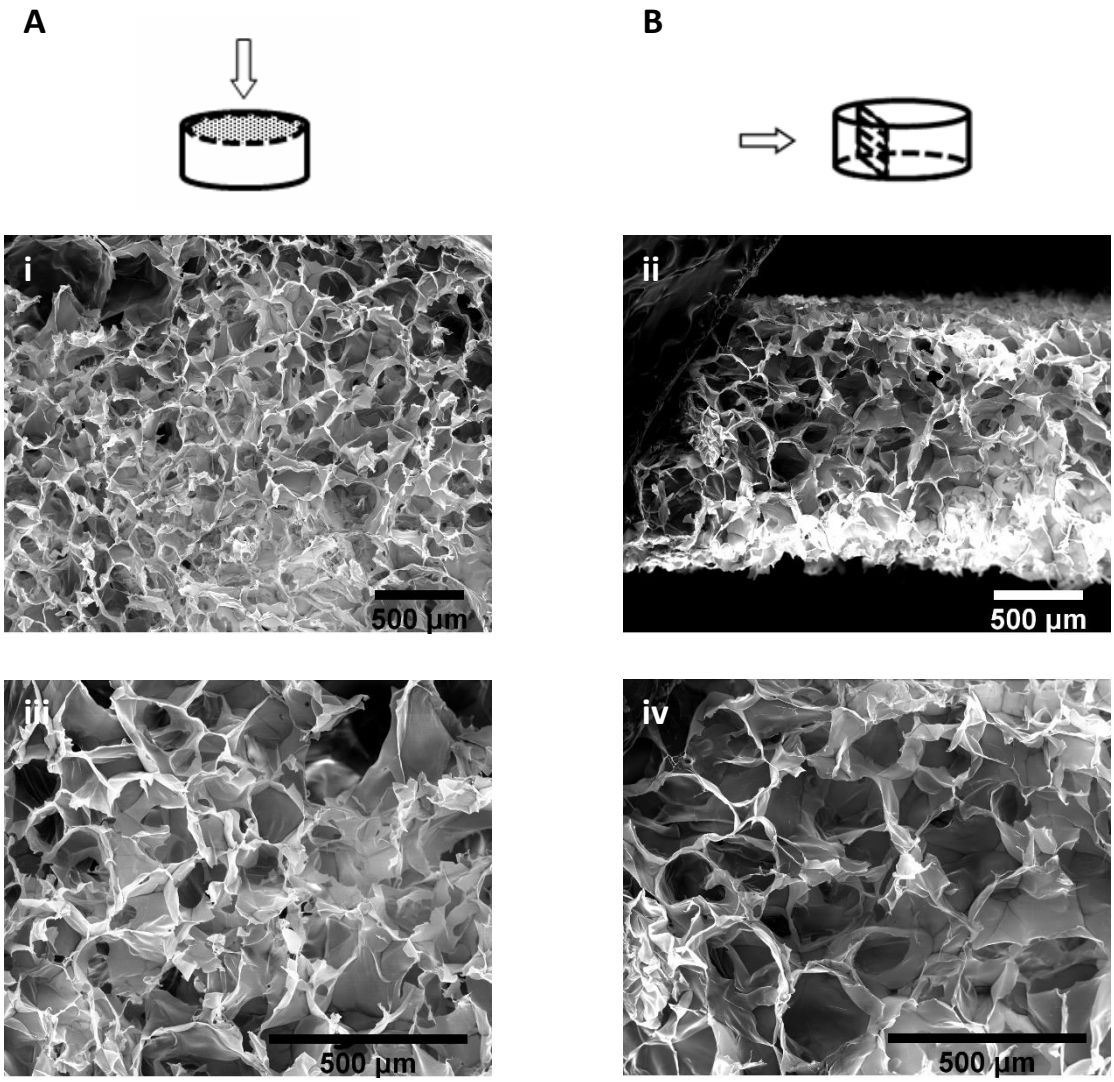

Figure 10 - SEM images of the porous structure: horizontal cross-section (A) and longitudinal cross-section (B). The images are shown in low (i and ii) and high (iii and iv) magnifications (45x and 100x, respectively). Scale bar: 500 µm.

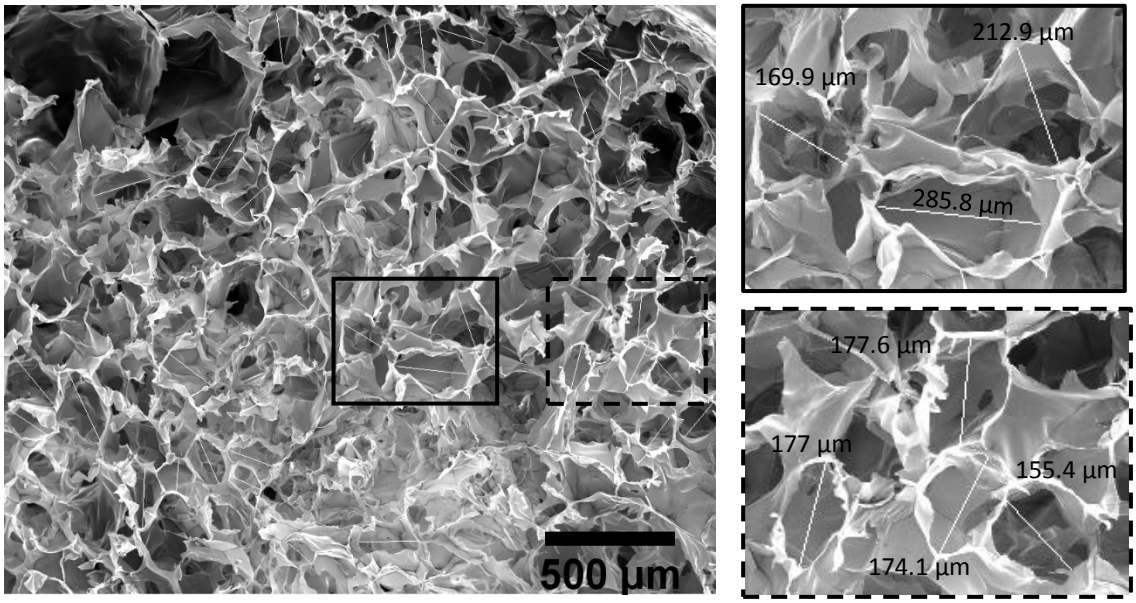

Figure 11 - Schematic illustration of the pore size measurement technique used. SEM images of the 2 wt.% alginate porous scaffold showed the presence of pores with pore size between 105.6 and 288.3 µm.

1.2. Monoculture of hMF and OECs

It is currently well established that ECs network formation is enhanced in the presence of stromal cells, which may not only produce important soluble factors and ECM components, but may also stabilize vascular structures via cell-cell interactions[131,132]. For example, Levenberg *et al* showed that it is possible to promote vascularization of a 3D tissue engineered constructs by combining ECs with fibroblasts and/or myoblasts[133]. Significantly, even though OEC present high proliferative capacity and phenotypic stability in long-term monolayer cultures,[134] these cells cannot form capillary like structures when cultured alone. Here, porous scaffolds were co-seeded with human mammary fibroblasts and OEC, but first the behavior of each cell type in monoculture was analyzed. hMF and OEC were seeded at a density of $25x10^4$ cells/scaffold in 30 µL, of the respective culture medium. Two seeding strategies were tested to select the one leading to a better cell distribution throughout the scaffold. In one of them the total volume of cell suspension was directly added on top of the scaffold. In the other one, cells were seeded on both sides of the scaffolds, with half of the volume being added on top of the scaffold, which was turned upside down 1 h later so that the reaming volume could be added on the other side.

ECs distribution within scaffolds was analyzed by CD31 (endothelial marker) and laminin staining (Fig. 12). Due to the presence of RGD peptides, ECs were able to adhere and

spread on the scaffold, and also produced laminin, an ECM protein that is considered to be the primary determinant of basement membrane assembly[135]. Importantly, we observed cell alignment along the pores' walls, as illustrated in Fig. 12Aii, 12Bii and 12Biv. In both seeding approaches we observed a higher cell density on the top of the scaffold, as compared to the bottom. After 11 days of culture, when cells were seeded on top only (first strategy) a higher cell number was detected on that side, compared to the bottom, as expected. Yet, in the case of the second strategy, cell distribution was also non-uniform and a higher amount of cells was also detected on top (where cells were seeded at the last stage). Therefore, the first strategy, which was also less time-consuming, was the one selected for subsequent experiments.

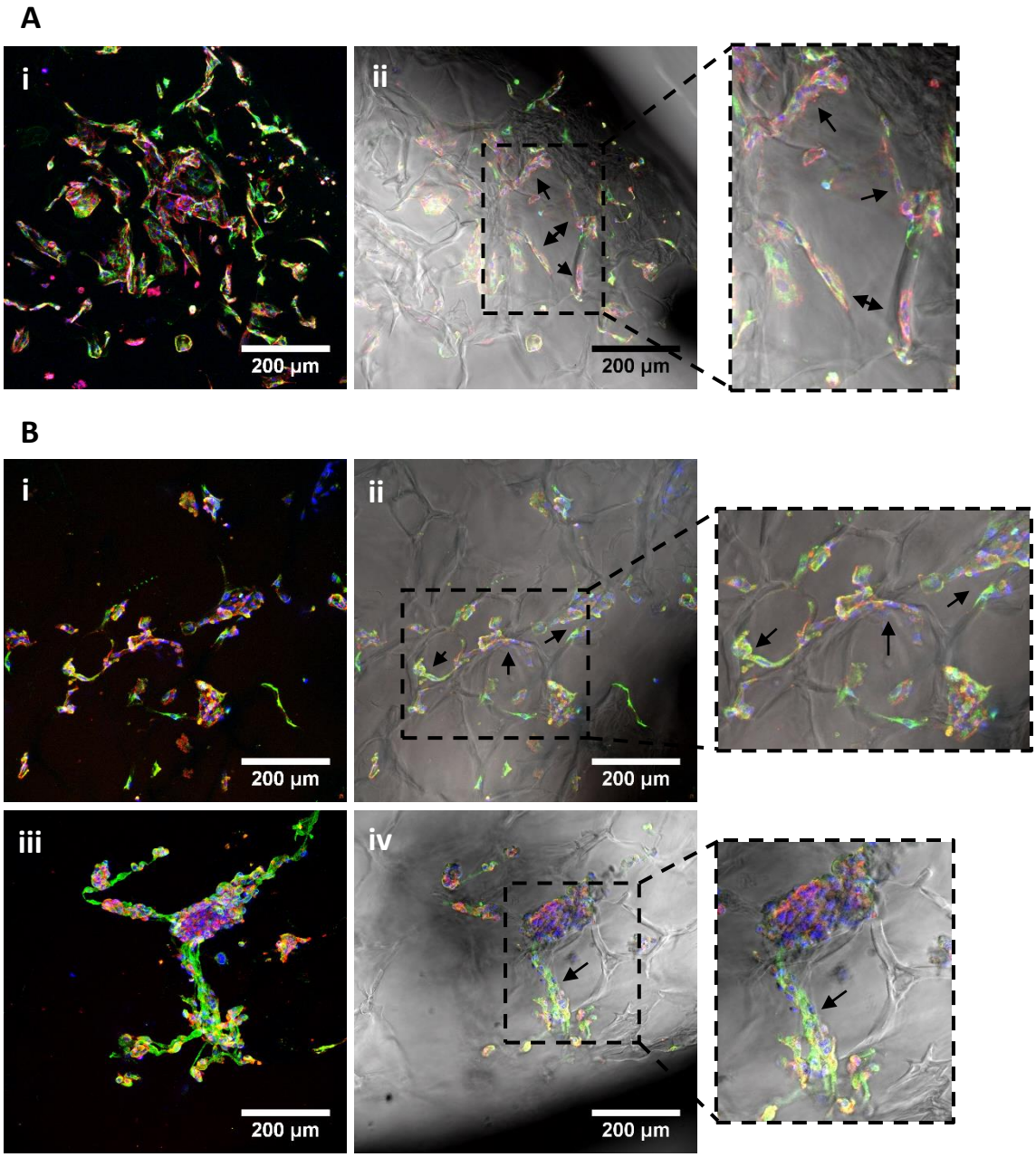

Figure 12 - Endothelial cells attachment, distribution and morphology on RGD-alginate scaffolds. OECs were stained for laminin (green), CD31 (red) and DAPI (blue). Seeding the cells only on top of the scaffolds showed a high cell density on top of the scaffold after 11 days of cell culture (A). Seeding the cells on both sides of the scaffold we can see the difference between the top (B, i-ii) and the bottom (B, iii-iv), after 14 days of culture. The cells were able to attach to the scaffold and align along the pore wall (A ii and B ii and iv, black arrows). Scale bars: 200 µm.

Fibroblasts seeded only on top of the scaffold presented a similar cell distribution profile, as depicted in Fig. 13. Again, the amount of cells on top of the scaffold (Fig. 13A and 13B) was higher than that at the bottom (Fig. 13E and 13F). In the proposed model, fibroblasts are expected to play a critical role in supporting the angiogenic process at the microenvironment scale, not only through ECM production and remodeling, but also via local delivery of key growth factors[136]. Thus, since it would be important to achieve high amounts of ECM deposition, we also tested a higher cell density of $50x10^4$ cells/scaffold, adding half of the cell suspension volume on both sides of the scaffold (Fig. 14A and 14B). This condition showed a better cell distribution compared to the scaffold seeded with only $25x10^4$ cells/scaffold, with the same strategy (Fig. 14A and 14C). Irrespectively of the approach, fibroblasts showed ability to assemble extensive fibronectin networks throughout the scaffold.

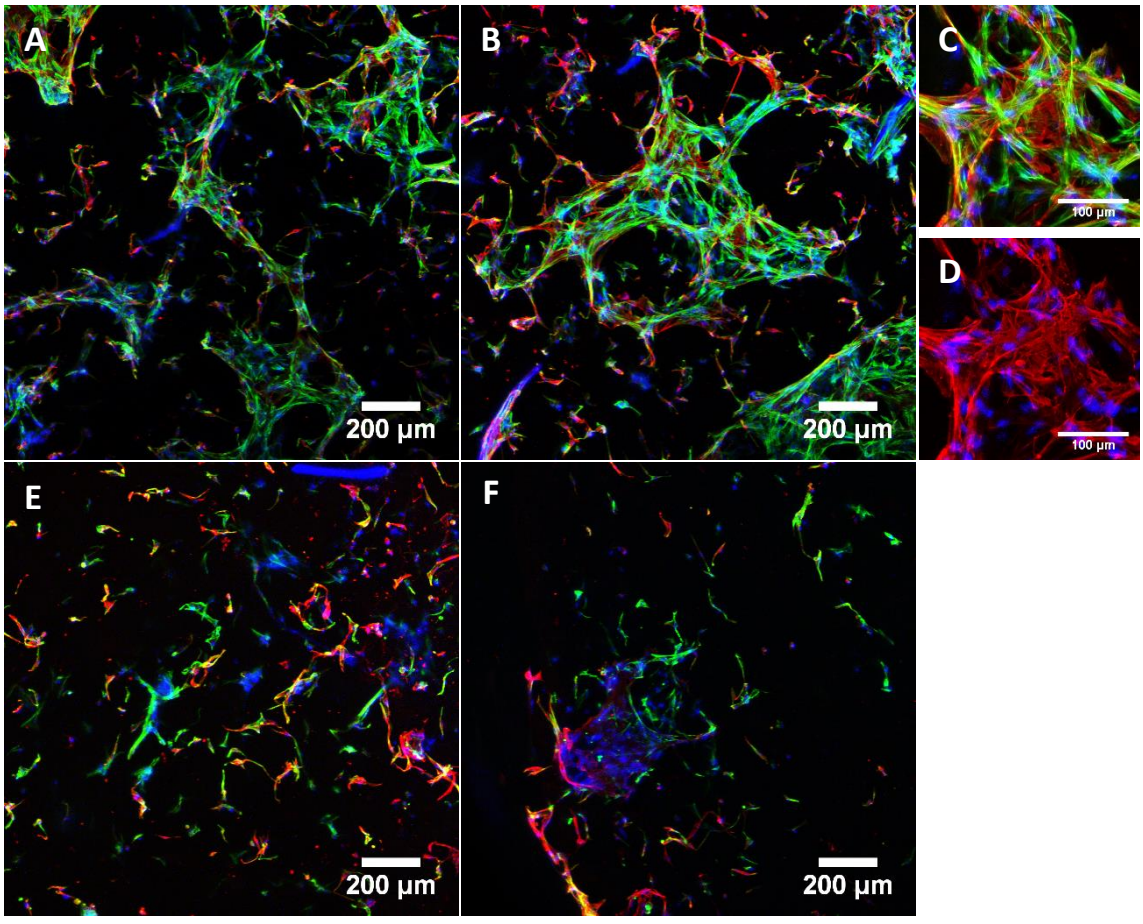

Figure 13 - Fibroblast cells attachment, distribution and morphology on RGD-alginate scaffolds. Cytoskeletal organization of fibroblasts grown on the scaffolds at day 14, was observed under a CLSM and demonstrated by F-actin (green), fibronectin (red) and DAPI (blue) staining. Seeding the fibroblasts only on top of the scaffold we saw that the number of cells on top (A and B) is higher compared to the bottom (E and F) of the scaffold (Scale bars: 200 µm). Fibronectin was clearly detected around the cells after 14 days of culture. (C and D, scale bar: 100 µm).

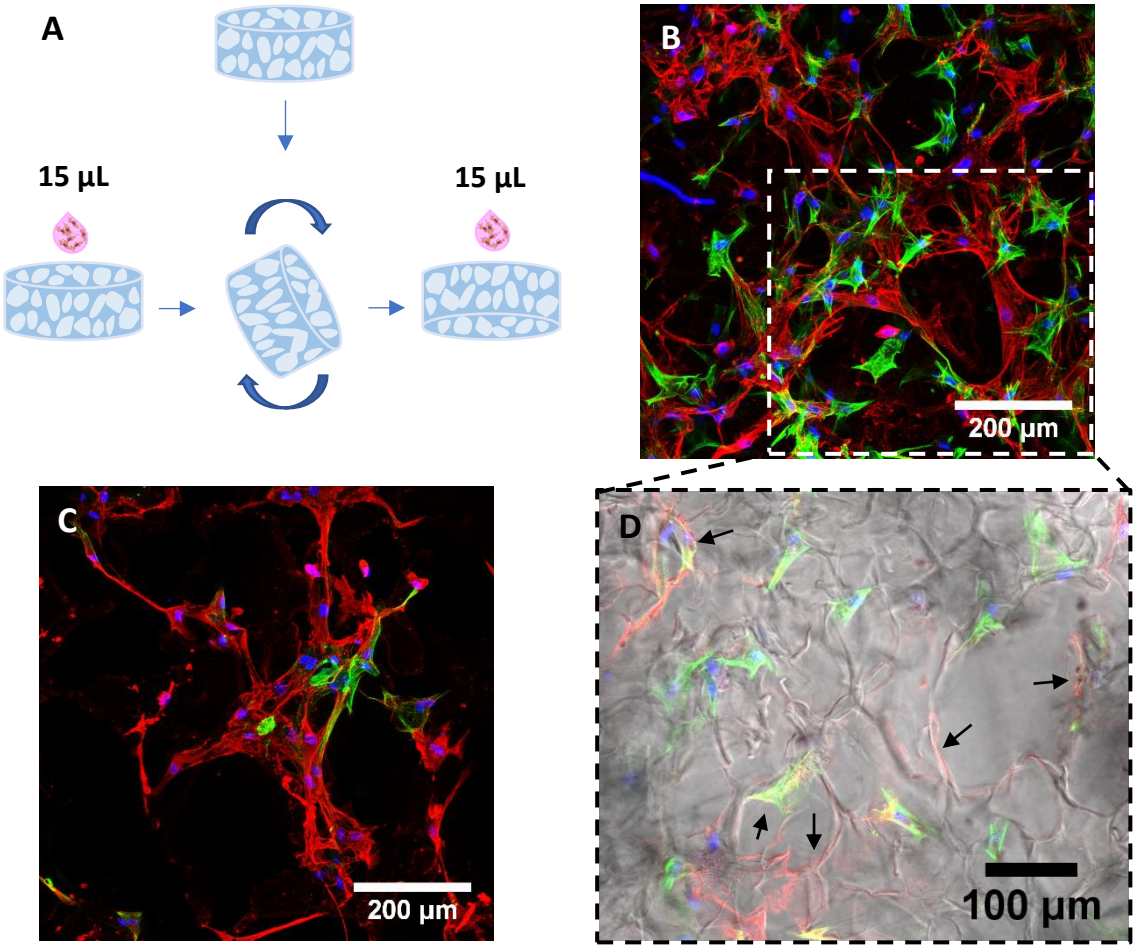

Figure 14 - Fibroblasts attachment, distribution and morphology on RGD-alginate scaffolds when using two different cell densities. Cytoskeletal organization of fibroblasts grown on the scaffolds at day 14, was observed under a CLSM and demonstrated by F-actin (green), fibronectin (red) and DAPI (blue) staining. Fibroblasts were seeded on both sides of the scaffold (A) with two different cell densities, (B and D) $50x10^4$ and (C) $25x10^4$ cells/scaffold. Fibronectin was clearly detected around the cells after 14 days of culture in both conditions but using a higher cell density allowed a better cell distribution on top of the scaffold (Scale bar of B and C: 200 µm). The cells were able to attach to the scaffold and align along the pore wall (D, black arrows; Scale bar: 100 µm).

1.3. Co-culture of hMF and OECs

The cell-cell ratio used in the co-culture should be optimized according to factors such as cell viability and the desired phenotypic expression within the system. Some groups used high ratios of ECs to make sure that these would be sufficient to form tubular structures, even if some cell death could occur[130,137]. Other groups use a higher ratio of non-ECs in order to induce the tissue engineered construct towards a specific phenotype[138,139]. While there is no consensus on the optimal cell ratio of ECs to stromal cells in co-culture studies, the 1:1 ratio has been used in most studies for the sake of

simplicity[140,141]. Here, the ratio was also set at 1:1, but different study designs were tested aiming optimal formation of capillary-like structures. The rationale for seeding cells sequentially (ECs after fibroblasts) was to give enough time for fibroblasts to produce sufficient amounts of ECM, which would later provide support for OEC. In this sense, we tested two timelines, where OEC were seeded at day 4 or 7 after hMF pre-seeding (Fig. 15A and 15B, respectively). Immunofluorescence images of both conditions showed that hMF pre-seeding led to the formation of a dense monolayer of cells with fibronectin deposition that unfortunately seemed to impair OECs 3D organization. In fact, as illustrated by CD31 staining (Fig. 15 A ii and B ii), OEC presented a spread morphology, as typically seen in a 2D monolayer culture, instead of organizing into aligned tubular-like structures. Considering these preliminary results, another strategy was tested, where the two cell types were seeded simultaneously at 1:1 cell ratio, with a total number of cells per scaffold of $25x10^4$ or $50x10^4$ (Fig. 15C and 15D). As we can observe in Fig. 15C and 15D this strategy successfully led to formation of endothelial tubular-like structures. Noteworthy, it seems that the lower cell density led to better OEC alignment (Fig. 15C and S2A). According to these results, the simultaneous seeding of both cell types at the lower density appeared to be the best option, which was thus selected for further experiments.

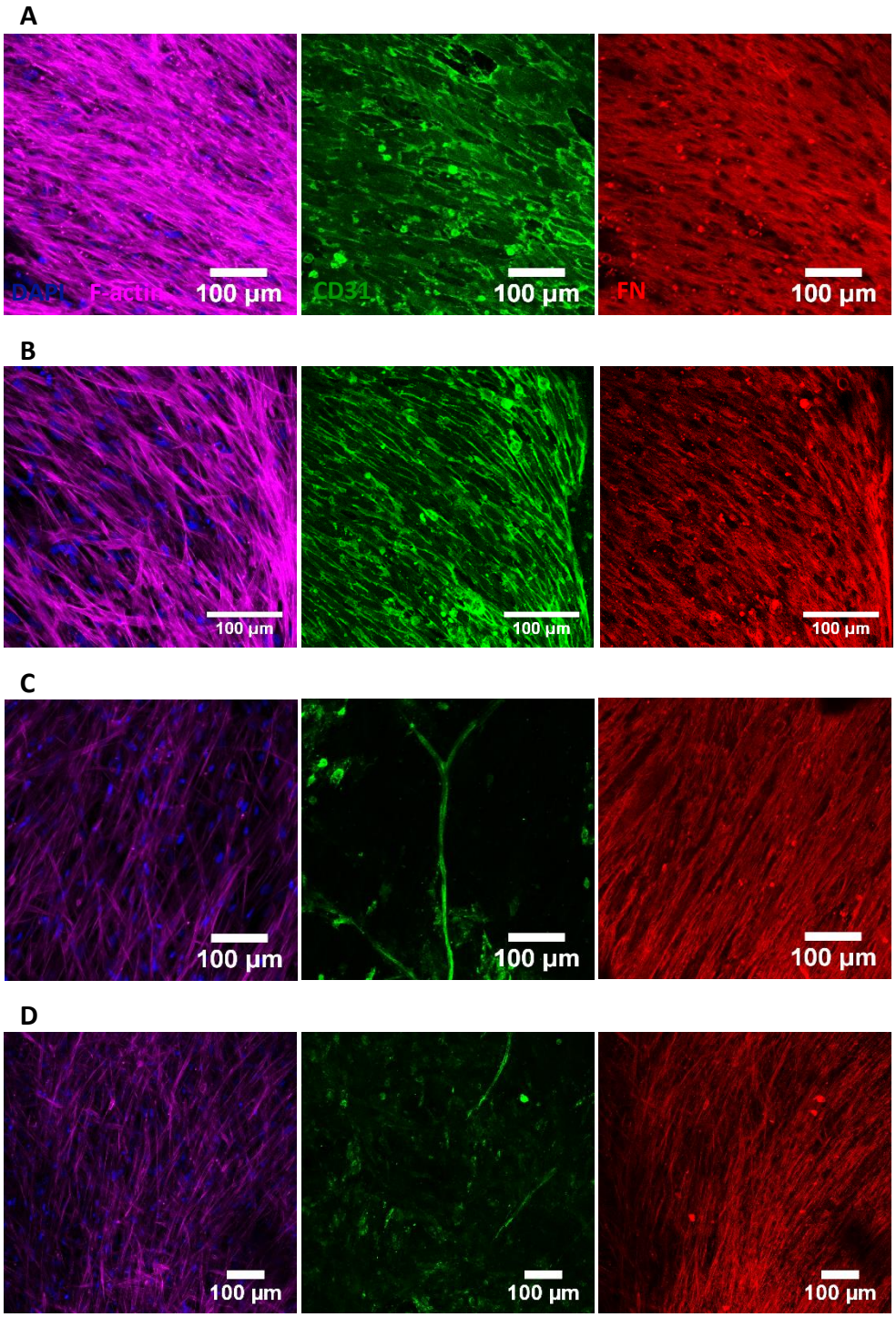

Figure 15 - Co-culture of hMF with OEC. Sequential (A and B) and simultaneous (C and D) co-culture strategies were studied, with the following cell densities per scaffold: Pre-seeding with $50x10^4$ hMF and (A) after 4 days or (B) 7 days $50x10^4$ OEC were added to the scaffold; (C) $25x10^4$ hMF + $25x10^4$ OEC, (D) $50x10^4$ hMF + $50x10^4$ OEC; Cytoskeletal organization of fibroblasts and ECs morphology on top of the co-cultured scaffolds, were observed under a CLSM and demonstrated by F-actin (purple), fibronectin (red), CD31 (green) and DAPI (blue).

2. 3D culture of human mammary epithelial cells within alginate-RGD matrices

Our group had previously developed an optimized alginate-based 3D matrix to study the inter-conversion between epithelial and mesenchymal states during epithelial-mesenchymal transition (EMT) and its reversion. Soft alginate hydrogel functionalized with RGD peptides was used to mimic the 3D microenvironment of normal murine mammary epithelial EpH4 cells. Using 1 wt.% RGD-alginate hydrogels and a cell density of 5×10^6 cells/mL showed to be ideal for culturing EpH4 cells in a 3D *in vitro* environment, enabling the formation of large spheroids with higher cell viability[142]. Using a RGD peptide density similar to the common ECM-derived biological matrices, including tumor ECM, is essential and leads to higher cell metabolic activity[142,143].Therefore, here we used these same conditions to establish 3D cultures of human mammary epithelial cells. We used three different cell lines that present distinct cell behavior both *in vitro* and *in vivo* as described in[144,145,146]. In order to validate the proposed engineered tumor model, we primarily assessed the morphology, metabolic activity and proliferation of three different cell lines: highly invasive human breast cancer MDA-MB-231 cells, non-invasive, tumorigenic human breast cancer MCF7 cells, and normal mammary epithelial MCF10A cells.

Their proliferative capacity in 3D was examined using the ki-67 immunofluorescence marker. While were able to detect ki-67 positive cells at day 1 in all cell lines (data not shown), the MCF7 showed the highest number of proliferative cells. After 2 weeks of culture, proliferative cells were essentially restricted to spheroids (Fig. 16A). We also observed that MCF7 presented the highest levels of metabolic activity, as compared to MCF10A and MDA-MB-231 (Fig. 16B), which gradually increased until day 10. While the metabolic activity profiles of the other two cell lines were less uniform, all of them exhibited a significant increase along the first 3 days of culture, suggesting that cells were actively proliferating. In fact, the fold increase was similar between the cell lines (around 1.5, Fig. 16C). After day 3 no significant differences were observed, except for MCF10A whose metabolic activity significantly decreased from day 10 to day 14.

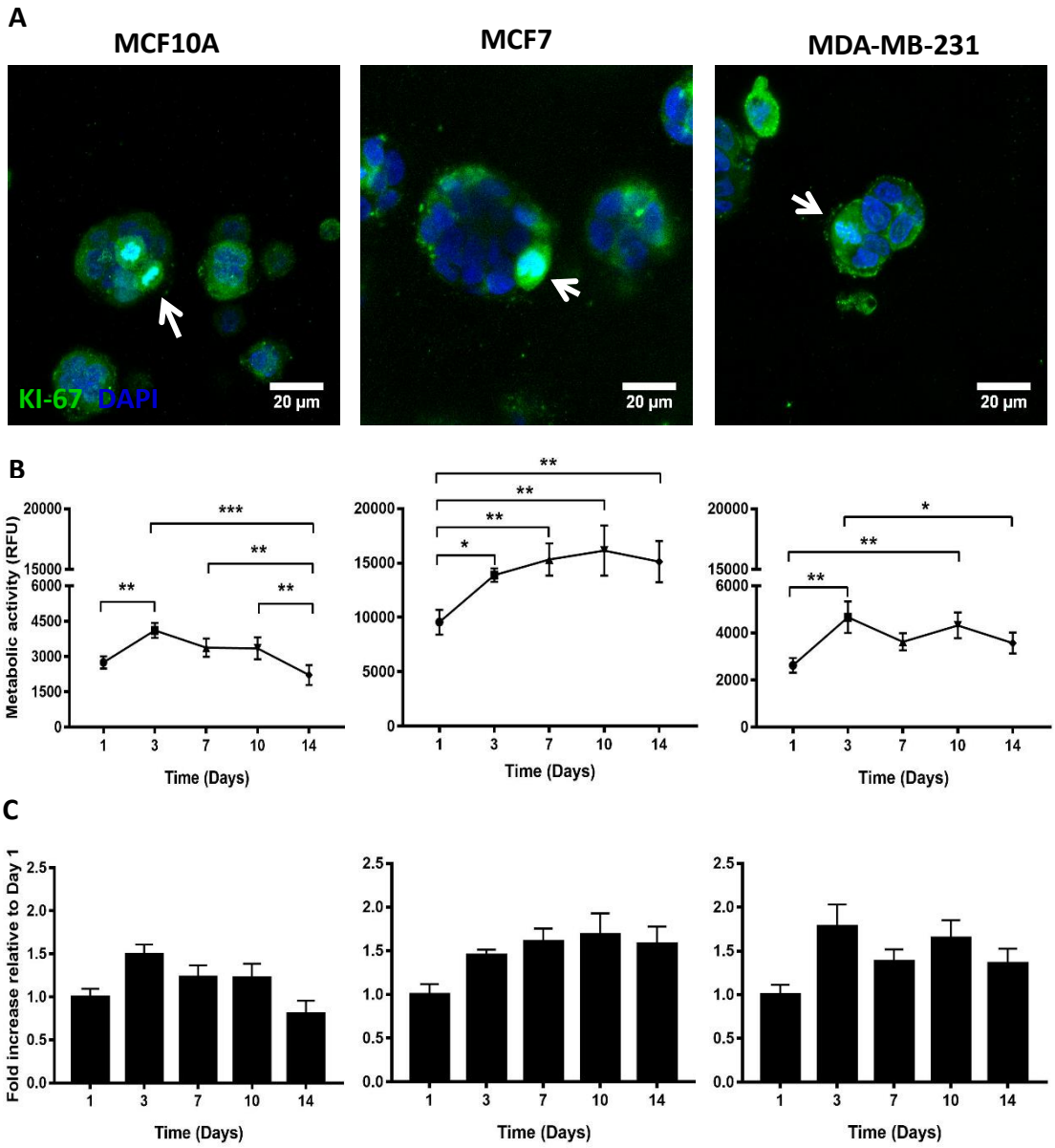

Figure 16 - Behaviour of MCF10A, MCF7 and MDA-MB-231 cells within 3D RGD-alginate matrix. (A) Proliferating epithelial cells (Ki-67 positive cells, arrows) after 14 days of culture (scale bar: 20 µm). (B) The metabolic activity profile in relative fluorescence units (RFU) showed a significant increase after 3 days of culture, then no significant differences were observed, except for MCF10A whose metabolic activity on day 14 was lower than day 1. Data is presented as mean ± stdev (n=4) (* $p<0.05$, ** $p<0.01$ and *** $p<0.0001$). (C) Fold increase of metabolic activity relative to day 1.

In the 3 cell lines, cells were initially distributed as single cells within the alginate matrix, generating spheroids as they proliferated, as depicted in Fig. 17. After 7 days the formation of small spheroids could already be detected, with their size increasing throughout time until day 14. Noteworthy, both MCF7 and MDA-MB-231 cell lines formed larger cell clusters as compared to the non-tumorigenic cell line, MCF10A.

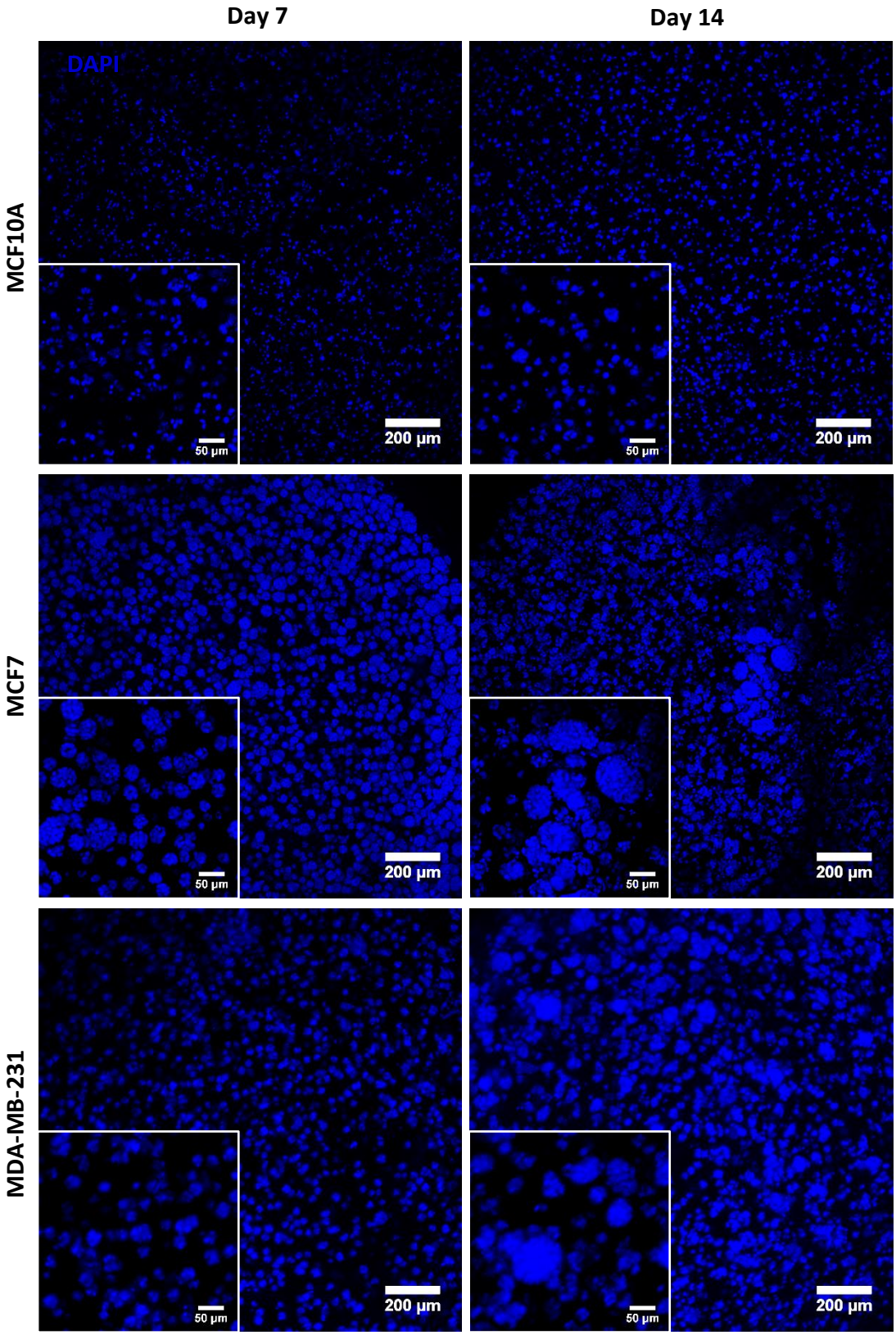

Figure 17 - Epithelial cell-laden hydrogels after 7 and 14 days of culture. MCF10A, MCF7 and MDA-MB-231 formed spheroids that increase in size and number along 14 days of culture. Spheroids were visualized with DAPI staining (scale bar: 200 µm, with zoom- 50 µm).

E-Cadherin/β-catenin complex plays an important role in maintaining epithelial integrity and disrupting this complex destabilizes cell-cell contact[147]. In fact, the loss of cell-cell adhesion is associated with a wide range of human malignancies in which EMT is implicated. Therefore, we assessed the presence of these cell-cell junction markers in the different epithelial cell lines cultured in 3D. Although all the cell lines formed multicellular clusters, only MCF10A and MCF7 cells expressed E-cadherin and ß-catenin at the cell-cell junctions as depicted in Figs. 18A and 18B. Therefore, it seems that MCF10A and MCF7 present a more stable cell-cell interactions within 3D spheroids as, compared to the MDA-MB-231, which suggests that the later probably retains its mesenchymal-like phenotype. This is in accordance with the literature, where MDA-MB-231 cell line is described as an invasive and metastatic tumor cell line lacking expression of E-cadherin and ß-catenin at the cell membrane[148–151]. This is corroborated by studies in 2D monolayer culture, which show that MCF10A and MCF7 cells typically present a cobblestone morphology, with cell-cell interactions being preserved during proliferation, whereas MDA-MB-231 cells exhibit a fibroblastic-like morphology in which single cells are spindle-shaped due to the absence of cell adhesion[152,153].

After 14 days in culture, was possible to detect the formation of acini-like structures within MCF10A-laden hydrogels, presenting an organized layer of single cells oriented around a central lumen (Fig. 18A). Similar behaviors have also been described in the literature not only with MCF10A cells but also with other non-malignant human mammary epithelial cells, such as HMT-3522 S1 and 184[154–157]. When cultured in a 3D reconstituted basement membrane (e.g. lrECM) these cells are able to form organotypic mammary acini characterized by growth arrest, apicobasal polarization, lumen formation and basement membrane formation. Here, these structures also stained positively for E-cadherin at the cell-cell junctions, suggesting robust cell-cell interaction. Overall, these results suggest that 3D culture of MCF10A in soft RGD-alginate promotes epithelial morphogenesis.

In contrast, the two tumorigenic cell lines formed dense spheroids. This was expected as, according to literature, MCF7 and MDA-MB-231, along with other malignant cells, adopt a variety of colony morphologies with common aspects such as loss of polarity, a disorganized architecture and a failure to arrest growth[154,158].

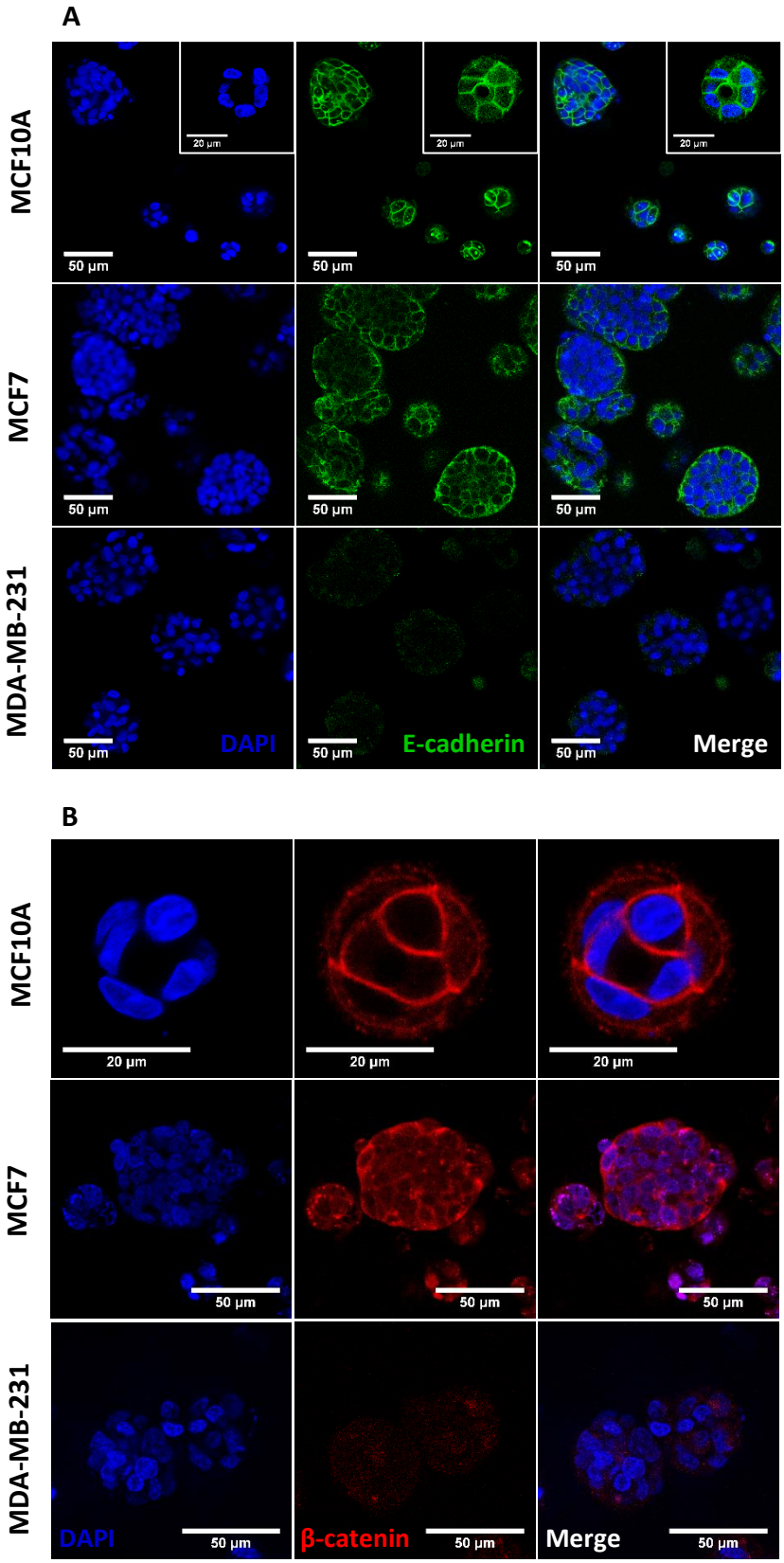

Figure 18 - Assessment of the expression of cell-cell junction markers in MCF10A, MCF7 and MDA-MB-231 cells cultured within 3D RGD-alginate matrix after 14 days of culture. Immunofluorescence for (A) E-cadherin (Green) (Scale bar: 50 µm; MCF10A with zoom is 20 µm) and (B) β-catenin (Scale bar: 50 µm except for MCF10A which is 20 µm).

3. Establishment of a heterotypic 3D breast cancer model

3.1. Tube formation assay

The environmental stresses in the tumor core, characterized by hypoxia, glucose deprivation, and the accumulation of metabolic wastes and carbon dioxide is known to induce an angiogenic switch. This is characterized by the secretion of proangiogenic signals that act on the ECs from nearby vessels leading to their migration and sprouting around the tumor mass[49,50]. Studies have suggested that tumor vascularization involves not only angiogenesis (vessel sprouting from pre-existing vessels), but also alternative mechanisms such as vasculogenesis (recruitment of endothelial progenitor cells (EPCs) from bone marrow)[159].

Here, we addressed the impact of epithelial cells with different tumorigenic capacity on ECs tubulogenesis ability, by using a standard angiogenesis assay. OECs were seeded on Matrigel in presence of conditioned medium from the three epithelial cell lines and analyzed after 24 h. As shown in Fig. 19, tube formation was observed in the presence of the three CMs, even though the number of capillary-structures formed in the presence of MCF10A and MDA-MB-231 CM was higher as compared to the MCF7 CM. This suggests that the secretion of angiogenic growth factors by MCF7 cells is lower compared to the other two cell lines. This is consistent to other studies described in the literature, which compared the angiogenic potential of MDA-MB-231 and MCF7 using an *in vitro* tumor angiogenesis model to assess paracrine signaling between breast cancer cells and endothelial cells (TIME)[99]. Bioengineered MDA-MB-231-based tumors were shown to promote endothelial proliferation and VEGF expression, thus inducing the formation of capillary-like tubular network with lumen formation and anastomosing branches. In contrast, bioengineered MCF7-based tumor did not elicit an angiogenic response[99]. Here, comparing the MCF10A and MDA-MB-231 cell lines, we could see that the later promoted the formation of larger and better-defined tubular structures. This result was expectable, since previous studies reported that MDA-MB-231 cells present higher angiogenic activity than MCF10A cells[95].

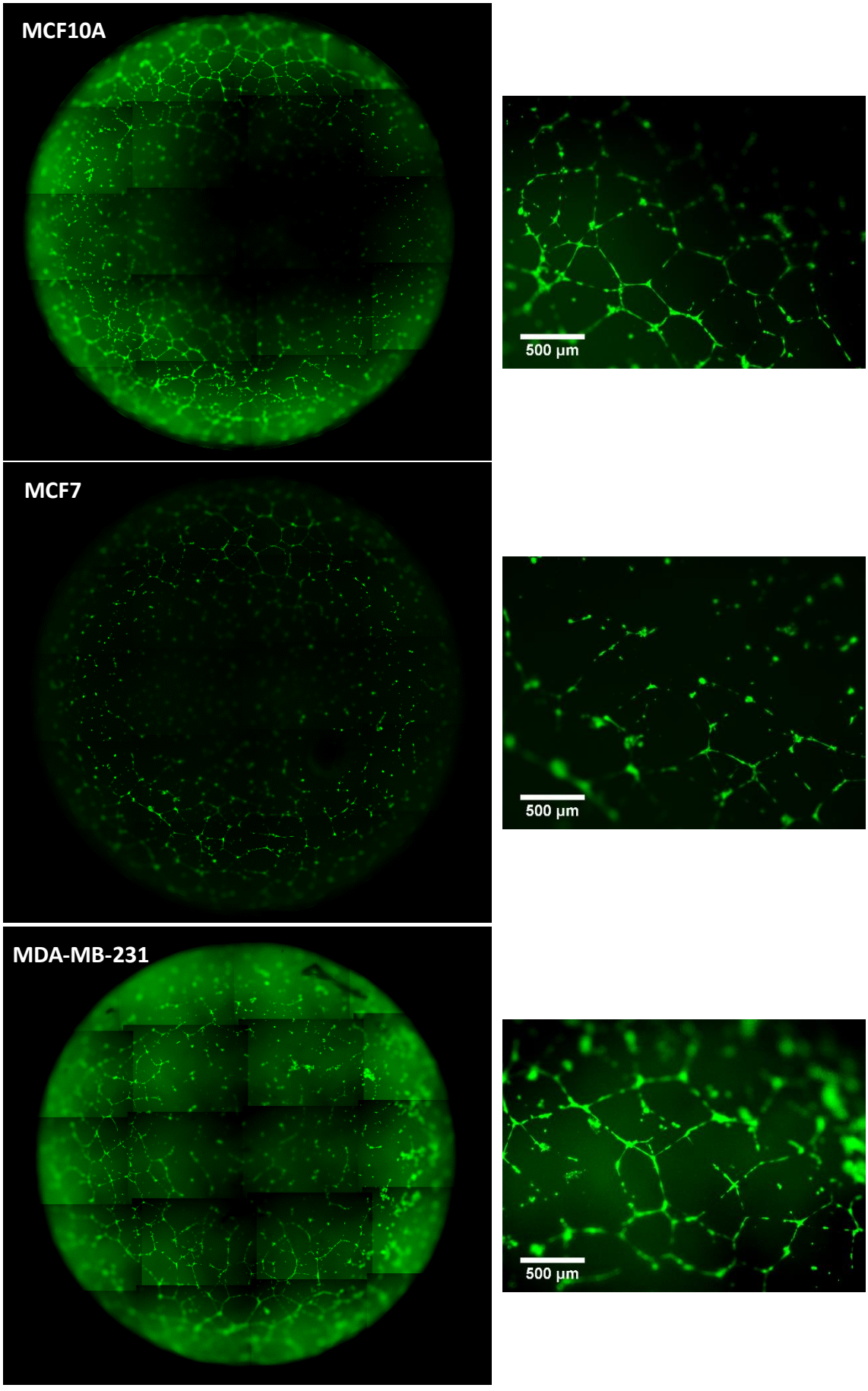
MCF10A
500 µm
MCF7
500 µm
MDA-MB-231
500 µm

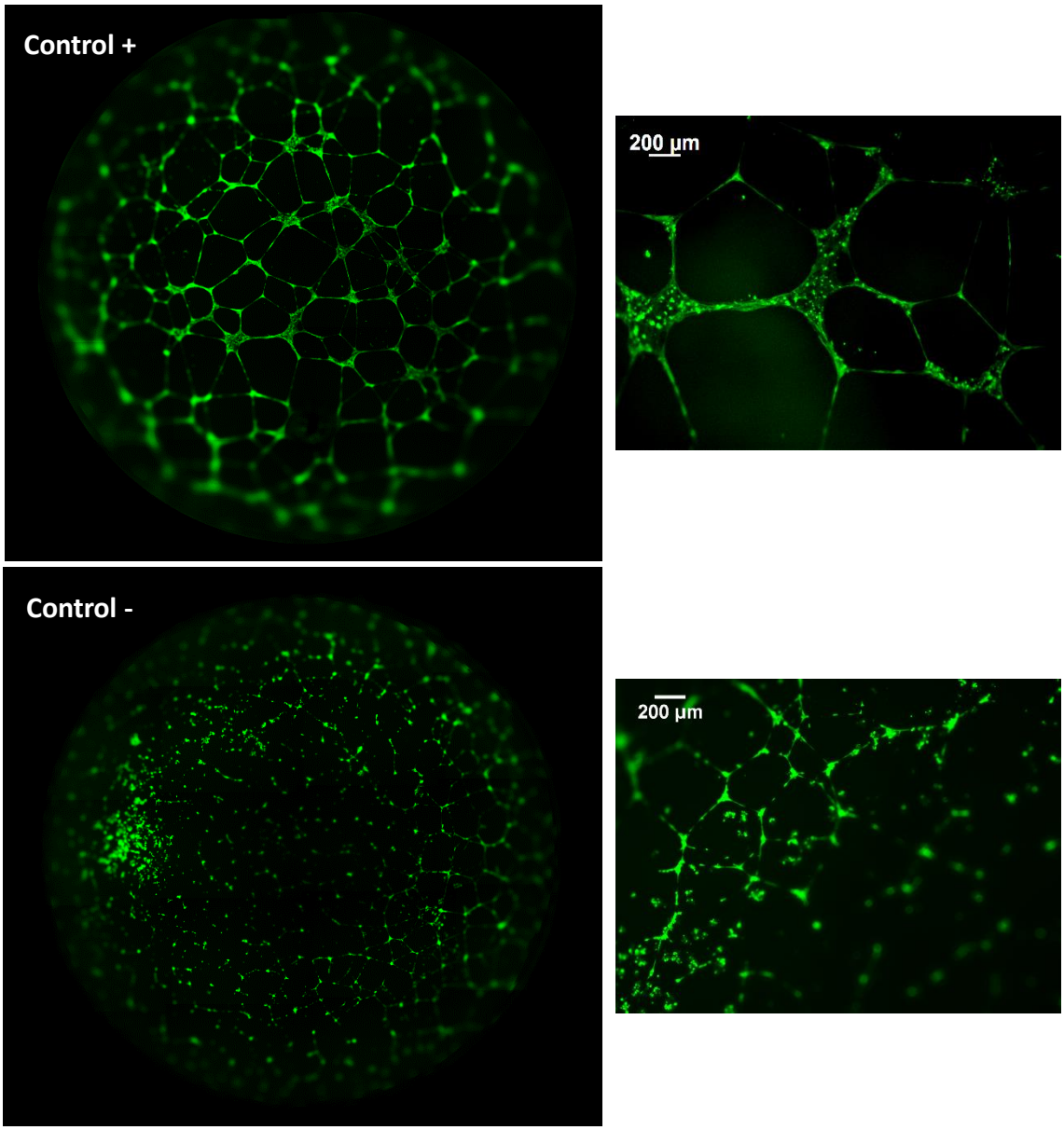

B

	Control +	Control -	MCF10A	MCF7	MDA-MB-231
# of capillary-like structures	345	281	466	338	451

Figure 19 - Outgrowth endothelial cell tube formation after 24 hours of culture on reduced growth factor basement membrane. A total of $5x10^4$ cells were seeded per well (in a 96-well plate) with conditioned media from MCF10A, MCF7 and MDA-MB-231. A) Fluorescence microscopy images of endothelial tube formation in Matrigel treated with calcein AM. Scale bar (right images): 500 µm (CMs) and 200 µm (controls) (B) Quantification of tube formation by Fiji.

3.2. Development of a tumor angiogenesis model

To create the tumor angiogenesis model, we combined the two previously developed 3D models, i.e. the hydrogel-embedded breast epithelial cells with the vascularized porous scaffold. To this end, epithelial cells embedded were suspended in 1 wt.% RGD-alginate hydrogel precursor solution and added to the porous scaffolds previously co-cultured with endothelial cells and fibroblasts for 8 days. Immunostaining of the 3D construct at day 8 revealed the presence of aligned CD31+ ECs (Fig. 20A), and the deposition of collagen IV at the periphery of ECs and of fibronectin throughout the scaffold (Fig. 20B). One week after adding the gel-embedded epithelial cells, we were able to detect the presence of small spheroids with all the three tested cell lines (Figs. 21 and 22). This can be more clearly observed with MCF10A cells, which not only formed spheroids at the periphery of the scaffold but also inside the pores, as depicted in Fig.21A and B. Interesting, some of these pores are surrounded by fibronectin produced by hMF cells. Unfortunately, with MCF7 and MDA-MB-231 cells, some of the hydrogel was also able to penetrate the scaffold's pores, but a significant amount remained at the top at the scaffold, where it ended up gelling, which results in a non-uniform distribution of the spheroids throughout the porous scaffold.

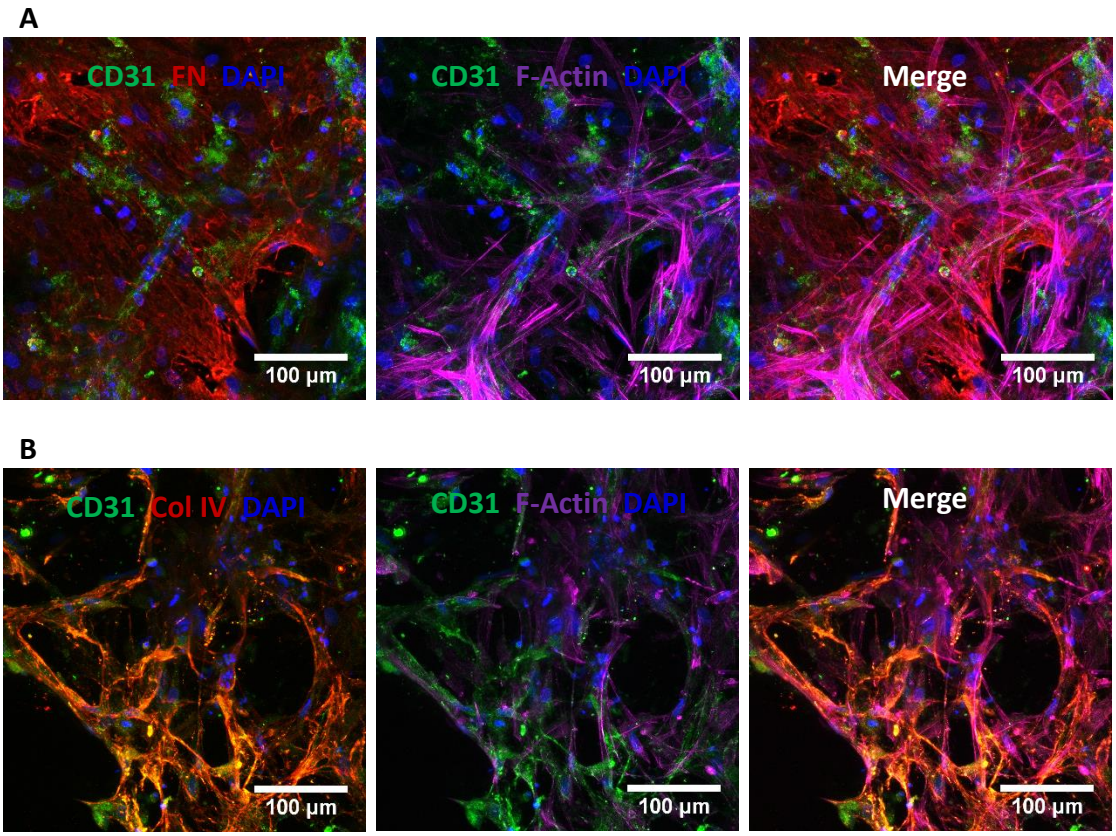

Figure 20 - Confocal fluorescent images of RGD-alginate scaffolds colonized with outgrowth endothelial cells and human mammary fibroblast for 8 days. Immunostaining of co-cultured scaffolds revealed the presence of oriented ECs that stained positive for CD31 (green) and the production of ECM proteins A) fibronectin (FN, red) and B) collagen IV (Col IV, red). Overall cell organization can be visualized through F-actin (purple) and nuclei (blue) staining. Scale bars: 100 µm.

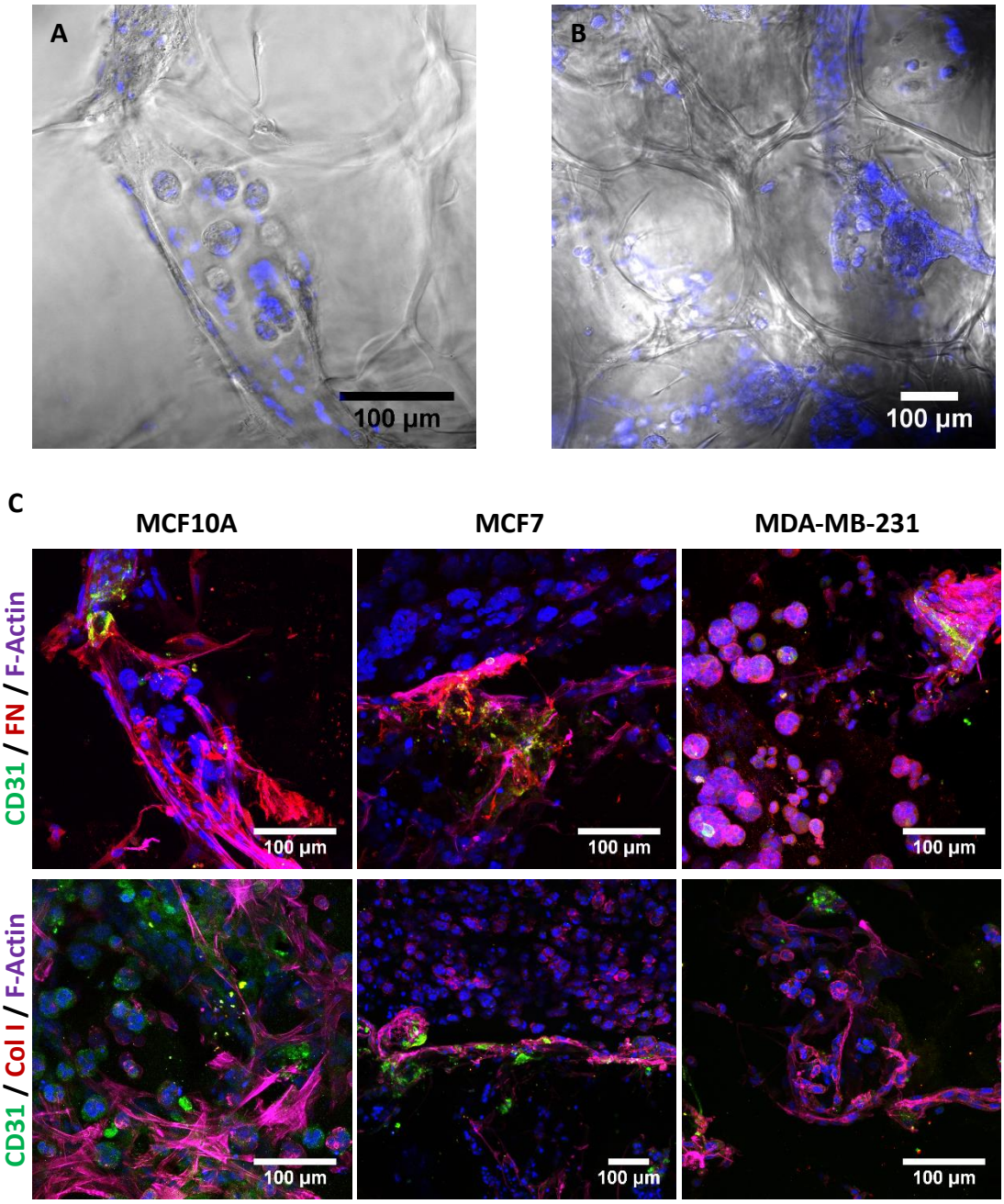

Figure 21 - Confocal fluorescent images of 3D tri-culture. The vascularized porous scaffolds combined with epithelial cell-laden hydrogel revealed the presence of spheroids within the porous scaffold, after one week of culture. A and B) MCF10A spheroids (nuclei, blue) within the alginate porous (bright field). C) Immunostaining of tri-cultured scaffolds revealed the presence of endothelial cells clusters that stained positive for CD31 (green) and the production of ECM proteins fibronectin (FN, red) and collagen IV (COL IV, red). Overall cell organization can be visualized through F-actin (purple) and nuclei (blue) staining. Scale bar: 100 µm.

To better visualize the spatial distribution of spheroids, cross sections of paraffin-embedded 3D constructs were stained with Safranin, which stains alginate in orange/red, and nicely illustrated the presence of spheroids within the pores (Fig. 22 and S3). We can also see that all the scaffolds present a layer of cell-laden hydrogel on top, indicating that the gelation process was too fast and did not allow the hydrogel to successfully infiltrate through the scaffold. One way to overcome this problem could be by delaying the onset and duration of the gelation time, for instance by adjusting the $CaCO_3$/GDL molar ratio. Another strategy could be the optimization of the scaffold architecture, by increasing the amount and/or size of the pores. These parameter can be tailored by changing the freezing conditions such as freezing temperatures, freezing time, and the freezing moulds[160–162]. Another possibility would be to use other scaffold processing techniques. One possibility would be to combine freeze-drying with particulate leaching by using a porogen with a desired size and shape. Some preliminary results obtained using this strategy are presented in section 4.

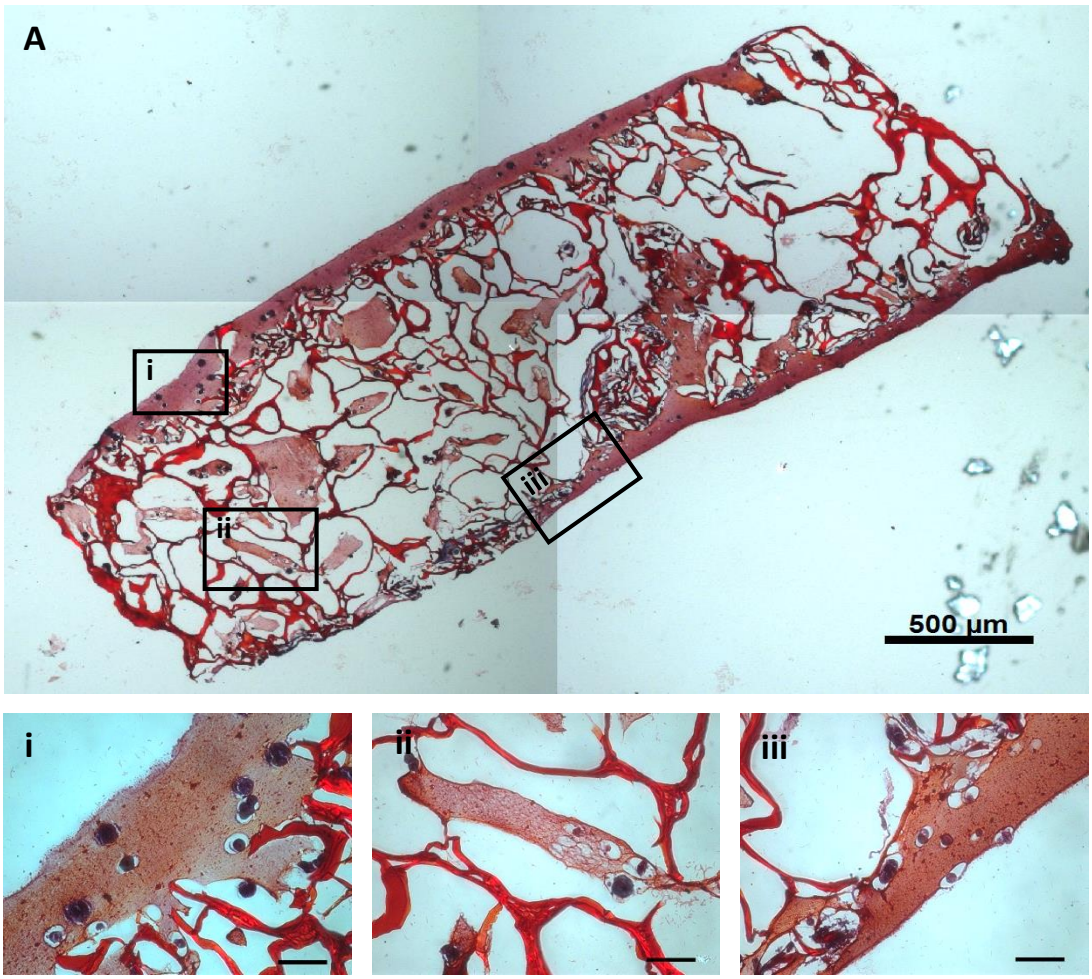
A
i
ii
iii
500 µm
i
ii
iii
B
i
ii
iii
500 µm
i
ii
iii

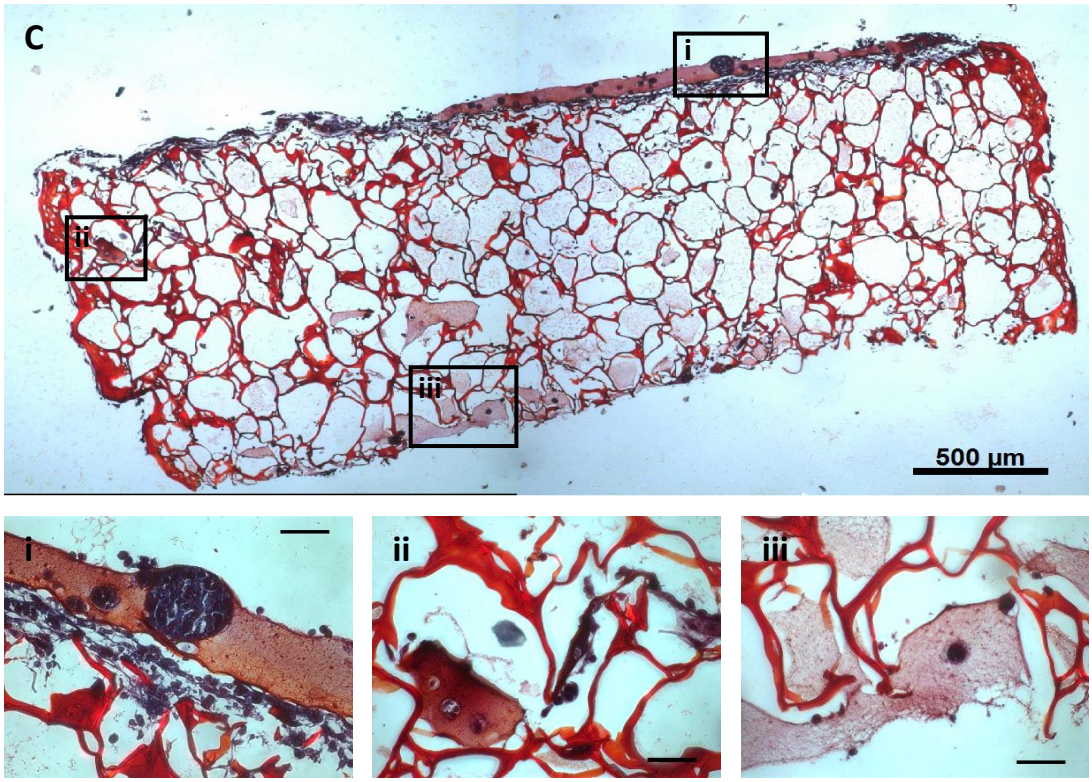

Figure 22 - Cell-laden hydrogel distribution within the vascularized scaffold. The cross-sections of the constructs with (A) MCF10A, (B) MCF7 and (C) MDA-MB-231-laden hydrogels were stained with Safranin, allowing to visualize the presence of spheroids within the pore structures. (Scale bar: 500 µm, with zoom- 50 µm).

In these studies, the heterotypic 3D breast cancer models were maintained in EGM-2MV, the same medium used for the OECs and hMF co-culture. Before establishing the combined model, we previously evaluated the metabolic activity of epithelial cells cultured in EGM-2MV. For that purpose, epithelial cell-laden hydrogels were maintained for one week in EGM-2MV medium. Results (Fig. 23A) showed that the metabolic activity of MCF10A and MDA-MB-231 cells in EGM-2MV was similar to the one they exhibited in their respective cultured medium, while the MCF7 cell line presented a lower metabolic activity. Macroscopic observation of the cell-laden hydrogels did not reveal differences on spheroids formation between the standard and the EGM-2MV medium (Fig. 23B).

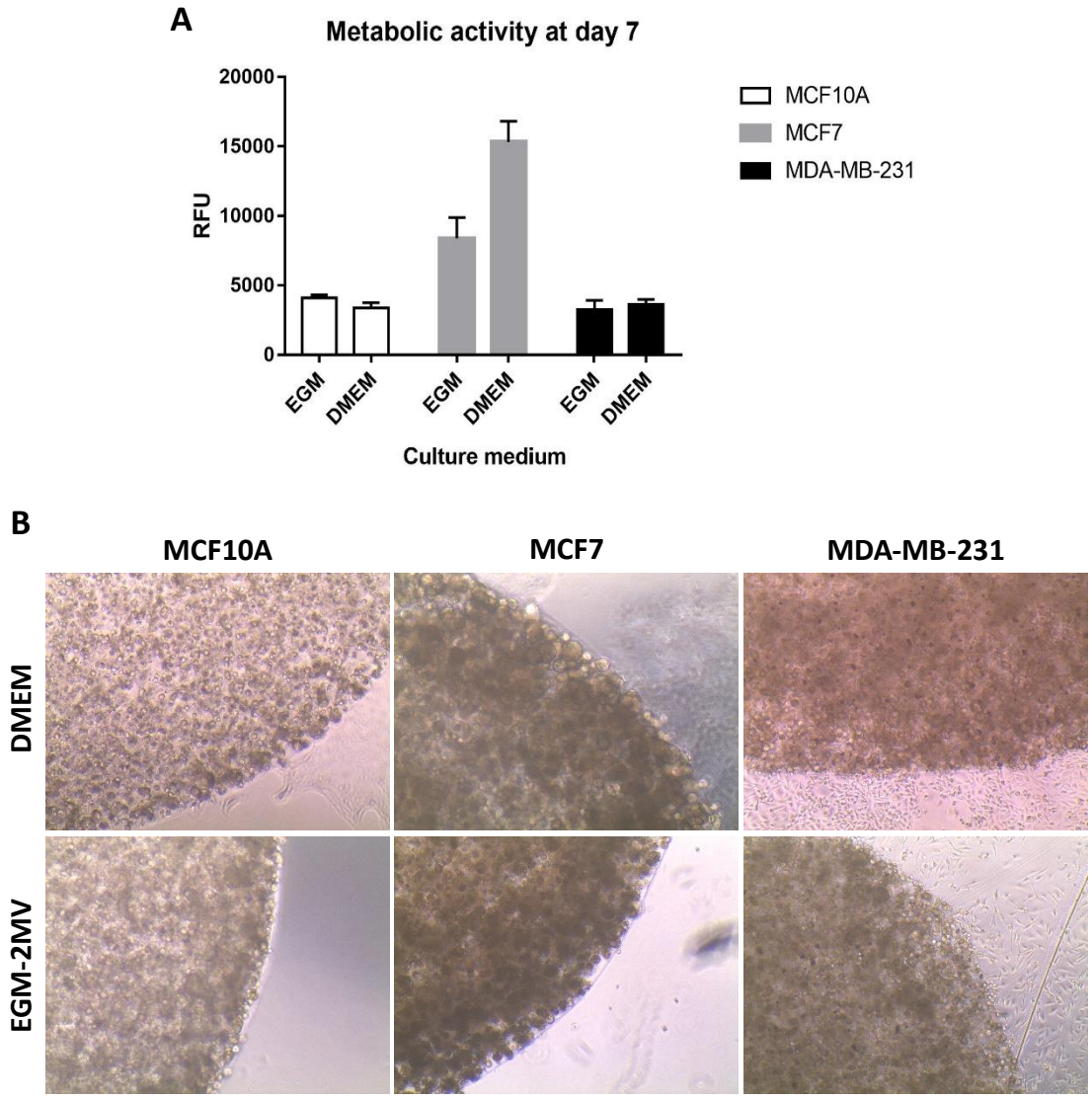

Figure 23 - The epithelial cell-laden hydrogels growth in EGM-2MV culture medium. (A) The metabolic activity profile showed no significant differences in both culture mediums, except for MCF7 whose metabolic activity on day 7 was lower when cultured in EGM-2MV (n=4). (B) Microscopic observation (5x magnification).

4. Preliminary results on an alternative strategy for the production of porous alginate scaffolds

4.1. Scaffold preparation and characterization

Alginate scaffolds were also prepared using freeze-drying combined with particle leaching, one technique widely used to fabricate scaffolds for tissue engineering applications[163,164]. Sodium chloride (NaCl) was used as porogen to form the porous structures. NaCl particles were broken/fractioned and sieved to a particle size of 150-250 µm. Alginate precursor solutions were prepared at a final alginate concentration of 2 and 4 wt.%, and different amounts of NaCl particles (0.6 and 1.1 mg/mL) were

subsequently incorporated into the hydrogel. After crosslinking samples were frozen and lyophilized, and salt particles were finally leached in distilled water. The leached samples were then freeze-dried again.

SEM observation (Fig. 24) showed that the size of pores of scaffolds prepared with 2 wt.% or 4 wt.%. alginate solutions are similar. Yet, the alginate concentration had an effect on the internal and surface morphology of the scaffold, with the 2 wt.% alginate solution leading to thicker pore walls. Regardless the alginate concentration used, increasing the amount of NaCl particles resulted on the formation of larger pores, although there were no significant differences in the scaffolds prepared with 4 wt.% alginate solution (Fig. 24). The control scaffolds did not contain NaCl, so the pores originated only from the sublimation of ice crystals by lyophilization. As we can see, the presence of the NaCl particles increased the pore size comparatively to the control (Fig. 24).

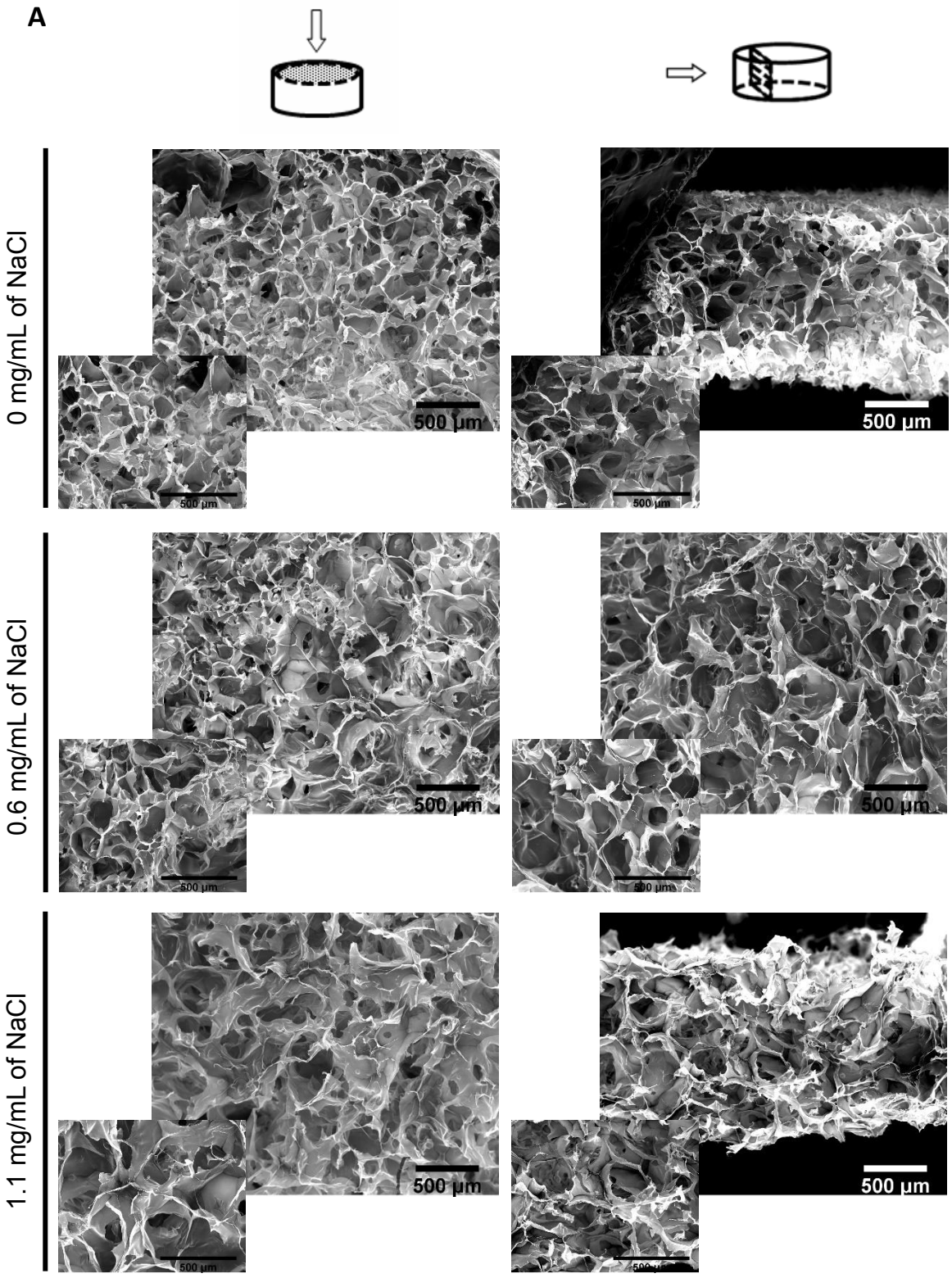

	2 wt.%	2 wt.% + 0.6 mg/mL	2 wt.% + 1.1 mg/mL
Average pore diameter (µm)	186.70 ± 47.58	218.07 ± 64.21	278.36 ± 95.05

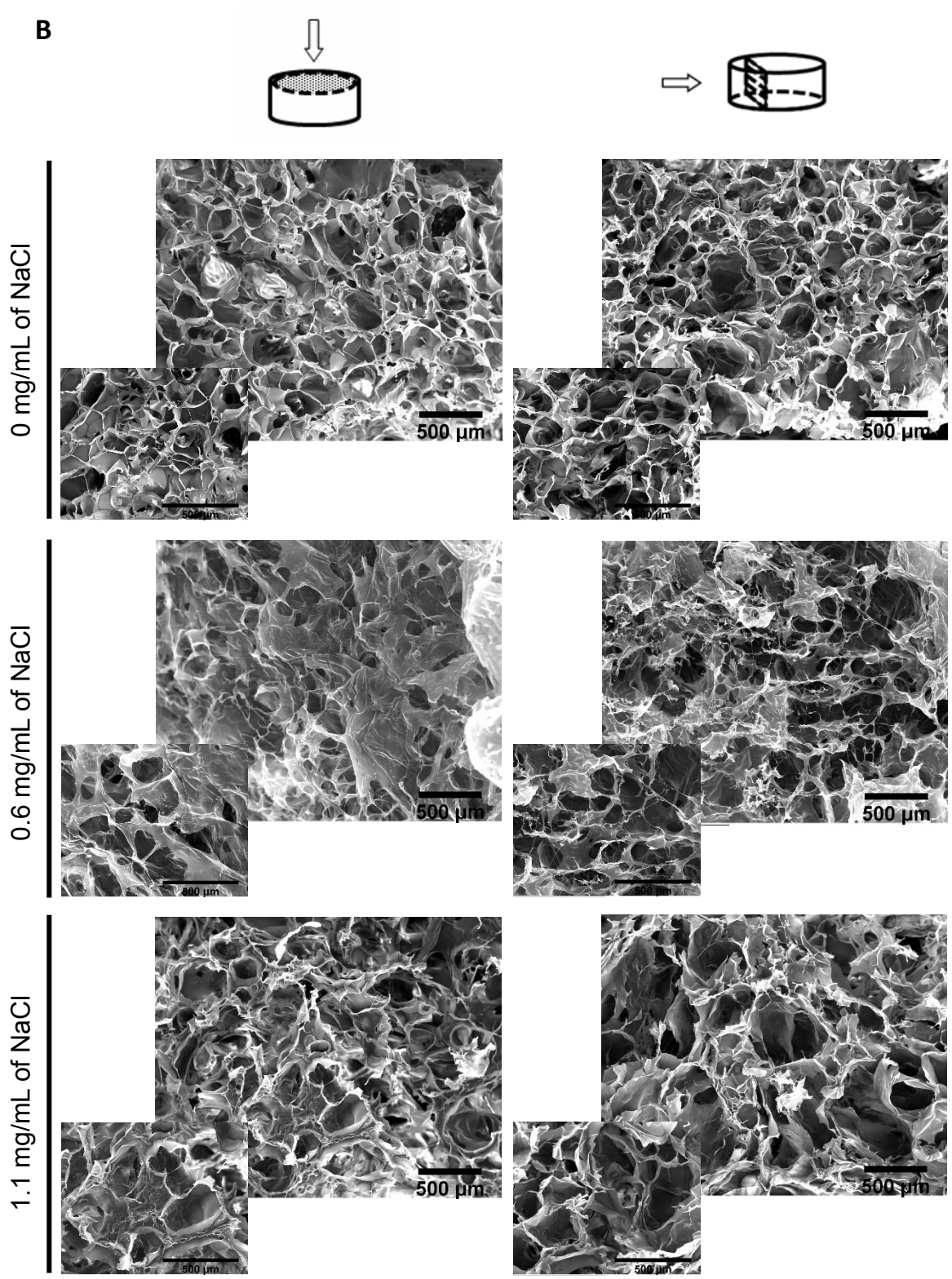

	4 wt.%	4 wt.% + 0.6 mg/mL	4 wt.% + 1.1 mg/mL
Average pore diameter (µm)	230.21 ± 70.44	231.97 ± 74.67	273.99 ± 67.39

Figure 24 - SEM images of the surface and one cross-section of alginate scaffolds prepared with different amounts of NaCl particles (0, 0.6 and 1.1 mg/mL). Scaffolds were prepared with two different alginate concentration A) 2 wt.% and B) 4 wt.%., with the respective pore size quantification (n=1). Scale bar: 500 µm.

- This page was intentionally left blank -

CONCLUDING REMARKS AND FUTURE PERSPECTIVES

Metastatic breast cancer is the most advanced stage of this type of cancer and profoundly affects woman daily life. Breast metastases are frequently found in the bones, liver, brain or lungs. While it is well established that tumor vascularization has a key role in metastisation, the underlying mechanisms remain poorly understood. This is partially due to the lack of adequate models to study these processes. An increasing number of cancer studies are now using 3D culture models as an intermediate step between the simplicity of 2D *in* vitro models and the complexity of *in vivo* animal models. Tissue engineering strategies provide a useful tool and have been widely used to develop advanced 3D models both for studies on angiogenesis and tumor morphogenesis. Yet integrative 3D models for studying tumor angiogenesis and cancer cells-ECs interactions are still scarce.

In this thesis we first focused on the development of 3D porous scaffolds to generate vascularized 3D constructs. This study revealed that the freeze-drying technique allowed the formation of disc-shaped alginate-based scaffolds with a sponge appearance and high porosity. OECs and mammary fibroblasts were able to adhere and spread within the scaffold and secrete extracellular matrix proteins. Furthermore, we concluded that the simultaneous seeding of both type of cells at the lower cellular density represented the best set-up, allowing the formation of tubular-like structures that were detected after 2 weeks of culture.

Secondly, we developed a 3D *in vitro* system by culturing human breast epithelial cells with different tumorigenic capacities within a soft RGD-modified alginate hydrogel. We concluded that the three cell lines formed spheroids with different characteristics. When cultured in this 3D system, MDA-MB-231 cells retained their mesenchymal-like phenotype, due to the lack of E-cadherin and β-catenin which is characteristic of this metastatic and invasive cell line. On the other hand, MCF10A and MCF7 established a stable cell-cell interaction within the 3D spheroids, characterized by the expression of both cell-cell junction markers. Additionally, we concluded that entrapment of MCF10A in soft RGD-alginate hydrogels promoted epithelial morphogenesis. This might be particularly interesting in itself, as the system could be used as a model to study normal epithelial morphogenesis and functional aspects of the human mammary gland. The inter-conversion between epithelial and mesenchymal states during TGF-β1-induced EMT could also be studied using this 3D matrix, as previously done in our group using murine mammary epithelial cells[142].

A 3D tri-culture platform was then developed by combining the vascularized porous scaffold with hydrogel-embedded breast epithelial cells. Although epithelial cells embedded within the hydrogel were able to form spheroids after 1 week of culture, a significant amount of cell-laden gel precursor solution was not able to efficiently penetrate the pores of the scaffold, forming a hydrogel at the surface. Due to this it was not possible to obtain a uniform distribution of the spheroids throughout the porous scaffold. Unfortunately, these experiments could not be repeated, due to time limitations, and so no solid conclusions about the effect of vascularization on spheroid formation could be taken. Future studies should be focused on the repetition and improvement of these experiments. For example, possible strategies to improve the infiltration of the cell-laden hydrogel through the scaffold could be i) delaying the onset of gelation and/or ii) optimizing the scaffold architecture (pore size and volume percentage of porosity), as previously mentioned. One way to improve scaffold architecture would be by tailoring the freezing conditions and/or by using porogen agents. In alternative other fabrication techniques could be explored, such as 3D printing, which provides much better control over scaffolds architecture and porosity[57,165].

Many other relevant aspects could be further investigated in the future using this 3D platform. For example, study the crosstalk between cells in different EMT states and vascular cells. We could induce the transition of epithelial cells along EMT/MET with TGF-β1 as previously described,[142] to generate cells in the other states (i.e. mesenchymal-like cells and reverted epithelial cells), and then evaluate the effect of vascularization on those stages. Due to platform compartmentalization, the 3D microenvironments can be optimized to each cell type to ensure optimal conditions for cell growth and maintenance. Furthermore, in the future, this bioengineered platform could be explored with primary patient-derived cells, in a precision medicine context.

Overall, continued advances in vascularized tumor models are expected to provide tools to identify novel therapeutic targets and more effective treatment options for breast cancer.

- This page was intentionally left blank -

REFERENCES

1. Huang, J., Li, H. & Ren, G. Epithelial-mesenchymal transition and drug resistance in breast cancer (Review). *International Journal of Oncology* **47,** 840–848 (2015).

2. Cheng, H. W. *et al.* Cancer cells increase endothelial cell tube formation and survival by activating the PI3K/Akt signalling pathway. *J. Exp. Clin. Cancer Res.* **36,** 1–13 (2017).

3. Ribatti, D. Epithelial-mesenchymal transition in morphogenesis, cancer progression and angiogenesis. *Experimental Cell Research* **353,** 1–5 (2017).

4. Flamini, V., Jiang, W. G., Lane, J. & Cui, Y. X. Significance and therapeutic implications of endothelial progenitor cells in angiogenic-mediated tumour metastasis. *Critical Reviews in Oncology/Hematology* **100,** 177–189 (2016).

5. Staton, C. A., Reed, M. W. R. & Brown, N. J. A critical analysis of current in vitro and in vivo angiogenesis assays. *International Journal of Experimental Pathology* **90,** 195–221 (2009).

6. Gill, B. J. & West, J. L. Modeling the tumor extracellular matrix: Tissue engineering tools repurposed towards new frontiers in cancer biology. *J. Biomech.* **47,** 1969–1978 (2014).

7. Bissell, M. J. & Radisky, D. Putting tumours in context. *Nat. Rev. Cancer* **1,** 46–54 (2001).

8. Erler, J. T. & Weaver, V. M. Three-dimensional context regulation of metastasis. *Clinical and Experimental Metastasis* **26,** 35–49 (2009).

9. Mintz, B. & Illmensee, K. Normal genetically mosaic mice produced from malignant teratocarcinoma cells. *Proc. Natl. Acad. Sci. U. S. A.* **72,** 3585–9 (1975).

10. Allen, M. & Louise Jones, J. Jekyll and Hyde: the role of the microenvironment on the progression of cancer. *J. Pathol.* **223,** 163–177 (2011).

11. Krause, S., Maffini, M. V, Soto, A. M. & Sonnenschein, C. The microenvironment determines the breast cancer cells' phenotype: Organization of MCF7 cells in 3D cultures. *BMC Cancer* **10,** 263 (2010).

12. Bissell, M. J., Radisky, D. C., Rizki, A., Weaver, V. M. & Petersen, O. W. The organizing principle: Microenvironmental influences in the normal and malignant breast. *Differentiation* **70,** 537–546 (2002).

13. Wang, C. *et al.* Three-dimensional in vitro cancer models: A short review. *Biofabrication* **6,** 022001 (2014).

14. Szot, C. S., Buchanan, C. F., Freeman, J. W. & Rylander, M. N. 3D in vitro bioengineered tumors based on collagen I hydrogels. *Biomaterials* **32,** 7905–7912 (2011).

15. Santos, E., Hernández, R. M., Pedraz, J. L. & Orive, G. Novel advances in the design of three-dimensional bio-scaffolds to control cell fate: Translation from 2D

to 3D. *Trends in Biotechnology* **30,** 331–341 (2012).

16. Chitcholtan, K., Asselin, E., Parent, S., Sykes, P. H. & Evans, J. J. Differences in growth properties of endometrial cancer in three dimensional (3D) culture and 2D cell monolayer. *Exp. Cell Res.* **319,** 75–87 (2013).

17. Carvalho, M. R., Lima, D., Reis, R. L., Correlo, V. M. & Oliveira, J. M. Evaluating Biomaterial- and Microfluidic-Based 3D Tumor Models. *Trends in Biotechnology* **33,** 667–678 (2015).

18. Weaver, V. M. *et al.* Reversion of the Malignant Phenotype of Human Breast Cells in Three-Dimensional Culture and In Vivo by Integrin Blocking Antibodies. *J. Cell Biol.* **137,** 231–245 (1997).

19. Huang, H., Ding, Y., Sun, X. S. & Nguyen, T. A. Peptide Hydrogelation and Cell Encapsulation for 3D Culture of MCF-7 Breast Cancer Cells. *PLoS One* **8,** e59482 (2013).

20. Jeanes, A. I., Maya-Mendoza, A. & Streuli, C. H. Cellular microenvironment influences the ability of mammary epithelia to undergo cell cycle. *PLoS One* **6,** e18144 (2011).

21. Chitcholtan, K., Sykes, P. H. & Evans, J. J. The resistance of intracellular mediators to doxorubicin and cisplatin are distinct in 3D and 2D endometrial cancer. *J. Transl. Med.* **10,** 38 (2012).

22. Luca, A. C. *et al.* Impact of the 3D Microenvironment on Phenotype, Gene Expression, and EGFR Inhibition of Colorectal Cancer Cell Lines. *PLoS One* **8,** e59689 (2013).

23. Tung, Y. C. *et al.* High-throughput 3D spheroid culture and drug testing using a 384 hanging drop array. *Analyst* **136,** 473–478 (2011).

24. Faute, M. A. D. *et al.* Distinctive alterations of invasiveness, drug resistance and cell-cell organization in 3D-cultures of MCF-7, a human breast cancer cell line, and its multidrug resistant variant. *Clin. Exp. Metastasis* **19,** 161–168 (2002).

25. Wang, F. *et al.* Reciprocal interactions between 1-integrin and epidermal growth factor receptor in three-dimensional basement membrane breast cultures: A different perspective in epithelial biology. *Proc. Natl. Acad. Sci.* **95,** 14821–14826 (1998).

26. Fallica, B., Maffei, J. S., Villa, S., Makin, G. & Zaman, M. Alteration of Cellular Behavior and Response to PI3K Pathway Inhibition by Culture in 3D Collagen Gels. *PLoS One* **7,** e48024 (2012).

27. Hongisto, V. *et al.* High-Throughput 3D Screening Reveals Differences in Drug Sensitivities between Culture Models of JIMT1 Breast Cancer Cells. *PLoS One* **8,** e77232 (2013).

28. Gurski, L. A., Petrelli, N. J., Jia, X. & Farach-carson, M. C. 3D Matrices for Anti-Cancer Drug Testing and Development. *Oncol. Issues* **25,** 20–25 (2010).

29. Edmondson, R., Broglie, J. J., Adcock, A. F. & Yang, L. Three-dimensional cell

culture systems and their applications in drug discovery and cell-based biosensors. *Assay Drug Dev. Technol.* **12,** 207–18 (2014).

30. Jong, B. K. Three-dimensional tissue culture models in cancer biology. *Seminars in Cancer Biology* **15,** 365–377 (2005).

31. Baker, B. M. & Chen, C. S. Deconstructing the third dimension – how 3D culture microenvironments alter cellular cues. *J. Cell Sci.* **125,** 3015–3024 (2012).

32. Xu, X. *et al.* Recreating the tumor microenvironment in a bilayer, hyaluronic acid hydrogel construct for the growth of prostate cancer spheroids. *Biomaterials* **33,** 9049–9060 (2012).

33. Yip, D. & Cho, C. H. A multicellular 3D heterospheroid model of liver tumor and stromal cells in collagen gel for anti-cancer drug testing. *Biochem. Biophys. Res. Commun.* **433,** 327–332 (2013).

34. Tibbitt, M. W. & Anseth, K. S. Hydrogels as extracellular matrix mimics for 3D cell culture. *Biotechnology and Bioengineering* **103,** 655–663 (2009).

35. Trédan, O., Galmarini, C. M., Patel, K. & Tannock, I. F. Drug resistance and the solid tumor microenvironment. *Journal of the National Cancer Institute* **99,** 1441–1454 (2007).

36. Price, K. J. *et al.* Matrigel Basement Membrane Matrix influences expression of microRNAs in cancer cell lines. *Biochem. Biophys. Res. Commun.* **427,** 343–348 (2012).

37. Fischbach, C. *et al.* Engineering tumors with 3D scaffolds. *Nat. Methods* **4,** 855–860 (2007).

38. Nelson, C. M. & Bissell, M. J. Modeling dynamic reciprocity: Engineering three-dimensional culture models of breast architecture, function, and neoplastic transformation. *Seminars in Cancer Biology* **15,** 342–352 (2005).

39. Nelson, C. M., Inman, J. L. & Bissell, M. J. Three-dimensional lithographically defined organotypic tissue arrays for quantitative analysis of morphogenesis and neoplastic progression. *Nat. Protoc.* **3,** 674–678 (2008).

40. Verbridge, S. S. *et al.* Oxygen-controlled three-dimensional cultures to analyze tumor angiogenesis. *Tissue Eng. Part A* **16,** 2133–41 (2010).

41. Raof, N. A., Raja, W. K., Castracane, J. & Xie, Y. Bioengineering embryonic stem cell microenvironments for exploring inhibitory effects on metastatic breast cancer cells. *Biomaterials* **32,** 4130–4139 (2011).

42. Cross, V. L. *et al.* Dense type I collagen matrices that support cellular remodeling and microfabrication for studies of tumor angiogenesis and vasculogenesis in vitro. *Biomaterials* **31,** 8596–8607 (2010).

43. Ruoslahti, E. RGD AND OTHER RECOGNITION SEQUENCES FOR INTEGRINS. *Annu. Rev. Cell Dev. Biol.* **12,** 697–715 (1996).

44. Fonseca, K. B., Bidarra, S. J., Oliveira, M. J., Granja, P. L. & Barrias, C. C. Molecularly designed alginate hydrogels susceptible to local proteolysis as three-

dimensional cellular microenvironments. *Acta Biomater.* **7,** 1674–82 (2011).

45. Chwalek, K. *et al.* Two-tier hydrogel degradation to boost endothelial cell morphogenesis. *Biomaterials* **32,** 9649–9657 (2011).

46. Silva, A. K. A., Richard, C., Bessodes, M., Scherman, D. & Merten, O. W. Growth factor delivery approaches in hydrogels. *Biomacromolecules* **10,** 9–18 (2009).

47. Hillen, F. & Griffioen, A. W. Tumour vascularization: Sprouting angiogenesis and beyond. *Cancer and Metastasis Reviews* **26,** 489–502 (2007).

48. Lovett, M., Lee, K., Edwards, A. & Kaplan, D. L. Vascularization Strategies for Tissue Engineering. *Tissue Eng. Part B Rev.* **15,** 353–370 (2009).

49. Bray, L. J. & Werner, C. Evaluation of Three-Dimensional in Vitro Models to Study Tumor Angiogenesis. *ACS Biomater. Sci. Eng.* **4,** acsbiomaterials.7b00139 (2017).

50. V, B. & G, C. The angiogenic switch in carcinogenesis. *Semin Cancer Biol* **19,** 329–37 (2009).

51. Van Zijl, F., Krupitza, G. & Mikulits, W. Initial steps of metastasis: Cell invasion and endothelial transmigration. *Mutation Research - Reviews in Mutation Research* **728,** 23–34 (2011).

52. Levental, K. R. *et al.* Matrix Crosslinking Forces Tumor Progression by Enhancing Integrin Signaling. *Cell* **139,** 891–906 (2009).

53. Feng, X., Tonnesen, M. G., Mousa, S. A. & Clark, R. A. F. Fibrin and collagen differentially but synergistically regulate sprout angiogenesis of human dermal microvascular endothelial cells in 3-dimensional matrix. *Int. J. Cell Biol.* **2013,** 231279 (2013).

54. Chwalek, K., Tsurkan, M. V, Freudenberg, U. & Werner, C. Glycosaminoglycan-based hydrogels to modulate heterocellular communication in in vitro angiogenesis models. *Sci. Rep.* **4,** (2014).

55. Liu, J. *et al.* Soft fibrin gels promote selection and growth of tumorigenic cells. *Nat. Mater.* **11,** 734–741 (2012).

56. Tian, L. & George, S. C. Biomaterials to prevascularize engineered tissues. *Journal of Cardiovascular Translational Research* **4,** 685–698 (2011).

57. Loh, Q. L. & Choong, C. Three-Dimensional Scaffolds for Tissue Engineering Applications: Role of Porosity and Pore Size. *Tissue Eng. Part B Rev.* **19,** 485–502 (2013).

58. Fu, J. & Wang, D. A. In Situ Organ-Specific Vascularization in Tissue Engineering. *Trends in Biotechnology* **36,** 834–849 (2018).

59. Marshall, A. *et al.* Biomaterials with tightly controlled pore size that promote vascular in-growth. *ACS Polym. Prepr.* **45,** 100–101 (2004).

60. Lee, K. W., Wang, S., Dadsetan, M., Yaszemski, M. J. & Lu, L. Enhanced cell ingrowth and proliferation through three-dimensional nanocomposite scaffolds

with controlled pore structures. *Biomacromolecules* **11,** 682–689 (2010).

61. Kang, Y., Kim, S., Fahrenholtz, M., Khademhosseini, A. & Yang, Y. Osteogenic and angiogenic potentials of monocultured and co-cultured human-bone-marrow-derived mesenchymal stem cells and human-umbilical-vein endothelial cells on three-dimensional porous beta-tricalcium phosphate scaffold. *Acta Biomater.* **9,** 4906–4915 (2013).

62. Kook, Y.-M. *et al.* Promotion of Vascular Morphogenesis of Endothelial Cells Co-Cultured with Human Adipose-Derived Mesenchymal Stem Cells Using Polycaprolactone/Gelatin Nanofibrous Scaffolds. *Nanomaterials* **8,** 117 (2018).

63. Fuchs, S., Motta, A., Migliaresi, C. & Kirkpatrick, C. J. Outgrowth endothelial cells isolated and expanded from human peripheral blood progenitor cells as a potential source of autologous cells for endothelialization of silk fibroin biomaterials. *Biomaterials* **27,** 5399–5408 (2006).

64. Dziubla, T. D. & Lowman, A. M. Vascularization of PEG-grafted macroporous hydrogel sponges: A three-dimensional in vitro angiogenesis model using human microvascular endothelial cells. *J. Biomed. Mater. Res. - Part A* **68,** 603–614 (2004).

65. Sun, X. *et al.* Electrospun Photocrosslinkable Hydrogel Fibrous Scaffolds for Rapid In Vivo Vascularized Skin Flap Regeneration. *Adv. Funct. Mater.* **27,** 1604617 (2017).

66. Marchioli, G. *et al.* Fabrication of three-dimensional bioplotted hydrogel scaffolds for islets of Langerhans transplantation. *Biofabrication* **7,** 025009 (2015).

67. Zhao, X. *et al.* In vitro vascularization of a combined system based on a 3D printing technique. *J. Tissue Eng. Regen. Med.* **10,** 833–842 (2016).

68. Liu Tsang, V. & Bhatia, S. N. Three-dimensional tissue fabrication. *Advanced Drug Delivery Reviews* **56,** 1635–1647 (2004).

69. Yeong, W. Y., Chua, C. K., Leong, K. F. & Chandrasekaran, M. Rapid prototyping in tissue engineering: Challenges and potential. *Trends in Biotechnology* **22,** 643–652 (2004).

70. Leong, K. F., Chua, C. K., Sudarmadji, N. & Yeong, W. Y. Engineering functionally graded tissue engineering scaffolds. *Journal of the Mechanical Behavior of Biomedical Materials* **1,** 140–152 (2008).

71. Leong, K. F., Cheah, C. M. & Chua, C. K. Solid freeform fabrication of three-dimensional scaffolds for engineering replacement tissues and organs. *Biomaterials* **24,** 2363–2378 (2003).

72. Chu, T. M. G., Orton, D. G., Hollister, S. J., Feinberg, S. E. & Halloran, J. W. Mechanical and in vivo performance of hydroxyapatite implants with controlled architectures. *Biomaterials* **23,** 1283–1293 (2002).

73. Sherwood, J. K. *et al.* A three-dimensional osteochondral composite scaffold for articular cartilage repair. *Biomaterials* **23,** 4739–4751 (2002).

74. Yang, S., Leong, K.-F., Du, Z. & Chua, C.-K. The Design of Scaffolds for Use in Tissue Engineering. Part II. Rapid Prototyping Techniques. *Tissue Eng.* **8,** 1–11 (2002).

75. Silva, G. A. *et al.* Selective Differentiation of Neural Progenitor Cells by High-Epitope Density Nanofibers. *Science (80-.).* **303,** 1352–1355 (2004).

76. Nichol, J. W. & Khademhosseini, A. Modular tissue engineering: Engineering biological tissues from the bottom up. *Soft Matter* **5,** 1312–1319 (2009).

77. Li, C., Vepari, C., Jin, H. J., Kim, H. J. & Kaplan, D. L. Electrospun silk-BMP-2 scaffolds for bone tissue engineering. *Biomaterials* **27,** 3115–3124 (2006).

78. Griffon, D. J., Sedighi, M. R., Schaeffer, D. V., Eurell, J. A. & Johnson, A. L. Chitosan scaffolds: Interconnective pore size and cartilage engineering. *Acta Biomater.* **2,** 313–320 (2006).

79. Kim, H. J., Kim, U. J., Vunjak-Novakovic, G., Min, B. H. & Kaplan, D. L. Influence of macroporous protein scaffolds on bone tissue engineering from bone marrow stem cells. *Biomaterials* **26,** 4442–4452 (2005).

80. Druecke, D. *et al.* Neovascularization of poly(ether ester) block-copolymer scaffolds in vivo: Long-term investigations using intravital fluorescent microscopy. *J. Biomed. Mater. Res. - Part A* **68,** 10–18 (2004).

81. Mastrogiacomo, M. *et al.* Role of scaffold internal structure on in vivo bone formation in macroporous calcium phosphate bioceramics. *Biomaterials* **27,** 3230–3237 (2006).

82. Lu, J. X. *et al.* Role of interconnections in porous bioceramics on bone recolonization in vitro and in vivo. *J. Mater. Sci. Mater. Med.* **10,** 111–120 (1999).

83. Kuboki, Y., Jin, Q., Kikuchi, M., Mamood, J. & Takita, H. Geometry of Artificial ECM: Sizes of Pores Controlling Phenotype Expression in BMP-Induced Osteogenesis and Chondrogenesis. *Connect. Tissue Res.* **43,** 529–534 (2002).

84. Kuboki, Y., Jin, Q. & Takita, H. Geometry of carriers controlling phenotypic expression in BMP-induced osteogenesis and chondrogenesis. *J. Bone Joint Surg. Am.* **83–A Suppl,** S105–S115 (2001).

85. Karageorgiou, V. & Kaplan, D. Porosity of 3D biomaterial scaffolds and osteogenesis. *Biomaterials* **26,** 5474–5491 (2005).

86. Henry, J. A., Burugapalli, K., Neuenschwander, P. & Pandit, A. Structural variants of biodegradable polyesterurethane in vivo evoke a cellular and angiogenic response that is dictated by architecture. *Acta Biomater.* **5,** 29–42 (2009).

87. Lu, T., Li, Y. & Chen, T. Techniques for fabrication and construction of three-dimensional scaffolds for tissue engineering. *International Journal of Nanomedicine* **8,** 337–350 (2013).

88. Subia, B., Kundu, J. & C., S. in *Tissue Engineering* (2010). doi:10.5772/8581

89. Abdelaal, O. A. M. & Darwish, S. M. H. Review of rapid prototyping techniques for tissue engineering scaffolds fabrication. *Adv. Struct. Mater.* **29,** 33–54 (2013).

90. Peltola, S. M., Melchels, F. P. W., Grijpma, D. W. & Kellomäki, M. A review of rapid prototyping techniques for tissue engineering purposes. *Annals of Medicine* **40,** 268–280 (2008).

91. El-Sherbiny, I. & Yacoub, M. Hydrogel scaffolds for tissue engineering: Progress and challenges. *Glob. Cardiol. Sci. Pract.* **2013,** 316–42 (2013).

92. Hebner, C., Weaver, V. M. & Debnath, J. Modeling Morphogenesis and Oncogenesis in Three-Dimensional Breast Epithelial Cultures. *Annu. Rev. Pathol. Mech. Dis.* **3,** 070920153408001 (2007).

93. Davis, G. E. & Camarillo, C. W. An α2β1 integrin-dependent pinocytic mechanism involving intracellular vacuole formation and coalescence regulates capillary lumen and tube formation in three-dimensional collagen matrix. *Exp. Cell Res.* **224,** 39–51 (1996).

94. Katanasaka, Y., Asai, T., Naitou, H., Ohashi, N. & Oku, N. Proteomic characterization of angiogenic endothelial cells stimulated with cancer cell-conditioned medium. *Biol. Pharm. Bull.* **30,** 2300–7 (2007).

95. Buchanan, C. F. *et al.* Cross-talk between endothelial and breast cancer cells regulates reciprocal expression of angiogenic factors in vitro. *J. Cell. Biochem.* **113,** 1142–1151 (2012).

96. Nakatsu, M. N., Davis, J. & Hughes, C. C. W. Optimized Fibrin Gel Bead Assay for the Study of Angiogenesis. *J. Vis. Exp.* 186 (2007). doi:10.3791/186

97. Janvier, R., Sourla, A., Koutsilieris, M. & Doillon, C. J. Stromal fibroblasts are required for PC-3 human prostate cancer cells to produce capillary-like formation of endothelial cells in a three-dimensional co-culture system. *Anticancer Res.* **17,** 1551–1557 (1997).

98. Correa de Sampaio, P. *et al.* A heterogeneous in vitro three dimensional model of tumour-stroma interactions regulating sprouting angiogenesis. *PLoS One* **7,** e30753 (2012).

99. Szot, C. S., Buchanan, C. F., Freeman, J. W. & Rylander, M. N. In Vitro Angiogenesis Induced by Tumor-Endothelial Cell Co-Culture in Bilayered, Collagen I Hydrogel Bioengineered Tumors. *Tissue Eng. Part C Methods* **19,** 864–874 (2013).

100. Lochter, A. *et al.* Matrix metalloproteinase stromelysin-1 triggers a cascade of molecular alterations that leads to stable epithelial-to-mesenchymal conversion and a premalignant phenotype in mammary epithelial cells. *J. Cell Biol.* **139,** 1861–1872 (1997).

101. Weigelt, B., Ghajar, C. M. & Bissell, M. J. The need for complex 3D culture models to unravel novel pathways and identify accurate biomarkers in breast cancer. *Advanced Drug Delivery Reviews* **69–70,** 42–51 (2014).

102. Mukai, N. *et al.* A comparison of the tube forming potentials of early and late endothelial progenitor cells. *Exp. Cell Res.* **314,** 430–440 (2008).

103. Shekhar, M. P. V., Werdell, J. & Tait, L. Interaction with endothelial cells is a

prerequisite for branching ductal-alveolar morphogenesis and hyperplasia of preneoplastic human breast epithelial cells: Regulation by estrogen. *Cancer Res.* **60,** 439–449 (2000).

104. Shekhar, M. P. V, Werdell, J., Santner, S. J., Pauley, R. J. & Tait, L. Breast stroma plays a dominant regulatory role in breast epithelial growth and differentiation: Implications for tumor development and progression. *Cancer Res.* **61,** 1320–1326 (2001).

105. Walter-Yohrling, J., Pratt, B. M., Ledbetter, S. & Teicher, B. A. Myofibroblasts enable invasion of endothelial cells into three-dimensional tumor cell clusters: A novel in vitro tumor model. *Cancer Chemother. Pharmacol.* **52,** 263–269 (2003).

106. Freudenberg, U. *et al.* A star-PEG-heparin hydrogel platform to aid cell replacement therapies for neurodegenerative diseases. *Biomaterials* **30,** 5049–5060 (2009).

107. Prokoph, S. *et al.* Sustained delivery of SDF-1α from heparin-based hydrogels to attract circulating pro-angiogenic cells. *Biomaterials* **33,** 4792–4800 (2012).

108. Zieris, A. *et al.* FGF-2 and VEGF functionalization of starPEG-heparin hydrogels to modulate biomolecular and physical cues of angiogenesis. *Biomaterials* **31,** 7985–7994 (2010).

109. Chwalek, K., Tsurkan, M. V., Freudenberg, U. & Werner, C. Glycosaminoglycan-based hydrogels to modulate heterocellular communication in in vitro angiogenesis models. *Sci. Rep.* **4,** 4414 (2014).

110. Bray, L. J. *et al.* Multi-parametric hydrogels support 3D invitro bioengineered microenvironment models of tumour angiogenesis. *Biomaterials* **53,** 609–620 (2015).

111. Nguyen, D. T., Fan, Y., Akay, Y. M. & Akay, M. TNP-470 reduces glioblastoma angiogenesis in three dimensional Gel MA microwell platform. *IEEE Trans. Nanobioscience* **15,** 683–688 (2016).

112. Nguyen, D. T., Fan, Y., Akay, Y. M. & Akay, M. Investigating Glioblastoma Angiogenesis Using A 3D in Vitro GelMA Microwell Platform. *IEEE Trans. Nanobioscience* **15,** 289–293 (2016).

113. Roudsari, L. C., Jeffs, S. E. & West, J. L. Lung Adenocarcinoma Cell Responses in a 3D in Vitro Tumor Angiogenesis Model Correlate with Metastatic Capacity. *ACS Biomater. Sci. Eng.* **4,** 368–377 (2018).

114. Roudsari, L. C., Jeffs, S. E., Witt, A. S., Gill, B. J. & West, J. L. A 3D Poly(ethylene glycol)-based Tumor Angiogenesis Model to Study the Influence of Vascular Cells on Lung Tumor Cell Behavior. *Sci. Rep.* **6,** 32726 (2016).

115. Seano, G. *et al.* Modeling human tumor angiogenesis in a three-dimensional culture system. *Blood* **121,** e129–e137 (2013).

116. Moll, C. *et al.* Tissue engineering of a human 3D in vitro tumor test system. *J. Vis. Exp.* 2–7 (2013). doi:10.3791/50460

117. Buchanan, C. F. *et al.* Three-Dimensional Microfluidic Collagen Hydrogels for Investigating Flow-Mediated Tumor-Endothelial Signaling and Vascular Organization. *Tissue Eng. Part C Methods* **20,** 64–75 (2014).

118. Smith, S. J., Ward, J. H., Tan, C., Grundy, R. G. & Rahman, R. Endothelial-like malignant glioma cells in dynamic three dimensional culture identifies a role for VEGF and FGFR in a tumor-derived angiogenic response. *Oncotarget* **6,** 22191–22205 (2015).

119. Dai, X., Ma, C., Lan, Q. & Xu, T. 3D bioprinted glioma stem cells for brain tumor model and applications of drug susceptibility. *Biofabrication* **8,** 045005 (2016).

120. Torres, A. L. *et al.* Guiding morphogenesis in cell-instructive microgels for therapeutic angiogenesis. *Biomaterials* **154,** 34–47 (2018).

121. Rowley, J. A., Madlambayan, G. & Mooney, D. J. Alginate hydrogels as synthetic extracellular matrix materials. *Biomaterials* **20,** 45–53 (1999).

122. Maia, F. R., Fonseca, K. B., Rodrigues, G., Granja, P. L. & Barrias, C. C. Matrix-driven formation of mesenchymal stem cell-extracellular matrix microtissues on soft alginate hydrogels. *Acta Biomater.* **10,** 3197–3208 (2014).

123. Bidarra, S. J. *et al.* Injectable in situ crosslinkable RGD-modified alginate matrix for endothelial cells delivery. *Biomaterials* **32,** 7897–7904 (2011).

124. Lemos, E. E. M. F., Patrício, P. S. O. & Pereira, M. M. 3D nanocomposite chitosan/bioactive glass scaffolds obtained using two different routes: An evaluation of the Porous structure and mechanical properties. *Quim. Nova* **39,** 462–466 (2016).

125. Lee, K. Y. & Mooney, D. J. Alginate: properties and biomedical applications. *Prog. Polym. Sci.* **37,** 106–126 (2012).

126. O'Brien, F. J., Harley, B. A., Yannas, I. V & Gibson, L. Influence of freezing rate on pore structure in freeze-dried collagen-GAG scaffolds. *Biomaterials* **25,** 1077–1086 (2004).

127. Sun, K., Li, R., Jiang, W., Sun, Y. & Li, H. Comparison of three-dimensional printing and vacuum freeze-dried techniques for fabricating composite scaffolds. *Biochem. Biophys. Res. Commun.* **477,** 1085–1091 (2016).

128. Zhang, Y., Wang, C., Jiang, W., Zuo, W. & Han, G. Influence of Stage Cooling Method on Pore Architecture of Biomimetic Alginate Scaffolds. *Sci. Rep.* **7,** 16150 (2017).

129. Tsuruga, E., Takita, H., Itoh, H., Wakisaka, Y. & Kuboki, Y. Pore size of porous hydroxyapatite as the cell-substratum controls BMP-induced osteogenesis. *J. Biochem.* **121,** 317–324 (1997).

130. Unger, R. E. *et al.* Tissue-like self-assembly in cocultures of endothelial cells and osteoblasts and the formation of microcapillary-like structures on three-dimensional porous biomaterials. *Biomaterials* **28,** 3965–3976 (2007).

131. Ghajar, C. M., Blevins, K. S., Hughes, C. C. W., George, S. C. & Putnam, A. J.

Mesenchymal Stem Cells Enhance Angiogenesis in Mechanically Viable Prevascularized Tissues via Early Matrix Metalloproteinase Upregulation. *Tissue Eng.* **12,** 060928131519005 (2006).

132. Koike, N. *et al.* Creation of long-lasting blood vessels. *Nature* **428,** 138–139 (2004).

133. Levenberg, S. *et al.* Engineering vascularized skeletal muscle tissue. *Nat. Biotechnol.* **23,** 879–884 (2005).

134. Fuchs, S., Hermanns, M. I. & Kirkpatrick, C. J. Retention of a differentiated endothelial phenotype by outgrowth endothelial cells isolated from human peripheral blood and expanded in long-term cultures. *Cell Tissue Res.* **326,** 79–92 (2006).

135. Davis, G. E. & Senger, D. R. Endothelial extracellular matrix: Biosynthesis, remodeling, and functions during vascular morphogenesis and neovessel stabilization. *Circulation Research* **97,** 1093–1107 (2005).

136. Newman, A. C., Nakatsu, M. N., Chou, W., Gershon, P. D. & Hughes, C. C. W. The requirement for fibroblasts in angiogenesis: fibroblast-derived matrix proteins are essential for endothelial cell lumen formation. *Mol. Biol. Cell* **22,** 3791–3800 (2011).

137. Unger, R. E. *et al.* The rapid anastomosis between prevascularized networks on silk fibroin scaffolds generated in vitro with cocultures of human microvascular endothelial and osteoblast cells and the host vasculature. *Biomaterials* **31,** 6959–6967 (2010).

138. Xing, Z., Xue, Y., Finne-Wistrand, A., Yang, Z. Q. & Mustafa, K. Copolymer cell/scaffold constructs for bone tissue engineering: Co-culture of low ratios of human endothelial and osteoblast-like cells in a dynamic culture system. *J. Biomed. Mater. Res. - Part A* **101 A,** 1113–1120 (2013).

139. Ekaputra, A. K., Prestwich, G. D., Cool, S. M. & Hutmacher, D. W. The three-dimensional vascularization of growth factor-releasing hybrid scaffold of poly (ε-caprolactone)/collagen fibers and hyaluronic acid hydrogel. *Biomaterials* **32,** 8108–8117 (2011).

140. Chen, Y. C. *et al.* Functional human vascular network generated in photocrosslinkable gelatin methacrylate hydrogels. *Adv. Funct. Mater.* **22,** 2027–2039 (2012).

141. Buschmann, J. *et al.* Three-Dimensional Co-Cultures of Osteoblasts and Endothelial Cells in DegraPol Foam: Histological and High-Field Magnetic Resonance Imaging Analyses of Pre-Engineered Capillary Networks in Bone Grafts. *Tissue Eng. Part A* **17,** 291–299 (2011).

142. Bidarra, S. J. *et al.* A 3D in vitro model to explore the inter-conversion between epithelial and mesenchymal states during EMT and its reversion. *Sci. Rep.* **6,** 27072 (2016).

143. Huebsch, N. *et al.* Harnessing traction-mediated manipulation of the cell/matrix

interface to control stem-cell fate. *Nat. Mater.* **9,** 518–526 (2010).

144. Thompson, E. A. *et al.* Differential response of MCF7, MDA-MB-231, and MCF 10A cells to hyperthermia, silver nanoparticles and silver nanoparticle-induced photothermal therapy. *Int. J. Hyperth.* **30,** 312–323 (2014).

145. Geltmeier, A. *et al.* Characterization of dynamic behaviour of MCF7 and MCF10A cells in ultrasonic field using modal and harmonic analyses. *PLoS One* **10,** e0134999 (2015).

146. Kenny, P. A. *et al.* The morphologies of breast cancer cell lines in three-dimensional assays correlate with their profiles of gene expression. *Mol. Oncol.* **1,** 84–96 (2007).

147. Tian, X. *et al.* E-Cadherin/β-catenin complex and the epithelial barrier. *Journal of Biomedicine and Biotechnology* **2011,** 567305 (2011).

148. Wang, F. *et al.* Phenotypic reversion or death of cancer cells by altering signaling pathways in three-dimensional contexts. *J. Natl. Cancer Inst.* **94,** 1494–1503 (2002).

149. Tan, R., Wang, L., Song, J., Li, J. & He, T. Expression and significance of Twist, estrogen receptor, and E-cadherin in human breast cancer cells and tissues. *J. Cancer Res. Ther.* **13,** 707 (2017).

150. Xu, J., Prosperi, J. R., Choudhury, N., Olopade, O. I. & Goss, K. H. β-catenin is required for the tumorigenic behavior of triple-negative breast cancer cells. *PLoS One* **10,** e0117097 (2015).

151. Zhang, X. *et al.* MicroRNA-3646 Contributes to Docetaxel Resistance in Human Breast Cancer Cells by GSK-3β/β-Catenin Signaling Pathway. *PLoS One* **11,** e0153194 (2016).

152. Benton, G., Crooke, E. & George, J. Laminin-1 induces E-cadherin expression in 3-dimensional cultured breast cancer cells by inhibiting DNA methyltransferase 1 and reversing promoter methylation status. *FASEB J.* **23,** 3884–95 (2009).

153. Lacroix, M. & Leclercq, G. Relevance of breast cancer cell lines as models for breast tumours: An update. *Breast Cancer Research and Treatment* **83,** 249–289 (2004).

154. Petersen, O. W., Ronnov-Jessen, L., Howlett, A. R. & Bissell, M. J. Interaction with basement membrane serves to rapidly distinguish growth and differentiation pattern of normal and malignant human breast epithelial cells. *Proc. Natl. Acad. Sci.* **89,** 9064–9068 (1992).

155. Fournier, M. V *et al.* Gene expression signature in organized and growth-arrested mammary acini predicts good outcome in breast cancer. *Cancer Res.* **66,** 7095–7102 (2006).

156. Debnath, J., Muthuswamy, S. K. & Brugge, J. S. Morphogenesis and oncogenesis of MCF-10A mammary epithelial acini grown in three-dimensional basement membrane cultures. *Methods* **30,** 256–268 (2003).

157. Chaudhuri, O. *et al.* Extracellular matrix stiffness and composition jointly regulate the induction of malignant phenotypes in mammary epithelium. *Nat. Mater.* **13,** 970–978 (2014).

158. Park, C. C. *et al.* β1 integrin inhibitory antibody induces apoptosis of breast cancer cells, inhibits growth, and distinguishes malignant from normal phenotype in three dimensional cultures and in vivo. *Cancer Res.* **66,** 1526–1535 (2006).

159. Hillen, F. & Griffioen, A. W. Tumour vascularization: sprouting angiogenesis and beyond. *Cancer Metastasis Rev.* **26,** 489–502 (2007).

160. Zmora, S., Glicklis, R. & Cohen, S. Tailoring the pore architecture in 3-D alginate scaffolds by controlling the freezing regime during fabrication. *Biomaterials* **23,** 4087–4094 (2002).

161. van der Heide, D. J., Verbraeken, B., Hoogenboom, R., Dargaville, T. R. & Hickey, D. K. Porous poly (2-oxazoline) scaffolds for developing 3D primary human tissue culture. *Biomater Tissue Technol.* **1,** 1–5 (2017).

162. Davidenko, N. *et al.* Biomimetic collagen scaffolds with anisotropic pore architecture. *Acta Biomater.* **8,** 667–676 (2012).

163. Ma, P. X. & Langer, R. Fabrication of biodegradable polymer foams for cell transplantation and tissue engineering. *Methods Mol. Med.* **18,** 47–56 (1999).

164. Lu, L. *et al.* In vitro and in vivo degradation of porous poly(DL-lactic-co-glycolic acid) foams. *Biomaterials* **21,** 1837–1845 (2000).

165. Plikk, P., Målberg, S. & Albertsson, A. C. Design of resorbable porous tubular copolyester scaffolds for use in nerve regeneration. *Biomacromolecules* **10,** 1259–1264 (2009).

166. Roudsari, L. C. & West, J. L. Studying the influence of angiogenesis in in vitro cancer model systems. *Advanced Drug Delivery Reviews* **97,** 250–259 (2016).

- This page was intentionally left blank -

SUPPLEMENTARY INFORMATION

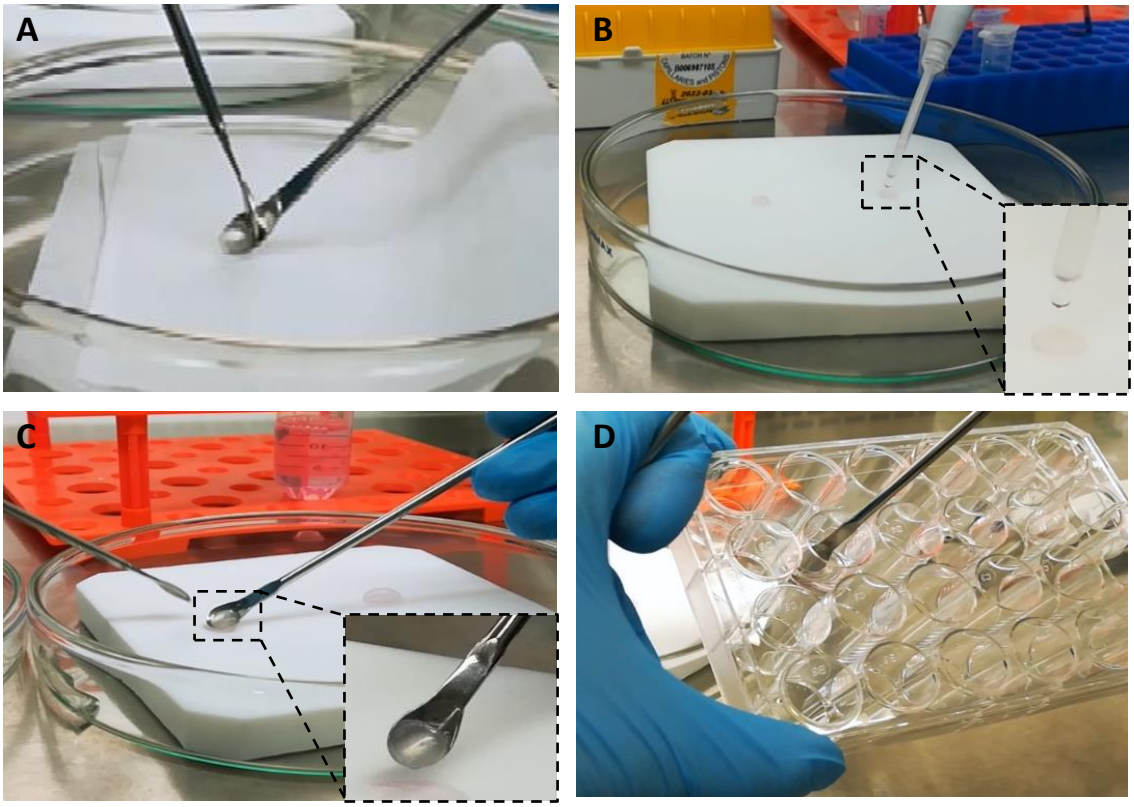

Figure S1 - Experimental procedure for the 3D tri-culture. (A) Placement of the co-cultured scaffold on sterilized filter paper to remove excess culture medium from the pores, then (B) it was placed on top of a Teflon plate and 40 µL of the mixture was applied in small drops on top of it. (C) The Teflon plate with the embedded scaffolds were kept in a petri dish, at 37°C in a 5% v/v CO_2 humidified atmosphere and removed after the gelling time. (D) Being then transferred to a 24-well culture plate and incubated with culture medium at 37°C and after 30 minutes fresh medium was added.

A

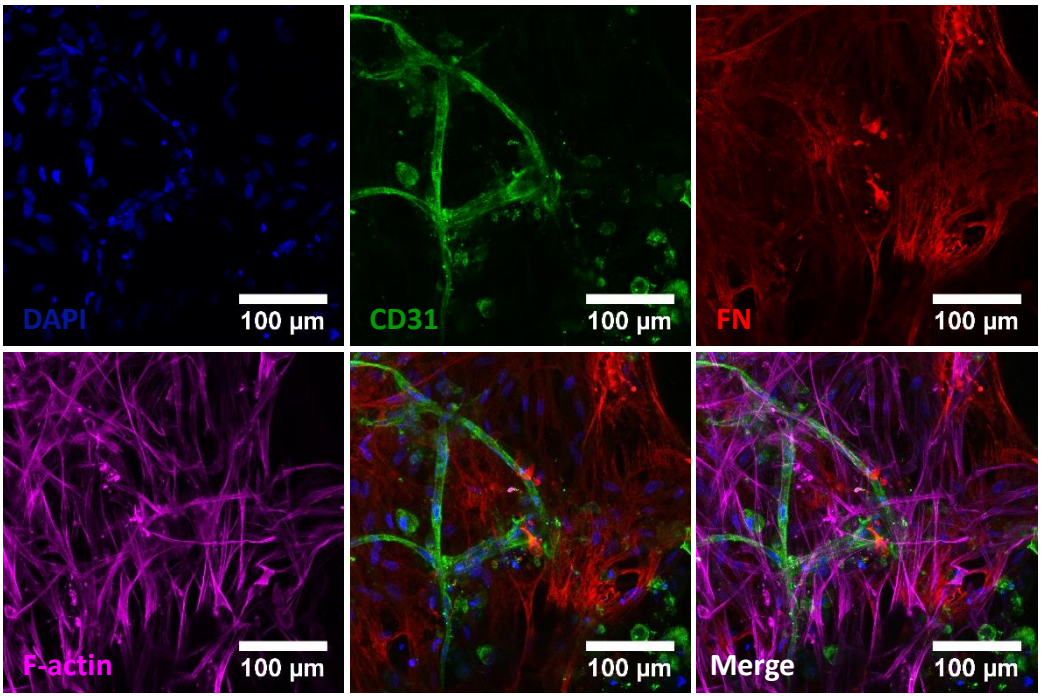
DAPI
100 μm
CD31
100 μm
FN
100 μm
F-actin
100 μm
100 μm
Merge
100 μm

B

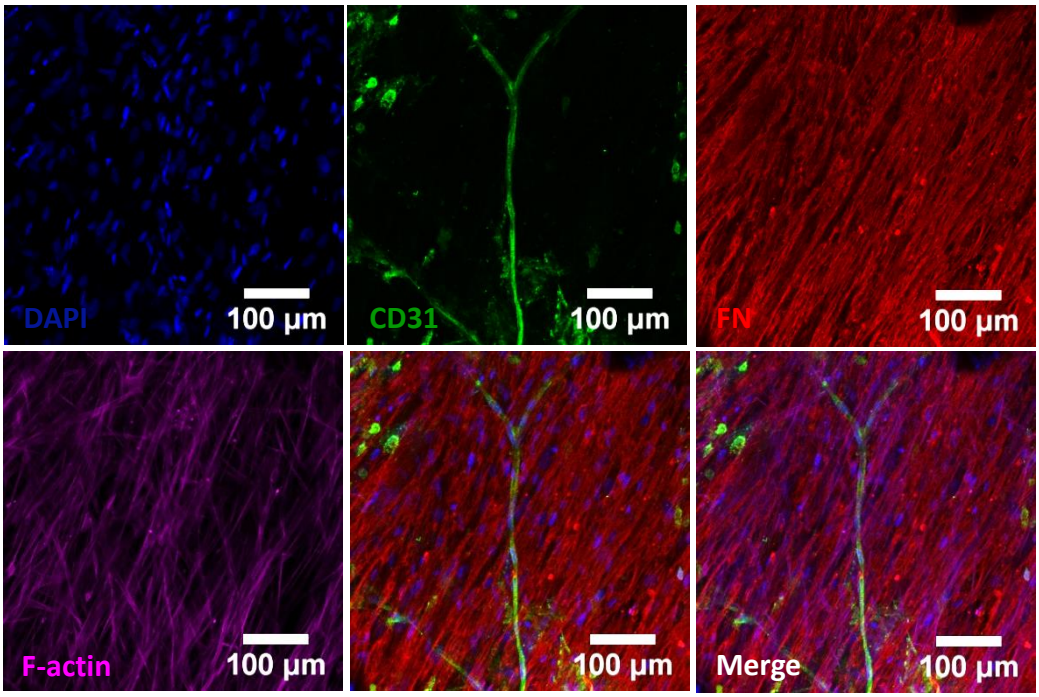
DAPI
100 μm
CD31
100 μm
FN
100 μm
F-actin
100 μm
100 μm
Merge
100 μm

C

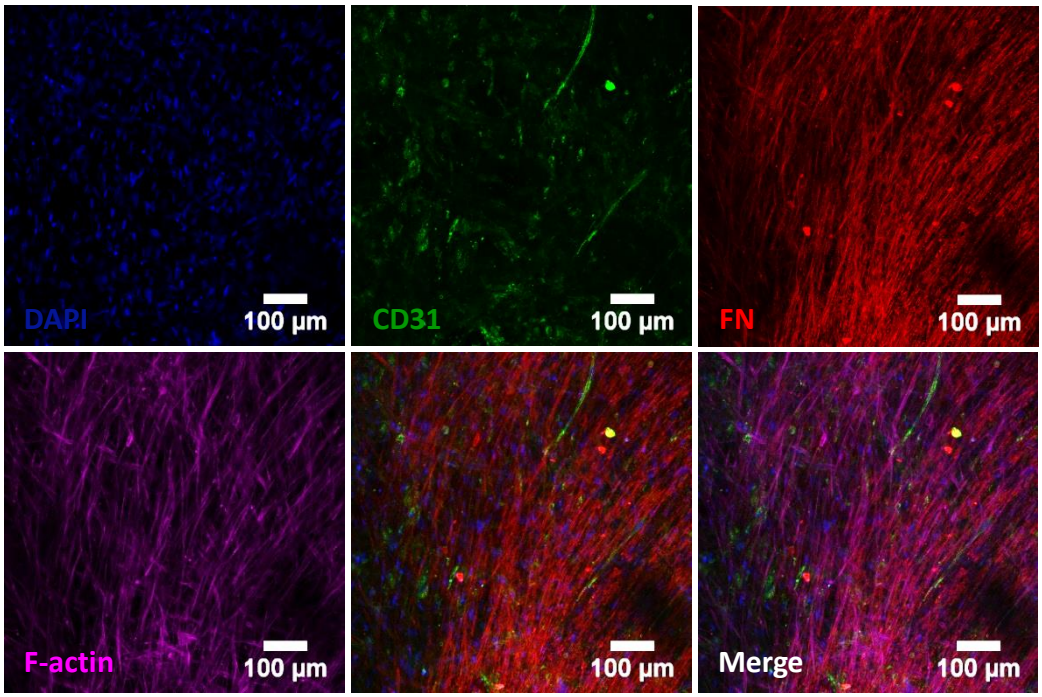
DAPI
100 μm
CD31
100 μm
FN
100 μm
F-actin
100 μm
100 μm
Merge
100 μm

D

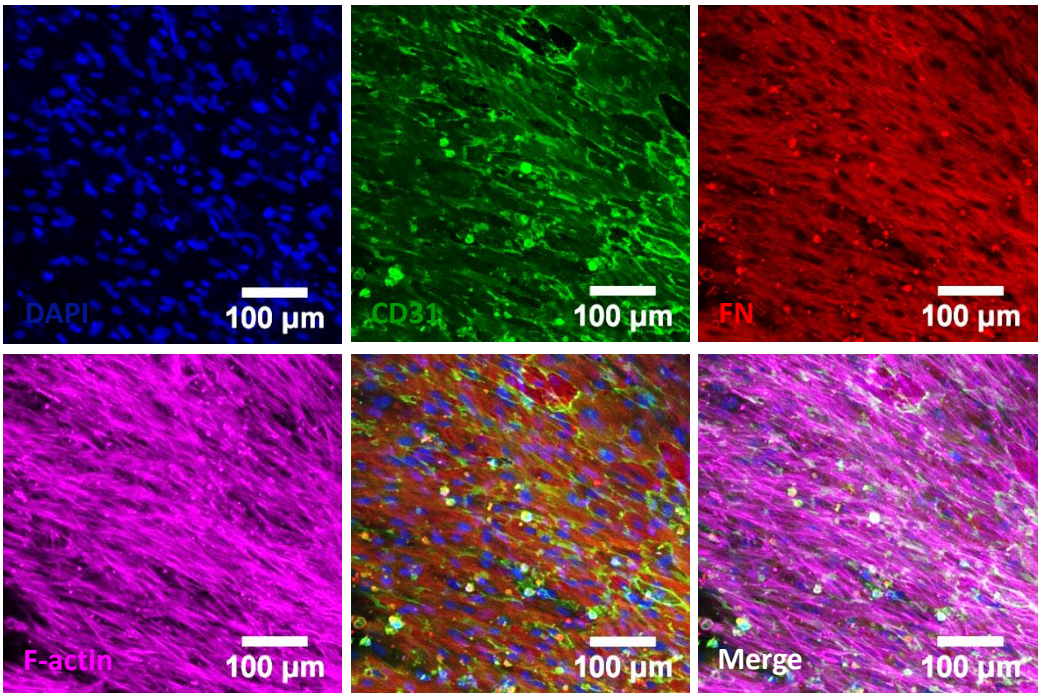
DAPI
100 μm
CD31
100 μm
FN
100 μm
F-actin
100 μm
100 μm
Merge
100 μm

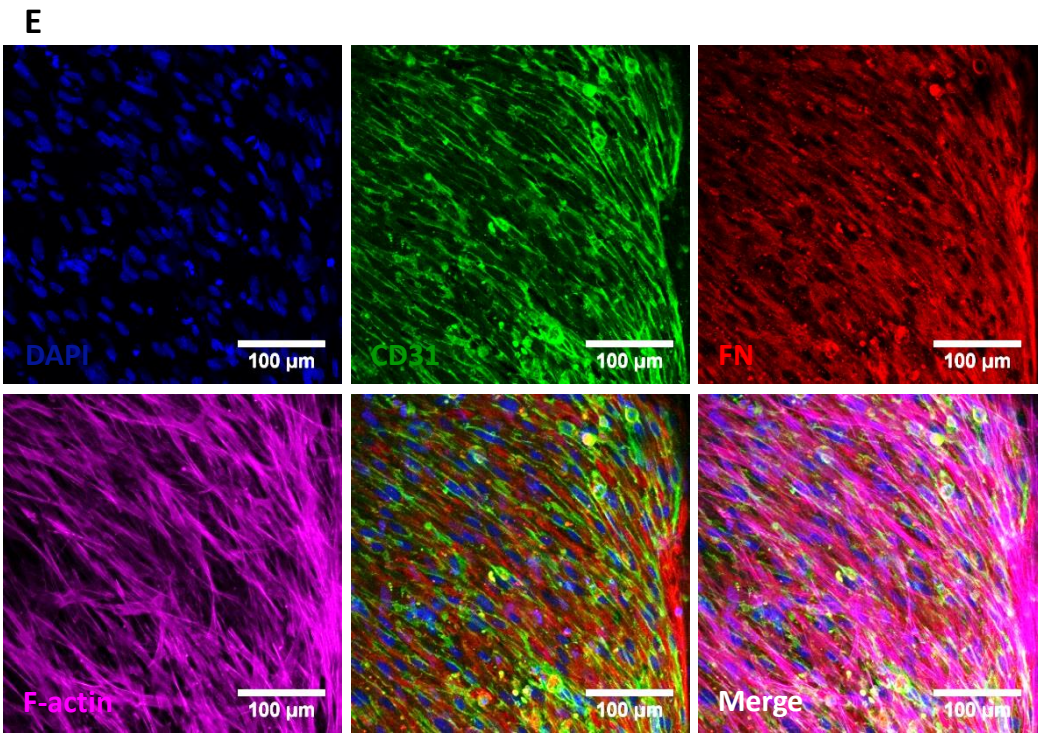

Figure S2 - Co-culture of hMF with OECs. Simultaneous (A, B and C) and sequential (D and E) co-culture strategies were studied, with the following cell densities per scaffold: (A and B) $25x10^4$ hMF + $25x10^4$ OEC, (C) $50x10^4$ hMF + $50x10^4$ OEC; Pre-seeding with $50x10^4$ hMF and (D) after 4 days or (E) 7 days $50x10^4$ OEC were added to the scaffold.

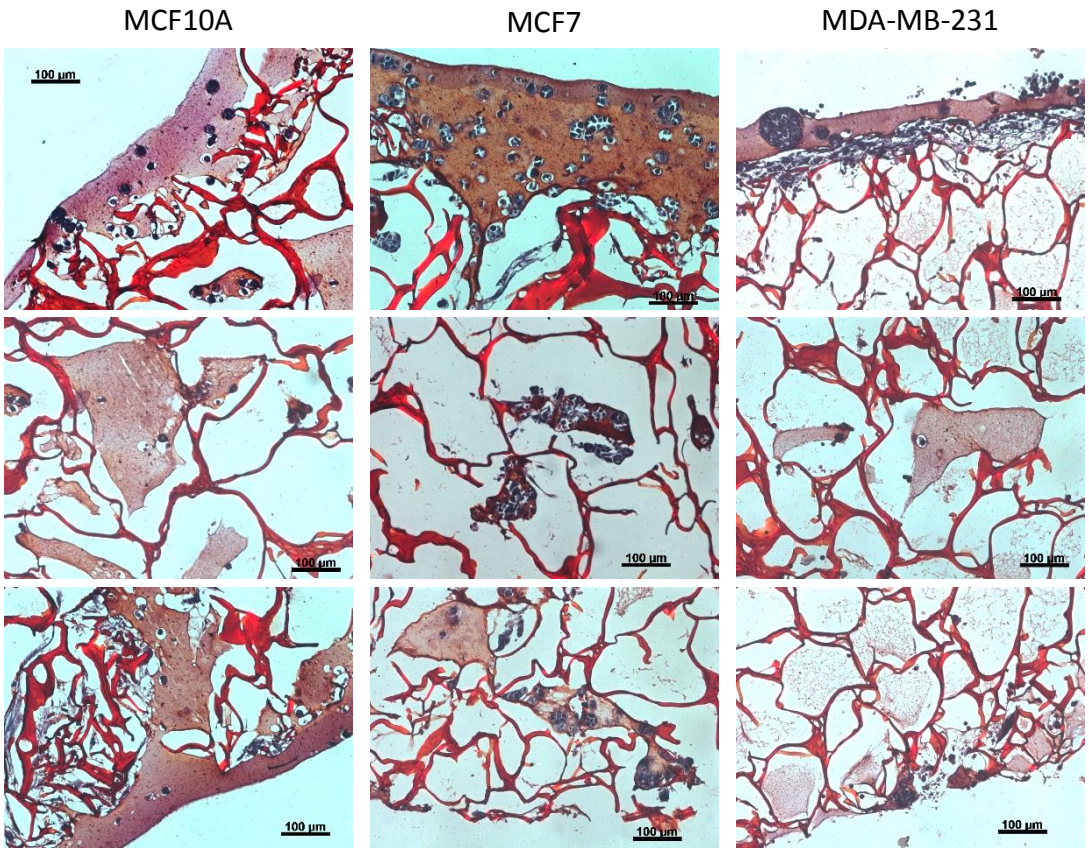

Figure S3 - Cell-laden Hydrogel distribution within the vascularized scaffold. The cross-sections of the constructs with MCF10A, MCF7 and MDA-MB-231-laden hydrogels were stained with Safranin, allowing to visualize the presence of spheroids within the pore structures. (Scale bar: 100 µm).